THE UNIVERSITY
of EDINBURGH

Molecular characterisation of human prion amplification in cell-free systems and diagnostic applications

Gabriele Piconi

Doctor of Philosophy

~

2020

Declaration

I declare that this thesis has been composed solely by myself and that it has not been submitted, in whole or in part, in any previous application for a degree. Except where states otherwise by reference or acknowledgment, the work presented is entirely my own.

Gabriele Piconi Ph.D.

Acknowledgements

I wish to thank the members of the supervising panel Dr Alison J.E. Green, Dr Alexander H. Peden and Dr Marcelo A. Barria for their trust and guidance throughout my Ph.D. degree. Thank you all for allowing me to manage my time and for entrusting me with the practical and theoretical means I needed to pursue and complete a research project as well as to experience science independently. Special thanks to Dr Mark W. Head, who I had the pleasure to be supervised by during my first year, for his kindness and for taking the time to read through and critically assessing the drafts of my writings.

I also wish to thank all the other staff, lab and front office members of the National CJD Research and Surveillance Unit for making me feel welcomed from day one. The NCJDRSU is such a great place to work at because of the amazing people that are there. Thank you all.

My gratitude also goes towards the relative of patients for the opportunity to conduct research on tissue specimens.

This Thesis is dedicated to my family. Nothing of what this work is and represents could have been achieved without your constant love and support.

Gabriele Piconi Ph.D.

Abstract

Prion diseases are a group of fatal neurodegenerative diseases associated with proteopathy occurring in humans and other mammals. The mechanism of prion replication is thought to be based on the induced misfolding of the host encoded prion protein and can be emulated *in vitro* by methodologies termed cell-free conversion (CFC) systems. Currently, the two most common implementation of CFC systems are the Protein Misfolding Cyclic Amplification (PMCA) reaction and the Real Time Quaking Induced Conversion (RT-QuIC) reaction. The overarching aim of this thesis is to describe and compare the human prion amplification *in vitro* by PMCA and RT-QuIC and to extend the diagnostic applicability of the latter, which is currently employed for the diagnosis of sporadic Creutzfeldt-Jakob disease (sCJD). Therefore, in this thesis, PMCA and RT-QuIC differential amplification abilities were systematically investigated and, for the first time, PMCA and RT-QuIC reaction kinetics compared using a specifically defined set of conditions. In addition, the research performed in this thesis has shown that the sCJD cerebrospinal fluid and brain samples seed the conformational change of the full-length hamster recombinant prion protein in a similar way in RT-QuIC, and that the RT-QuIC analysis of sCJD urine samples is possible, however, it has low sensitivity and, therefore, a limited diagnostic potential.

Lay summary

Prions are the causative agent of prion diseases, a group of infectious neurodegenerative diseases affecting humans and other mammals. Prions are unique among infectious agents because, at variance with viruses and bacteria, they are able to replicate themselves without relying on DNA or RNA to store the information needed. Cell-free systems are methodologies that allow emulating prion replication *in vitro*. The two most commonly used prion replication cell-free systems are the PMCA

reaction and the RT-QuIC reaction. These methods are powerful tools to study prion biology and have found application to aid prion disease diagnosis in humans. In this thesis, with the aim of gaining insight into the molecular mechanism of prion replication, the PMCA and the RT-QuIC reactions are compared on the basis of their differential abilities in amplifying and detecting human prions. Moreover, the results of a biochemical characterization of the RT-QuIC reaction products is presented, as well as a study regarding the possibility of achieving prion disease diagnosis by the RT-QuIC analysis of human urine samples.

Table of Content

List of Abbreviation

βME	Beta mercaptoethanol
129 MM	Methionine homozygote at *PRNP* codon 129
129 MV	Methionine/Valine heterozygote at *PRNP* codon 129
129 VV	Valine homozygote at *PRNP* codon 129
90-231Ha-rPrP	N-terminally truncated form of hamster rPrP
A	Ampere
ACDP	Advisory Committee on Dangerous Pathogens
AD	Alzheimer's disease
BH	Brain Homogenate
BSE	Bovine Spongiform Encephalopathy
CD	Circular Dichroism
CFC	Cell-Free Conversion
CNS	Central Nervous System
Cryo-EM	Cryogenic Electron Microscopy
CSF	Cerebrospinal Fluid
CWD	Chronic Waiting Disease
CJD	Creutzfeldt-Jakob Diseases irrespective to the aetiology
DPBS	Dulbecco modified PBS without $CaCl_2$ and $MgCl_2$
EDTA	Ethylenediaminetetraacetic acid
FLHa-rPrP	Full Length Hamster recombinant Prion Protein
FLHu-rPrP	Full Length Human recombinant Prion Protein
FTIR	Fourier Transform Infrared spectroscopy
gCJD	genetic Creutzfeldt-Jakob Disease irrespective to the mutation
Gnd-HCl	Guanidine hydrochloride
GPI	Glycosylphosphatidylinositol

h	hours
IB	Inclusion Bodies
LDS	Lithium Dodecyl Sulphate sample buffer
mAb	monoclonal Antibody
MSC I	Class I Microbiological Safety Cabinet
MSC II	Class II Microbiological Safety Cabinet
MM1	sCJD subtype MM1
MM2c	sCJD subtype MM2 cortical
MM2t	sCJD subtype MM2 thalamic
MV1	sCJD subtype MV1
MV2	sCJD subtype MV2
NCJDRSU	National CJD Research and Surveillance Unit
Ni-NTA	Nickel-nitrilotriacetic acid
NPM	Nucleation-Polymerization Model
OM	Olfactory Mucosa
PBS	Phosphate Buffered Saline
PCR	Polymerase Chain Reaction
PD	Parkinson's disease
PIRIBS	Parallel In-Register Intermolecular β-Sheet
PK	Protease K
PMCA	Protein Misfolding Cyclic Amplification
PrD	Prion Disease
PRNP	Human gene encoding PrP
PrP	Prion Protein
PrP^C	Cellular Prion Protein, physiological conformer, degraded by PK treatment

PrP^{res}	Protease Resistant PrP, derived from limited proteolytic treatment of PrP^{Sc}
PrP^{Sc}	Disease-associated form of prion protein. Rich in β-sheet structure. Conformational alternated respective to PrP^{C}
rPrP	recombinant Prion Protein
PSWC	Periodic Sharp Wave Complexes
RFU	Relative Fluorescence Units
RT-QuIC	Real Time Quaking Induced Conversion
SA	Seeding Activity
sCJD	sporadic Creutzfeldt-Jakob Disease
SDS-PAGE	Sodium Dodecyl Sulphate – Poly-Acrylamide Gel Electrophoresis
SHa-rPrP	chimeric Sheep-Hamster recombinant Prion Protein
sPAINT	spectrally-resolved Points Accumulation for Imaging in Nanoscale Topography
TAM	Template Assisted Model
TBS	Tris-Buffered Saline
TBST	Tris-Buffered Saline with 0.1% Tween 20
Thr	Threshold, indicate the fluorescence threshold for positivity of an RT-QuIC signal
TIRFM	Total Internal Reflection Fluorescence Microscopy
t_{Lag}	Lag time, mean average of the t_{Thr}
t_{Thr}	Time to threshold expressed in hours
TP	True Positive
TSE	Transmissible Spongiform Encephalopathy
vCJD	variant Creutzfeldt-Jakob Disease
VV1	sCJD subtype VV1
VV2	sCJD subtype VV2

w/o	without
w/v	weight/volume
WB	Western Blot
WHO	World Health Organisation

List of Tables

Chapter 2

Chapter 3

Chapter 4

Chapter 5

List of Figures

Chapter 3

Chapter 4

Chapter 5

Chapter 1: General Introduction

1.1 The "protein-only" hypothesis and the concept of prions

In the late 1950s', William J. Hadlow, an American veterinarian, had the chance to attend an exhibition at the Wellcome Medical Museum in London, illustrating the clinical and neuropathological features of a recently described neurodegenerative disease affecting an isolated human population in the Eastern Highlands of Papua New Guinea. This endemic condition, named "kuru" (shivering) by the natives, was showing similarities at a neuropathological, clinical, and epidemiological level with "scrapie", a fatal transmissible disease of sheep and goats recognized in Europe for over 200 years. This observation lead Hadlow to suggest that kuru, as with scrapie, might be transmissible and that possibly kuru and scrapie were determined by a similar pathogen (Hadlow 1959). The transmissibility of kuru was demonstrated a few years later, by intracerebral inoculation of kuru brain homogenate (BH) to non-human primates (Gajdusek, Gibbs, and Alpers 1967), confirming Hadlow's intuition. Based on these results, Creutzfeldt-Jakob disease (CJD), another human neurodegenerative disease with neuropathological similarities with kuru and scrapie, was experimentally inoculated into non-human primates showing that it was also transmissible (Gibbs et al. 1968). Notwithstanding the transmissibility and neuropathological similarities linking kuru, scrapie and CJD, the hypothesis regarding a similar aetiological agent proved to be difficult to investigate at that time.

The adaptation of the natural scrapie agent to the common laboratory rodents (Chandler 1961) and chiefly the isolation of the scrapie strain 263K in Syrian hamsters (Kimberlin and Walker 1978) were key to further investigation of this issue. Indeed, the Syrian hamster adapted scrapie strain 263K, which produces high titres of infectivity in a relatively short time, made it easier to titre scrapie infectivity in biological samples and to more rapidly generate infectious material to be analysed. Data started

accumulating showing that semi-purified fractions prepared from brains of 263K-infected Syrian hamster enriched for scrapie infectivity were enriched in proteins but not in nucleic acids, leading to speculate that the scrapie aetiological agent was entirely proteinaceous (Prusiner et al. 1980). Inactivation studies of the scrapie agent in semi-purified fractions suggested that it was also devoid of nucleic acids (Prusiner et al. 1981). Moving from these bases, Prusiner postulated the "protein-only" hypothesis, proposing the existence of a novel biological infectious entity, termed "prion", composed mainly, if not entirely, of a hydrophobic protein. Consequently to the lack of nucleic acids, Prusiner also suggested that the prion was able to induce or template its own synthesis in order to replicate (Prusiner 1982).

The initial scepticism around the protein-only hypothesis and the existence of prions was overturned by the accumulation of evidence backing Prusiner's insight over time (Prusiner 1998; 2004). According to the current paradigm, the central molecular event in diseases like kuru, scrapie and CJD, classically identified as Transmissible Spongiform Encephalopathies (TSEs) and currently referred to as Prion Diseases (PrDs), is the conformational change that transforms the cellular form of the host encoded prion protein (PrP^{C}), into a β-sheet rich, amyloidogenic, partially proteinase resistant, conformer referred to as PrP Scrapie (PrP^{Sc}). Once PrP^{Sc} is formed, or exogenously acquired, it induces the conformational shift of PrP^{C} leading to precipitation of pathognomonic PrP^{Sc} aggregates. Hence, PrP^{Sc} appears to be able to transfer structural information without relying on informational molecules such as DNA or RNA.

The centrality of the host encoded PrP^{C} to PrDs pathology, was further confirmed by the observation that genetically modified mice lacking PrP^{C}, are resistant to prion disease transmission (Büeler et al. 1993; Sailer et al. 1994; Brandner et al. 1996; 2002). The latter observation, together with the *in vitro* generation of infectious

preparations (i.e. synthetic prions) from bacterially expressed recombinant PrP^C (rPrP) and minimal non-proteinaceous components, are among the strongest evidence in support of the protein-only hypothesis (Deleault et al. 2007; Legname et al. 2004; Colby et al. 2009; Wang et al. 2010; Barria et al. 2009). The study of synthetic prions also revealed that, under specific conditons, it is possible to separate prion ability to induce misfolding from the generation of infectivity (Noble and Supattapone 2015).

Notably, the generalization of the biological concept that prions, as proteins, are capable of storing and transferring structural information, without necessarily displaying infectious properties, has been highly influential. Specifically, a prion-like behaviour has been proposed to explain the spreading within the peripheral and Central Nervous System (CNS) of the protein α-synuclein, which aggregates constitute the distinctive neuropathological hallmark of Parkinson's disease (PD), Lewy Body Dementia, and other 'synucleinopathies'. Similarly, the aggregation and spreading of the tau protein (τ-protein) which can be observed in Alzheimer's disease (AD) brains has been proposed to rely on a prion-like mechanism. In addition to pathological processes, a number of physiological and biological processes have also been proposed to follow the prion-like model (Scheckel and Aguzzi 2018; Hafner-Bratkovič 2017).

1.2 Molecular and structural biology of prions

In humans the gene *PRNP*, encoding for the prion protein, is expressed ubiquitously (including skin, kidney, urinary bladder and spleen) but at the highest level in the brain (https://www.ncbi.nlm.nih.gov/gene/5621). Both *PRNP* and its product are highly conserved throughout the mammalian taxon (http://www.ensembl.org/). PrP^C is synthesized in the rough endoplasmic reticulum (RER) as a polypeptide chain of 253 aminoacid residues in humans, 254 in Syrian hamster and mice, 264 in bovines (*Bos*

taurus) and 256 in sheep (*Ovis aries*). PrP^C post-translational modifications include: the cleavage of an N-terminal signal peptide (residues 1-22, human numbering, UniProt database accession number P04156), the addition of two facultative N-linked oligosaccharide chains (at asparagine residues 181 and 197), the formation of a disulfide bond (between the cysteine residues at 189 and 214), the insertion of a glycosylphosphatidylinositol (GPI) anchor with the simultaneous removal of a C-terminal signal peptide (residues 231-254). The facultative glycosylation at asparagine residues 181 and 197 results in mono-, di-, and un-glycosylated forms of PrP^C present in cells at the same time. The GPI anchor is responsible for PrP^C association with lipid-rafts at the plasma membrane (Stahl et al. 1990).

Nuclear Magnetic Resonance (NMR) spectroscopy and X-ray crystallography studies on bacterially expressed rPrPs from hamster, human, and other mammals, showed that they have essentially the same conformation. While the N-terminal portion from residues 23 to 127 is largely unfolded in solution, the C-terminus(residues 128 to 230) has a well-defined secondary and tertiary structure and is often referred to as the globular domain (GD) (Wüthrich and Riek 2001; Rossetti and Carloni 2017; Zahn et al. 2000). The GD is characterised by three α-helices at residues 144-154, 173-194, and 200-228 (hereafter referred to as α1 α2 and α3 respectively). The single disulfide bond connects α2 and α3.

As mentioned, the central molecular event in PrDs is the conformational change of PrP^C into PrP^{Sc}. Misfolded PrP^C may form small aggregates (*i.e.* oligomers) and eventually fibrillary, amyloid-like PrP^{Sc} forms that, because of their insolubility, eventually precipitate and can form amyloid plaques in the central nervous system (CNS). At variance with PrP^C, PrP^{Sc}, due to its amyloid-like conformation, is partially resistant to protease digestion. The resolution of PrP^{Sc} structure has been hampered by its insolubility in non-denaturing detergents. Fourier Transform Infrared (FTIR)

spectroscopy and Circular Dichroism (CD) spectroscopy data have shown that PrP^{Sc} structure has a high β-sheet content while α-helices dominate PrP^{C} conformation (Caughey et al. 1991; Pan et al. 1993). Currently, studies of rPrP fibrils by means of cryogenic Electron Microscopy (cryo-EM), X-ray diffraction and solid state NMR spectroscopy (ssNMR), have led to two competing models of the PrP^{Sc} fibrillar structure: the Parallel In-Register Intermolecular β-Sheet (PIRIBS), and the 4-rung β-solenoid model (Baskakov et al. 2019; Wille and Requena 2018; Groveman et al. 2014). A growing line of evidence, however, indicates that small, transient, and structurally heterogeneous oligomers of misfolded PrP, are the species responsible for prion infectivity and toxicity rather than PrP^{Sc} (Kayed *et al.*, 2003; Silveira *et al.*, 2005; Campioni *et al.*, 2010; Sang *et al.*, 2019).

The limited proteolysis in standardized conditions of samples known to contain PrP^{Sc}, or of fractions enriched for this component, yield a fragment usually referred to as protease resistant prion protein (PrP^{res}). Specifically, PrP^{res} is defined operationally as the fragment obtained following limited proteolysis of PrP^{Sc} with Proteinase K (PK) and detected by immunochemical assay, typically a western blot (WB), with PrP specific monoclonal antibodies (mAb). PrP^{res} is composed of the C-terminal part of the PrP sequence spanning residues from ~90 to 230 (231 in hamster). Beside its historical importance for the identification of the scrapie agent (Bolton, Mckinley, and Prusiner 1982), PrP^{res}, is currently acknowledged internationally as the immunochemically detectable, decisive hallmark, for diagnosis of PrDs in humans.

The molecular characterization of PrP^{res} from human and animal PrD biological samples, has shown that the position of the N-terminal cleavage site is not fixed. Namely, the limited proteolysis of PrP^{Sc} yields a limited number of major PrP^{res} types (*e.g.* two, in humans and hamster), that are defined on the basis of the size of the un-glycosylated PrP^{res} as assessed by standardized WB analysis. It has been

hypothesized that such observable diversity is due to slightly different PrP^{Sc} conformations (*i.e.* isotypes) exposing different regions of the prion protein polypeptide chain to degradation by PK. Adding to this, the relative abundance of di-mono- and un-glycosylated forms (*i.e.* glycotype) and the size of the un-glycosylated PrP^{res} (*i.e.* PrP^{res} type) as assessed by standardize WB analysis, vary in correlation with the different phenotypes of PrDs. This process, in combination with the status of certain polymorphic codons on the prion protein gene, have been exploited to achieve a molecular classification of human forms as well as animal forms of PrDs (Parchi et al. 1999; Telling et al. 1996; Bessen and Marsh 1992; Biacabe et al. 2004; Parchi et al. 1996).

The conformational heterogeneity of PrP^{Sc} isotypes, which can be inferred by the detection of PrP^{res} types upon PK digestion, has also been hypothesised to be the molecular determinant of the prion strain phenomenon. The concept of prion strains arose from the observation of the existence of several distinct isolates of agents, from phenotypically different PrDs that, when passaged in inbred mice of the same prion protein genotype, show reproducible incubation time and patterns of neuropathology (Collinge et al. 1996; Collinge and Clarke 2007; Safar et al. 1998; Bishop, Will, and Manson 2010; Moda et al. 2012; Fraser and Dickinson 1973; Pattison and Millson 1961). Similarly, minor differences in PrP^{C} primary and secondary structures have been used to explain the molecular basis of the “species barrier” phenomenon, typical of PrDs. The concept of the species barrier arose from the observation that transmission of PrDs between xenogeneic hosts, is typically far less efficient than between syngeneic individuals (Scott et al. 1989; 1997; Crozet et al. 2001; Vilotte et al. 2001; Tessier and Lindquist 2007; Sigurdson et al. 2010; Collinge et al. 1995; Kocisko et al. 2006). Exceptions to the species barrier phenomenon, however, do exist. It has been reported that the primary transmission of certain animal and human

prion diseases, including CJD, to bank voles (Clethrionomys Glareolus), occurs without the loss of efficiency typically observed with other laboratory animals (Nonno et al. 2006; Di Bari et al. 2008; Watts et al. 2014).

1.4 Models of PrP conversion

The idea that the replication of the scrapie agent involved a process resembling crystal formation was firstly suggested by James Stanley Griffith in 1967 (Griffith 1967). The autocatalytic formation of crystals can, indeed, be seen as analogous to the process of protein misfolding, aggregation and amyloid fibril formation that was integrated in the framework of the prion concept to explain prion replication without the aid of nucleic acids (Cohen et al. 1994; Prusiner 1998; Jarrett and Lansbury 1993; Prusiner et al. 1990).

Two models for the prion replication mechanism were conceived based on experimental evidence: the autocatalysis mechanism, usually referred to as Template-Assisted Model (TAM, Prusiner *et al.*, 1990), and the nucleation-dependent polymerization or Nucleation-Polymerization Model (NPM, Jarrett and Lansbury, 1993). The TAM postulates a low rate of production of PrP^{Sc} by spontaneous conversion of PrP^{C}. The newly formed PrP^{Sc} then catalyses the conformational change of PrP^{C} by direct contact (*i.e.* by forming a heterodimer), which in turn dissociate at a faster rate into two molecules of PrP^{Sc}. The mathematical description of this model, however, showed that unrealistic high values for the rate constants were required (Eigen 1996). Namely, this model does not accommodate the long incubation period typical of PrDs. In the same work, however, a simulation of the NPM model was given, showing that it had a higher potential to describe the characteristics of prion replication.

In the NPM, conversion is initiated when oligomers of misfolded PrP^{C} act as nuclei for the incorporation and conversion of PrP^{c} into growing polymers of PrP^{Sc}. The

fragmentation of these fibril polymers provides nuclei for further polymerisation. The NPM is characterized by four key aspects: i) a threshold of nuclei size below which no replication occurs, ii) a lag-time before polymerization for nuclei just above the critical threshold, iii) a relatively rapid polymerisation for nuclei above the critical size, iv)a slow nucleation process that can be accelerated by the introduction of exogenous nuclei or “seeds”. The mathematical formalisation of the NPM describes in a more realistic way that, when PrP aggregates of a certain size are formed (*i.e.* oligomers), they can either elongate by the incorporation of a PrP^C monomer or break into new aggregates (Nowak et al. 1998). Further modification to the NPM formulation by Nowak and collaborators facilitated the validation of this model with *in vitro* data (Masel, Jansen and Nowak, 1999). Notwithstanding the progress made in the mathematical modelling of prion replication and in the broader research field of protein misfolding aggregation, to which the modelling of prion replication is integral (Dobson 2003; Walker and LeVine 2003), a gap still exists with the *in vitro* experimental observations (Giehm and Otzen 2010). This can be ascribed to the technological hurdles posed by the direct observation of transient molecular events in chemically crowded environments such as the one typical of biological systems. In a recent publication, Sang and colleagues (Sang *et al.*, 2019), reported the direct observation of mouse recombinant prion protein oligomer formation *in vitro* using Total Internal Reflection Fluorescence Microscopy (TIRFM) and spectrally-resolved Points Accumulation for Imaging in Nanoscale Topography (sPAINT). These methodologies might be the key for further elucidating the prion replication mechanism as well as the misfolding of other pathologically relevant proteins.

1.5 Prion diseases

Prion diseases (PrDs) or Transmissible spongiform encephalopathies (TSEs) are a group of fatal neurodegenerative diseases associated with proteopathy, affecting

humans and other mammals. PrDs may have sporadic or genetic aetiology but PrDs are also transmissible and hence can be exogenously acquired. The following paragraphs present a general description of human PrDs focussing on certain forms that presented the subjects of the experimental work in this thesis. Next, a brief description of the current criteria and methods for the clinical diagnosis of human PrDs is given.

1.5.1 Human prion diseases

As a group, human PrDs are rare diseases of middle aged and elderly people with a wide spectrum of clinical phenotypes. Based on the aetiology, clinical signs and neuropathology, distinct human PrDs are now recognised. Sporadic Creutzfeldt-Jakob disease (sCJD) (*i.e.* idiopathic, unknown cause) is the most common form accounting for ~85% of all PrD cases. Genetic forms are due to point or insertional mutation in the *PRNP* gene and represent ~10% of all PrD cases. The acquired forms are characterized by a long incubation period (years) and, although being the rarest, are of high concern to public health. Iatrogenic CJD (iCJD, *i.e.* CJD due to inadvertent transmission during medical procedure) has occurred in a substantial number of dura mater graft recipients and recipients of human growth hormone derived from cadaveric pituitary glands (Brown et al. 2012; Ironside, Knight, and Head 2011; Ritchie et al. 2017). Likewise, the epidemic of variant CJD (vCJD, see Section 1.5.1.2), that peaked between the late 1990s' and early 2000s' (World Health Organisation 2003), has been ascribed to inadvertent animal-to-human transmission (*i.e.* zoonotic transmission) of Bovine Spongiform Encephalopathy (BSE, *i.e.* PrD typical of bovines) (Bruce et al. 1997; Ward et al. 2006) and there have been cases of vCJD secondary transmission by transfusion of contaminated blood products (Peden et al. 2004) or professional accidental exposure (ISS 2019).

1.5.1.1 Sporadic Creutzfeldt-Jakob disease

Among human PrDs, sporadic CJD (sCJD) is the most common form, with an incidence of 1.5-2 cases per million people world-wide (Ladogana et al. 2005; Masters et al. 1979). The combination of dementia and myoclonic movements, often associated with cerebellar features, progressing over weeks to a state of total disability is the classic presentation of sCJD. Variation in the clinical presentation largely correlates with the genotype at the polymorphic codon 129 (encoding for either methionine M or valine V) of the *PRNP* gene in combination with the molecular mass of the un-glycosylated PrP^{res}. Indeed, PrP^{res} from different sCJD subtypes shows distinct physicochemical properties, (*i.e.* electrophoretic mobility, glycoform patterns, infrared spectrum) and, based on the molecular mass of the un-glycosylated form, two types of PrP^{res} can be distinguished in WB assay: type 1 migrating at 21 kDa and type 2 at 19 kDa. Based on these observations, molecular characterization of sCJD has defined six possible genotype/protein isotype combinations (*i.e.* MM1, MV1, MM2, MV2, VV1 and VV2 referred to as sCJD subtypes) that have been proposed to correlate with the major clinic-pathological phenotypes (Parchi et al. 1996; 1999).

While MM1 and MV1 cases are phenotypically indistinguishable and are, therefore, merged in an individual subtype termed MM1/MV1, the MM2 cases show two distinct phenotypes based on cortical (MM2c) or thalamic (MM2t) histopathology. Age at onset, disease duration, frequency, evolution of symptoms and signs are all discriminating features of the different sCJD subtypes. The median age at onset of sCJD subtype MM1/MV1 is 68 years (range 31-86 years) slightly higher than MM2c (64 years, range 49-77 years) which is similar to the median age at onset of VV2 (64 years, 40-83 years) and MV2 (65 years, 36-83 years) (Zerr and Parchi 2018). The rarer subtypes VV1 and MM2t show a significant lower median age at onset of 44 years (range 19-55 years) and 52 (26-71 years) respectively. The median disease

duration of sCJD is 6 months but it is strongly influenced by the molecular disease subtype. Namely, while the disease duration of MM1/MV1 and VV2 cases is typically shorter than 12 months, in all the other cases the median disease duration is between 1 and 2 years.

The most common sCJD phenotypical presentation is associated with subtype MM1/MV1 (~65% of sCJD cases). Symptoms and signs at onset in sCJD subtype MM1/MV1 are variable and include cognitive decline and visual signs of central origin. Aphasia, ataxia and myoclonus occur, in different combination, in a substantial number of patients with subtype MM1/MV1. The histopathologic investigation reveals the classic spongiform change with vacuolization located in the neuropil and in all the layers of the cerebral cortex and subcortical nuclei. Thalamus and basal ganglia are also affected, while hippocampus and brainstem are relatively spared. Upon immunohistochemical examination, granular deposition of PrP^{res} is most abundant in the cerebral cortex and cerebellum and basal ganglia. The sCJD subtype VV2 accounts for 15-20% of sCJD cases and is characterized by early onset of cerebellar symptoms and signs as well as oculomotor abnormalities and behavioural disturbances (Head *et al*. 2008) . Cognitive decline, other than memory loss and myoclonus, are late features. Distribution of PrP^{res} and spongiform change depends on disease duration, but in contrast with subtype MM1/MV1, neocortex is generally spared. About 10% of sCJD cases are subtype MV2. The clinical phenotype of subtype MV2 shows significant similarities with VV2 but is characterized by a lower progression rate and slightly longer disease duration. Likewise, histopathology is similar between VV2 and MV2 although the latter typically present cerebellar plaques referred to as kuru plaques. Subtype VV1, MM1c and MM2t are the rarest. Around 1% of sCJD cases are VV1. Early symptoms and signs include psychiatric and cognitive abnormalities followed later during the disease course by extrapyramidal

signs and ataxia. Histopathology generally shows that cortical-striatal regions are affected while subcortical regions are spared. The subtype MM2t is also referred to as sporadic Familial Insomnia (sFI) and early signs and symptoms include insomnia with inability to initiate and maintain sleep, although this is not invariably detected. The histopathology shows atrophy of the thalamus while spongiform changes may be absent or limited to the cerebral cortex where PrP^{res} deposit may also be present. Progressive dementia and frequent aphasia and apraxia characterize sCJD subtype MM2c. In this subtype, the pathology shows a lesion profile similar to MM1/MV1 with the exception of the cerebellum, which is generally spared (Head et al. 2008; Head and Ironside 2012; Zerr and Parchi 2018). The sCJD classification system has been further refined (Parchi and Saverioni 2012) to accommodate the substantial minority of cases that contain both type 1 and type 2 PrP^{res}, but this more subtle sub-classification system has not yet been employed internationally, is difficult to apply retrospectively and is beyond the scope of this thesis.

Notably, transmission studies to selected inbred strains of mice have shown that the above-mentioned six sCJD subtypes comprise four major human strains of prions (M1, M2, V1, V2) as defined by the length of incubation time, susceptibility and disease phenotype, as well as by the conservation of characteristic neuropathological lesion patterns upon serial passage in the same host (Bishop, Will, and Manson 2010; Moda et al. 2012). Interestingly, the V2 strain that has been proposed to account for both MV2 and VV2 sCJD, has been indicated as the possible contaminant to have caused the kuru epidemic (see Section 1.1) as well as the iCJD epidemic linked to growth hormone treatment in the United Kingdom (Kobayashi et al. 2014; Ritchie et al. 2017). Currently, the full characterization of the different sCJD subtypes require *post mortem* investigation, however, a means to discriminate sCJD *intra vitam* would

be of importance for the clinical management of patients and for caregivers as well as for the enrolment in future clinical trials.

1.5.1.2 Variant Creutzfeldt-Jakob disease

During the late 1990s, a new variant form of CJD (variant CJD, vCJD) was identified (Will et al. 1996). vCJD is an acquired form of PrD, which likely emerged as the result of human consumption of mechanically recovered meat derived from cattle affected by Bovine Spongiform Encephalopathy (BSE), a PrD which emerged in UK cattle in the late 1980s and early 1990s. (Bruce et al. 1997; Ward et al. 2006; Hill et al. 1997). The BSE outbreak highlighted the threat to public health posed by PrDs and resulted in coordinated national and international surveillance networks which allowed the identification of vCJD as a new form of PrD. From the clinical standpoint, variant CJD starts at an earlier age (mean age at onset is 29 years in UK patients) than sCJD, with prominent psychiatric symptoms and a mean disease duration of 14 months (Head et al. 2008). The vast majority of the reported vCJD cases present homozygosity with respect to codon 129 status, being almost exclusively MM. Transmission and biochemical studies have shown that the biological phenotype and PrP^{res} isotype of vCJD is almost indistinguishable from the one found in BSE. These observations corroborated the hypothesis that vCJD emerged from the infection of susceptible individuals by the BSE strain of agent (Collinge et al. 1996; Bruce et al. 1997; Head et al. 2004). In recent years, however, one case of definite vCJD (Mok et al. 2017) and one case of possible vCJD (Kaski et al. 2009) heterozygous at codon 129 (*i.e.* 129MV) were described. This appears to be in line with a previous transmission study of vCJD in transgenic mouse lines expressing the human prion protein gene of 129MM, MV or VV genotype, at physiological levels (i.e. single copy of the human PrP^{C} gene replacing the mouse one). The results of this study predicted a 129 genotype-specific susceptibility to vCJD, with 129MM subjects showing the shortest

incubation time, followed by 129MV and 129VV individuals having the longest incubation time, so long that in fact they may never show signs of the (Bishop et al. 2006).

1.5.1.3 Human prion disease diagnosis

Criteria for human PrD diagnosis are defined by guidelines compiled by the World Health Organization (WHO). According to WHO guidelines, the diagnosis of PrD firstly depends on the recognition of the possibility of this type of disorder upon neurological investigation. Electroencephalogram (EEG) registration of Periodic Sharp Wave Complexes (PSWC) represents an important aid for sCJD diagnosis despite having no definite diagnostic value, because some of the identified sCJD molecular subtypes and vCJD do not show alteration in EEG. Similarly, alterations in Diffusion Weighted Magnetic Resonance Imaging (DW-MRI) signals from specific brain structures (*e.g.* basal ganglia) and cortical ribbon are also taken into account to inform CJD diagnosis. Cerebrospinal Fluid (CSF) screening for the presence of 14-3-3 protein is currently routinely performed in suspected CJD cases. However, CSF 14-3-3 is a biomarker of neuronal damage and its detection in the CSF may be the result of several other pathologies acquiring diagnostic value only within the framework of a specific clinical context (Ladogana et al. 2009; Stoeck et al. 2012; Collins et al. 2006). Ultimately, according to the WHO diagnostic criteria, PrDs definite diagnosis is achieved only at *post mortem* (World Health Organisation 2003). Neuropathological observation typically reveals characteristic change in the CNS: spongiform changes, neuronal loss, glial activation, and PrP^{Sc} deposition, which may form amyloid plaques. PrP^{Sc} is the only currently available direct biomarker for PrDs and its presence in brain tissue is usually inferred by immunoblot detection of PrP^{res} (see Section 1.2) following PK treatment in standardized conditions. The limited sensitivity of the currently available methods for the immuno-detection of PrP^{res}, however, hinder their application to

peripheral biological tissues or fluid for diagnostic purposes. In the last decade, however, *in vitro* biochemical methodologies based on the prion replication mechanism have been described, which have shown the potential overcome this hurdle and eventually allow the *intra vitam* diagnosis of PrDs based the analysis of peripheral biological fluids.

1.6 Cell-free conversion systems

Cell-free conversion (CFC) systems are methodologies that emulate prion replication mechanism *in vitro* and allow amplification and, thereby, detection of otherwise undetectable amounts of prions. The general elements constituting a CFC system are: a source of PrP^{Sc} (termed seed), a source of PrP^{C} (termed substrate), an energy input, tailored chemical conditions and a method to detect the conformational change of the substrate. CFCs were originally developed to test the protein-only hypothesis and investigate prion biology. Kocisko and colleagues firstly demonstrated, in an *in vitro* cell-free reaction environment, the ability of brain-derived, semi-purified PrP^{Sc} to convert recombinant PrP to forms that resemble naturally occurring PrP^{Sc}, by showing resistance to limited proteolysis (Kocisko et al. 1994). Currently, after 25 years of technical refinements, two methodologies represent the most common implementation of CFCs: the Protein Misfolding Cyclic Amplification (PMCA) and the Real Time Quaking Induced Conversion (RT-QuIC).

1.6.1 Protein Misfolding Cyclic Amplification (PMCA)

In 2001, the group led by Claudio Soto described the Protein Misfolding Cyclic Amplification (PMCA) reaction for the *in vitro* amplification of tiny amounts of PrP^{Sc} otherwise undetectable by immunoblotting (Saborio, Permanne, and Soto 2001). The archetypical PMCA reaction is a tube-based reaction that employs crude Brain Homogenate (BH) as a source of PrP^{C} (substrate), which is induced by the PrP^{Sc} that is present in the test sample (seed) to convert into more PrP^{Sc}. The PMCA reaction

involves cycles of incubation at constant temperature and sonication in the ultrasound frequency range. The latter element constitutes the energy input and is the distinctive, invariant, characteristic of the PMCA method. The homogeneous distribution of the sound waves is achieved by partially submerging tubes in a water bath. PMCA reaction products are detected in a separate step by a biochemical assay. The typical detection system relies on the detection of PrP^{res} by WB analysis following PK digestion. PMCA results are typically qualitative (*i.e.* Yes/No), but quantitative protocols have been described (Chen et al. 2010; Morales et al. 2012).

The PMCA reaction conditions are thought to enhance the kinetics of the natural prion replication mechanism. Evidence has shown prion replication (involving nucleated aggregation and misfolding of PrP into PK resistant structures) can occur spontaneously in *in vitro* systems consisting of mouse cell lysate expressing tagged PrP^{C}, mixed with semi-purified PrP^{Sc} preparations (Saborio et al. 1999) and incubated at constant temperature. However, in PMCA, the ultra-sound waves are thought to directly break PrP^{Sc} fibrils, generating new nuclei of polymerization (Saborio, Permanne, and Soto 2001; Moda, Pritzkow, and Soto 2013; Piening et al. 2005), therefore, increasing the kinetics of the reactions. At the same time, sonication in the ultrasound frequency range causes the repeated expansions and collapse of microbubbles, generating high local pressure and temperature (*i.e.* acoustic cavitation), as well as the sonolysis of water. These two latter phenomena generate an environment enriched in air-liquid interfaces as well as in reactive species (*e.g.* •OH and •H) that favour the misfolding of the substrate PrP and contribute to fibrils breaking (Haigh and Drew 2015). It has been shown that PMCA kinetics can be further increased by adding teflon or ceramic beads to the reaction mixture (Barria et al. 2018; Moudjou et al. 2016).

The PMCA reaction has been crucial for the investigation into critical aspects of prion biology. Indeed, specific PMCA protocols have allowed the production of *de novo* infectious prions from preparations of bacterially expressed recombinant PrP^{C} and minimal components, corroborating the protein-only hypothesis (Deleault et al. 2007; Legname et al. 2004; Colby et al. 2009; Wang et al. 2010; Barria et al. 2009). Likewise, the observation that the PMCA reaction products, seeded with PrD samples, retain infectivity, PrP^{Sc} isotype and prion strain properties when inoculated in mice (Castilla et al. 2008; Cali et al. 2019), sustains the hypothesis that the characteristics of prion strain do not require a functional cell machinery to propagate and are enciphered in PrP^{Sc} structure. Similarly, the species barrier phenomenon is, at least in part, recapitulated in PMCA. Hence, PMCA has been used to investigate the potential of certain animal PrDs to be transmitted to humans (Barria et al. 2014; Levavasseur et al. 2014; Fernández-Borges, De Castro, and Castilla 2009) as well as to gain insights into how the transmission of sCJD and vCJD is influenced by different genotypes of the polymorphic codon 129 of human *PRNP* (Jones et al. 2008).

Furthermore, PMCA protocols have been described that allow the detection of PrP^{Sc} in urine (Moda et al. 2014), blood plasma (Concha-Marambio et al. 2016; Bougard et al. 2016) and CSF (Barria et al. 2018) samples from vCJD cases. Nonetheless, the deployment of PMCA diagnostic applications on a large-scale has been limited. This is likely due to the fact that the substrate used for the PMCA diagnostic applications is the BH of transgenic mice expressing the human PrP^{C} (Concha-Marambio et al. 2016; Moda et al. 2014; Barria et al. 2018). Not all the laboratories involved in clinical diagnosis have access to animal facilities and, to maintain transgenic animal production is costly. The transferability of the method between laboratories is further hampered by the difficulties in standardizing the sonication procedure.

1.6.2 Real Time Quaking Induced Conversion (RT-QuIC)

The Real Time Quaking Induced Conversion (RT-QuIC) reaction is the evolution of the assay developed by Kocisko and colleagues (Kocisko et al. 1994) in combination with certain technical features of the Amyloid Seeding Assay (ASA) developed by Colby and colleagues (Colby et al. 2007). RT-QuIC employs a recombinant PrP (rPrP) as substrate for conversion. At variance with PMCA, RT-QuIC uses intermittent shaking rather than sonication as energy input and does not require a separate step for signal detection. The RT-QuIC reaction can be followed in real time because of the presence of Thioflavin T (ThT) in the reaction mixture, an amyloidotropic fluorescent dye. ThT binds to the amyloid and amyloid-like fibril structures that are formed by the prion seeded misfolding of the rPrP substrate during the RT-QuIC reaction. The typical RT-QuIC reaction is a 96-well plate based assay, performed in a plate-reader that incubates samples at constant temperature, performs cycles of intermittent shaking and is able to detect the fluorescence emission from ThT upon binding to amyloid structures (Wilham *et al.*, 2010; Atarashi, *et al.*, 2011a; Atarashi, *et al.*, 2011b).

Since its first introduction (Wilham et al. 2010), RT-QuIC has attracted attention as diagnostic test for animal and human PrDs. The first studies regarding the application of RT-QuIC to sCJD diagnosis used the full-length (*i.e.* 23-230) human rPrP (FLHu-rPrP) or the full-length (*i.e.* 23-231) hamster recombinant PrP (FLHa-rPrP) as the reaction substrate for the analysis of human CSF and brain samples (Atarashi *et al.*, 2011b; McGuire *et al.*, 2012). A subsequent study using sCJD and vCJD brain material showed that the use of the FLHu-rPrP, FLHa-rPrP, as well as a truncated (*i.e.* 90-231) form of the hamster rPrP (90-231Ha-rPrP), allowed the detection of highly diluted sCJD BH but not of vCJD BH (Peden et al. 2012). A few years later, the use of the FLHa-rPrP, FLHu-rPrP, and chimeric full-length sheep-hamster rPrP (SHa-

rPrP) (Cramm et al. 2015) were internationally validated as the RT-QuIC substrates for the diagnostic analysis of sCJD CSF samples (McGuire et al. 2016). Around the same time, a second generation RT-QuIC diagnostic test for the analysis of sCJD CSF samples was described with improved analytical sensitivity and speed that employed 90-231Ha-rPrP, included a denaturant (*i.e.* Sodium Dodecyl Sulphate, SDS) in the reaction mixture and required higher temperature and shaking frequency (Orrù et al. 2015a). Second generation RT-QuIC has also been validated to screen samples of CSF (Groveman et al. 2016). More recently, the analysis by first generation RT-QuIC of olfactory mucosa samples collected by means of nasal swab from CJD patient has shown the potential to further reducing the invasiveness of the diagnostic test (Bongianni et al. 2017; Orrú et al. 2014). Because of the high sensitivity, specificity and transferability between laboratories, the RT-QuIC analysis of CSF, has been included among the sCJD diagnostic criteria in the United Kingdom (https://www.cjd.ed.ac.uk/sites/default/files/criteria.pdf) and is under scrutiny to be considered internationally (Hermann et al. 2018).

1.7 Aims of the thesis

The overarching aim of this thesis is to compare human prion amplification in PMCA and RT-QuIC using human sCJD and vCJD samples. The following three hypotheses are addressed:

1 Comparison of RT-QuIC and PMCA kinetics of aggregation (Chapter 3)

Hypothesis: The PMCA and RT-QuIC reaction kinetics differ when seeded with the same seed.

With the aim of addressing this, the amplification performances for sCJD and vCJD prions of specific PMCA and RT-QuIC protocols are established by seeding the reactions with brain homogenate from the same sCJD and vCJD cases. Next, a methodology for the comparison of PMCA and RT-QuIC respective kinetics of aggregation is applied, which takes the specifics of the two technologies into account.

2 Molecular Characterization of RT-QuIC products (Chapter 4)

Hypothesis: the epitope mapping analysis of the RT-QuIC protease resistant products allows discrimination between sCJD subtypes.

The products of the diagnostic RT-QuIC reaction seeded with sCJD brain or CSF samples, are analysed applying the same methodological principles employed for the molecular discrimination of PrP^{res} types that are part of sCJD molecular subtyping.

3 RT-QuIC seeding activity of sCJD urine samples (Chapter 5)

Hypothesis: RT-QuIC reaction can discriminate sCJD from non-CJD urine samples.

The RT-QuIC reaction is optimized and deployed to investigate the possibility of developing a clinical diagnostic test for sCJD based on the analysis of patient urine samples.

Chapter 2 General Materials and Methods

2.1 Laboratory requirements for safe handling of TSE samples

The Laboratory Code of Practice of the National CJD Research & Surveillance Unit (NCJDRSU) follows the Advisory Committee on Dangerous Pathogens (ACDP) indications on laboratory requirements and practices that needs to be in place to handle PrD tissue samples safely. According to this, all the experimental work presented in this thesis was carried out in a containment level 3 laboratory with certain derogation. Because the PrD agent is not air borne, the laboratory does not need to be sealable for fumigation and the laboratory extract air does not need to be HEPA filtered. CJD tissue sampling, homogenization to 10% weigh/volume (w/v) and handling of the homogenate, were performed in class 1 microbiology safety cabinet (MSC I) while non-CJD tissue homogenization to 10% w/v and homogenate handling were performed in class 2 microbiology safety cabinet (MSC II).

2.2 Biological samples

The CSF and tissue bank at the National CJD Research and Surveillance Unit (NCJDRSU), provided all the human brain, CSF and urine samples. All the human biological samples had ethical approval and full consent for use in research (Scotland A REC 05/MRE00/67, Edinburgh Brain Bank 16-ES-0084). Transgenic mouse brains, used as PMCA substrate (see Section 2.6), were kindly provided by Dr. Abigail Diack, Roslin Institute, the University of Edinburgh, UK.

2.2.1 Human brain samples

The brain frontal cortex of three cases of sCJD subtypes MM1, MV1, MM2 (of the cortical variant, MM2c), MV2, VV2 and two cases of sCJD subtype VV1 according to the Parchi nomenclature (Parchi et al. 1999) as well as three cases of vCJD and one non-CJD control (Table 2.1), were sampled and used throughout the study. Sample

selection was based on presence of a full consent for research, tissue availability as well as a previous use of the same tissue in published studies (Bishop, Will, and Manson 2010; Diack et al. 2012).

2.2.1.2 Preparation of 10% Brain Homogenates

All human brain samples were homogenized to 10% w/v. Table 2.1 lists all the brain samples used. Frontal cortex of each brain was sampled twice, and each pair of samples were homogenized in either RT-QuIC or PMCA homogenization buffer (Table 2.2) generating R or P samples respectively. The samples coding allows to identify samples taken from the same brain and homogenized to 10% w/v in either PMCA or RT-QuIC homogenization buffer. For details regarding the preparation of the 10%BHs used to seed RT-QuIC see Section 2.5.2, while details of PMCA seed preparation are described in Section 2.6.3.

Diagnosis	Codon 129	PrP^{res} Type	N of cases	RT-QuIC Coding	PMCA Coding
sCJD	MM	1	3	MM1BH1R	MM1BH1P
				MM1BH2R	MM1BH2P
				MM1BH3R	MM1BH3P
		2	3	MM2BH1R	MM2BH1P
				MM2BH2R	MM2BH2P
				MM2BH3R	MM2BH3P
	MV	1	3	MV1BH1R	MV1BH1P
				MV1BH2R	MV1BH2P
				MV1BH3R	MV1BH3P
		2	3	MV2BH1R	MV2BH1P
				MV2BH2R	MV2BH2P
				MV2BH3R	MV2BH3P
	VV	1	2	VV1BH2R	VV1BH2P
				VV1BH3R	VV1BH3P
		2	3	VV2BH1R	VV2BH1P
				VV2BH2R	VV2BH2P
				VV2BH3R	VV2BH3P
vCJD	MM		3	vCJDBH1R	vCJDBH1P
				vCJDBH2R	vCJDBH2P
				vCJDBH3R	vCJDBH3P
Brain tumour			1	-Ctrl BH	

Table 2.1 Human brain samples

Samples coding allow to identify the CJD type (vCJD or the sCJD subtype), the individual brain sampled of a certain CJD type (BH1, 2 or 3) and the preparation protocol (P for PMCA and R for RT-QuIC seed preparation protocol). All the cases selected had received a definite diagnosis.

	RT-QuIC	PMCA
PBS	1X	1X w/o Ca^{++} or Mg^{++}
NaCl	150 mM	150 mM
Triton X-100	0.5%	1%
EDTA	1 mM	none
Complete® Protease Inhibitor Cocktail Roche	1 tablet	1 tablet w/o EDTA
Homogenizers	FastPrep-24® MPbio	Plastic Mini-Pestels Eppendorf

Table 2.2 RT-QuIC and PMCA brain homogenization buffers composition and equipment

All the human brain samples were homogenized with either RT-QuIC or PMCA buffer. The latter was also used to homogenize the transgenic mice brain used as PMCA substrate.

2.2.2 Cerebrospinal fluid samples

CSF samples were selected based on volume availability, testing positive in a previous RT-QuIC analysis, being from patients with neuropathologically-confirmed sCJD and with a known sCJD subtype. The selected CSF samples included three cases of sCJD subtypes MM1, MV2 and VV2 and two cases of MV1 and MM2c. An additional CSF samples was selected as negative control based on being assigned with diagnosis of a non-prion related neurological disease, sample volume availability and testing negative in a previous RT-QuIC analysis. Table 2.3 lists the CSF samples used.

Diagnosis	Codon 129	PrP Type	N of cases	Coding
sCJD	MM	1	3	MM1CSF1 MM1CSF2 MM1CSF3
		2	2	MM2CSF1 MM2CSF2
	MV	1	2	MV1CSF1 MV1CSF2
		2	3	MV2CSF1 MV2CSF2 MV2CSF3
	VV	2	3	VV2CSF1 VV2CSF2 VV2CSF3
Negative				-Ctrl

Table 2.3 CSF samples used

All the samples were previously tested in RT-QuIC, received definite diagnosis and had a defined codon 129 genotype and PrP^{res} type.

2.2.3 Urine samples

Urine samples were selected based on availability of a full consent for research and sample volume availability (Table 2.4).

Code	Diagnosis
U1	sCJD
U2	sCJD
U3	sCJD
U4	sCJD
U5	sCJD
U6	sCJD
U7	sCJD
-Ctrl 1	suspected sporadic, non-CJD
-Ctrl 2	suspected sporadic, non-CJD
-Ctrl 3	suspected sporadic, non-CJD

Table 2.4 Urine samples used

2.2.4 Definition of Seeding Activity of a biological sample

In this thesis, the Seeding Activity (SA) is the ability or capacity of a biological sample to seed a cell-free conversion system *i.e.* to generate a True Positive (TP) signal according to PMCA and RT-QuIC respective detection system. The definition of TP signal for PMCA and RT-QuIC is given in the respective materials and methods Sections (see Section 3.3.10 for PMCA 2.5.4 for RT-QuIC). The definition of the SA of a sample is of importance for the analysis of the analytical performances of a specific CFC and is not included among the diagnostic criteria used to analyse the results of the RT-QuIC reaction.

2.3 SDS-PAGE

All SDS-PAGE analyses were performed using pre-cast 10% bis-tris gels (NuPAGE). Following preparation, samples were incubated at 100°C for 10 minutes in sample loading buffer (LDS4X, NuPAGE). When needed, reducing agent β-mercaptoethanol (βMA) was added directly to 2% in LDS4X (LSD4X/2%βMA). Electrophoretic separation was performed in MES-SDS buffer (NuPAGE) at 200V for a minimum 35 and a maximum of 45 minutes. Table 2.5 lists buffers and materials used for SDS-PAGE analysis.

Gel	10% Bis-Tris Gel NuPAGE
Sample loading buffer	LDS4X NuPAGE (NP0007)
β-mercaptoethanol	Sigma-Aldrich (60-24-2)
Running buffer	MES-SDS NuPAGE
Towbin buffer	Glycine: Fisher Scientific (BP381-5) Tris Base: Corning (61-233-RR) Methanol: Fisher Chemicals (M/4000/PC17)
TBST	Tris Base: Corning (61-233-RR) NaCl: VWR Chemicals (27810 295) Tween 20: (SLS CHE3852)
Blotting membrane	BioRad Immun-Blot PVDF (1620177)
Secondary Antibody	Goat anti-Mouse IgG-Peroxidase Novex (A16072)
Chemilumiscence system	ECL Prime Amersham
Photographic film	Hyperfilm ECL Amersham (28906837)

Table 2.5 List of buffers and materials used for SDS-PAGE and WB analysis

Catalogue numbers are reported in parenthesis following the name of the brand.

2.4 Western blot

Following SDS-PAGE, gels were blotted on polyvinylidene fluoride (PVDF, BioRad Immun-Blot) membrane by means of wet transfer (1 hour, 0.8 A constant) using Towbin buffer (Towbin, Staehelin, and Gordon 1979). Following transfer, PVDF membranes were blocked overnight in a 5% w/v solution of non-fat dry milk in 0.1% Tween 20 Tris buffered saline (TBST). The following day, blocking solution was removed and membrane was incubated according to the conditions specific for the primary antibody of choice. At the end, membrane was washed three times for 10 minutes with fresh TBST. Washed membrane was incubated for 1 hour at room temperature (RT) and gentle shaking with a solution of horseradish peroxidase conjugated secondary antibody (Goat anti-Mouse IgG, Novex) diluted 1:25000 in TBST. At the end, membrane was washed with two 10 minutes washes and two 5 minutes washes with TBST before applying enhanced chemiluminescence system (ECL Prime Amersham). The signal was detected by digital imaging with ChemiDoc XRS+ (BioRad).

2.4.1 Western Blot for the evaluation of PrP^{res} content in sCJD and vCJD 10% brain homogenates

For each sCJD and vCJD 10% BHs produced, PrP^{res} levels were evaluated by western blot. A sample from each 10% BH was digested with 50 µg/mL PK (Merck Novagen) for one hour at 37°C, digestion was blocked by protease inactivation with Pefabloc SC (Roche). Samples were then diluted 1:2 four times stepwise in 0.1%SDS/PBS and LSD4X was added to 2X. Following 10 minutes incubation at 100 °C, samples were loaded on 10% Bis-Tris gel and run in SDS-PAGE (see Section 2.3) along with FLHa-rPrP dilutions of known concentration. Gels were blotted as described in Section 2.4 and membranes probed with primary antibody 3F4 (Millipore) diluted 1:10000. Digital images were taken by means of ChemiDoc XRS+ (BioRad).

Densitometric analysis of the signal was performed using ImageLab 4.1 software (BioRad) as described in 2.4.2. The raw data used for the evaluation of the PrP^{res} content in all the vCJD and sCJD 10%BH are reported in Appendix III.

2.4.2 Densitometric analysis of western blot signals

All the densitometric analyses presented in this study were performed using ChemiDoc XRS+ (BioRad). The software was set to take pictures every 30 seconds for a minimum of 20 to a maximum of 40 minutes. The image that preceded the appearance of signal saturation (in either the standard, when used, or in a sample of interest) on an individual gel, was used to perform densitometric analysis of all the signals on that gel. The ChemiDoc XRS+ ImageLab 4.1 software (BioRad) has a built-in function for digital image analysis and it was used to perform all the densitometric analysis presented in this thesis as follows; an image area, termed volume, enclosing a signal of interest was defined, the same volume was used to individually encircle all the other signal of interest (including the standard when used) and determine the image signal background as well. The background signal was subtracted as a constant from all the other defined volumes. When a standard was used, the user assigned quantities to the volumes corresponding to the standard dilutions and the software calculated a standard curve and interpolated the unknown volumes.

2.5 RT-QuIC

2.5.1 RT-QuIC substrate: purification of the recombinant Hamster PrP

An individual batch of Full-length Syrian Golden Hamster recombinant prion protein (FLHa-PrP, residues 23-231) was purified and used for all the RT-QuIC experiments presented in this thesis. Purification was performed as previously described (Wilham et al. 2010). Syrian Golden Hamster *prnp* (accession K02234) expression and translation from transformed *E.coli* Rosetta cells (Invitrogen), was obtained with

Overnight Express Instant TB medium (Merck Novagen). Bacteria were collected and inclusion bodies (IB) isolated in pellets by means of Bug Buster Master Mix (Merck Novagen). IB Pellets were resuspended and bound to Ni-NTA Superflow resin beads (Qiagen) in denaturing buffer. Resin beads were packed in column and the denatured protein was refolded on column by running an isocratic gradient of refolding buffer. Refolded protein was eluted with elution buffer and dialysed against dialysis buffer. Concentration was adjusted to 0.69 mg/mL by means of Amicon Ultra-15 centrifugal Filter Units (Merck Millipore). One mL aliquots were prepared, flash frozen and stored at -80°C until use. Table 2.6 lists all the buffers and materials used for the recombinant protein expression and purification.

Overnight Express Instant TB medium	Merck Novagen (71491-4)
Bug Buster Master Mix	Merck Novagen (71456-4)
Ni-NTA Super flow resin beads	Qiagen (30430)
Denaturing buffer	100 mM $NaPO_4$, 10 mM Tris, 6M Gdn-HCl, pH 8
Refolding buffer	100 mM $NaPO_4$, 10 mM Tris, pH 8
Elution buffer	500 mM Imidazole HCl, 100 mM $NaPO_4$, 10 mM Tris pH 6
Dialysis buffer	10 mM $NaPO_4$ pH 5.8
Centrifugal filters	Amicon Ultra-15 Merck Millipore (UFC901008)

Table 2.6 List of buffers and materials used for the purification of the recombinant FLHa-rPrP.

Catalogue numbers are reported in parenthesis following the name of the brand.

2.5.2 Preparation of sCJD and vCJD brain samples as RT-QuIC seeds

As mentioned in paragraph 2.2.1, small pieces of frontal cortex were sampled from three cases of sCJD subtypes MM1, MV1, MM2c, VV2, two cases of sCJD subtype VV1 according to the Parchi nomenclature (Parchi et al. 1999) as well as three cases of vCJD and one non-CJD case (Table 2.1). To prepare the collected tissue samples as RT-QuIC seeds the samples were homogenised to 10% w/v (10%BH) in RT-QuIC homogenization buffer (Table 2.2) using a FastPrep-24® automated homogeniser (MPbio) and lysing matrix D.

2.5.2.1 Criteria for the normalization of RT-QuIC seed input from different 10%BH

As mentioned in Sections 2.4.1 and 2.4.2, the levels of PrP^{res} present in each sCJD and vCJD 10% BH was evaluated by WB allowing the input of seed from different brain samples to be normalized by PrP^{res} content. Unless otherwise indicated, all the RT-QuIC reactions were seeded with 2 µL of a dilution of 10% BH in PBS accounting for 50 fg/µL of PrP^{res}.

2.5.3 RT-QuIC reaction

RT-QuIC reaction buffer composition was as follows, PBS1X (*i.e.* 5 mM phosphate 154 mM NaCl), 170 mM sodium chloride, 1 mM EDTA, 10 µM ThT. All the RT-QuIC reaction buffer components were purchased as concentrated stock solutions from Sigma-Aldrich and diluted in cell culture grade water (Corning). ThT was purchased as powder from the same provider and ThT solution prepared monthly as 10 mM solution. ThT powder was weighed and dissolved in cell culture grade water, the solution was then syringe filtered through a 0.22 µm filter (Merck Millipore) and kept at +4 °C sheltered from direct light. Recombinant FLHa-rPrP substrate was thawed and filtered through a 100 kDa centrifuge filter (Nanosep, Pall). Following filtering, the

concentration of the substrate was calculated from measuring the absorbance at 280 nm at a 1:2 dilution in 0.1% sodium dodecyl sulphate in PBS (0.1%SDS/PBS) using a NanoDrop One^{C} (Thermo-Fisher Scientific), blanking with 0.05%SDS/PBS. The FLHa-rPrP was then incorporated into the reaction buffer at 0.1 µg/µL, generating a bulk reaction mixture. Bulk reaction mixture was aliquoted in individual reaction wells. The final reaction volume was 100 µL per well including seed. RT-QuIC reaction was performed in a sealed 96-well plate with clear bottom (Thermo-Fisher Scientific) incubated at 42 °C for at least 48 h in FLUOstar Optima or Omega (BMG Labtech) plate reader. Table 2.7 lists buffer and materials used in RT-QuIC. During the incubation, the plate reader performed cycles of intermittent shaking (60 seconds shake, 60 seconds rest) and took fluorescence bottom readings every 15 min (450 nm excitation, 480 nm emission, gain 2000). Standard shaking frequency between FLUOstar Optima and Omega was different to compensate for different shaking mechanism geometry (Table 2.8).

H_2O	Corning Cell Culture grade water (25-055-CI)
PBS 10X	Sigma-Aldrich (P5493)
NaCl 5M	Sigma-Aldrich (S6546)
EDTA 0.5 M	Sigma-Aldrich (03690)
Thioflavin T	Sigma-Aldrich (T3516-5G)
Filters	Nanosep 100 kDa Omega P/N (OD100C33) Merck Millipore Express MILLEXGP filter unit 0.22 µm
96-well plates	Thermo-Fisher Scientific NUNC (265301)
Plate sealing tape	Thermo-Fisher Scientific Sealing Tape (235307)
Plate readers	BMG Labtech FluoSTAR Optima or Omega

Table 2.7 List of buffer and materials used for RT-QuIC

Catalogue numbers are reported in parenthesis following the name of the brand.

	FluoSTAR Optima	**FluoSTAR Omega**
Temperature	42 °C	42 °C
Cycle structure (shaking/rest)	60 s/60 s	60 s/60 s
Fluorescence measuring	Every 15 minutes	Every 15 minutes
Double orbital shaking frequency	700	900

Table 2.8 Settings of plate readers used for RT-QuIC

2.5.4 RT-QuIC data analysis: fluorescence Threshold for True Positive signal and criteria for positivity of a sample

RT-QuIC datasets were processed in three stages. The first stage was the labelling of raw data set using the built-in function of the plate reader data analysis software MARS (version 3.20 R2, BMG Labtech). Labelled raw data sets were exported to Microsoft Excel for the second stage. Using Microsoft Excel, mean average and standard deviation were calculated on the first fluorescence reading on all the used reaction well. The sum of the mean average of all the first fluorescence reading plus five standard deviation defined the fluorescence Threshold (Thr) value. As the plate reader reads fluorescence emission every 15 minute, it often happens that a first fluorescence reading equal or above Thr is followed by two consecutive readings just below Thr followed by a fourth reading reaching fluorescence values above the very first one. In this thesis, to account for the stochastic fluctuations of the RT-QuIC fluorescence signal, only when three consecutive fluorescence readings on an individual reaction well were equal or above Thr, the signal was deemed a True Positive (TP) signal and the time of the third reading was deemed time to threshold (t_{Thr}). When for one sample more than 50% of the technical replicates resulted in TP signals the sample was deemed positive.

2.5.4.1 Lag-time as a measure of the seeding activity of a seed in RT-QuIC

For positive samples (*i.e.* 50% of the technical replicates resulting in TP signals) the mean average of the t_{Thr} on all the technical replicates (including those that did not result in TP signals) was calculated and termed lag-time (t_{Lag}). The latter value was used to evaluate the seeding activity of an individual seed in RT-QuIC and to compare different seeds for their seeding activity.

2.6 PMCA

A complete description of the PMCA method and the materials used to perform it, can be found in chapter 3 where all the PMCA experimental results are presented.

2.7 Statistical analysis

All the statistical analysis presented were performed in Microsoft Office 365 Excel or GraphPad Prism 8.

Chapter 3 - Comparison of PMCA and RT-QuIC reaction kinetics

Hypothesis: The PMCA and RT-QuIC reaction kinetics differ when seeded with the same seed.

3.1 Introduction

In order to investigate the hypothesis that PMCA and RT-QuIC reaction kinetics differ when seeded with the same seed, a set of aims were established to evaluate and compare PMCA and RT-QuIC as follow:

1 To evaluate the *in vitro* seeding activity of sCJD samples by PMCA and RT-QuIC.
2 To evaluate the *in vitro* seeding activity of vCJD samples by PMCA and RT-QuIC.
3 To evaluate the effect of differences in sample preparations between PMCA and RT-QuIC (*e.g.* different homogenization buffers).
4 To design and implement a specific protocol for the observation of PMCA reaction kinetics.

The results Section in this Chapter firstly addresses points 1 and 2 of the above list showing that, when using defined PMCA and RT-QuIC standard reaction conditions, at least one sCJD subtype presents a robust seeding activity (see Section 2.2.4) when assayed in both PMCA and RT-QuIC. Therefore, this subtype can be used as a benchmark seed for comparing the two techniques. Secondly, to address point 3, and further validate the selected benchmark seed, the use of samples prepared following PMCA sample preparation protocol as RT-QuIC seeds is established. Lastly, the results of a kinetic observation of the PMCA reaction are presented and compared to the RT-QuIC reaction kinetics using the same sCJD seed.

3.2 Material and methods

The following paragraphs contain information specific to the experiments presented in this Chapter. When needed and to avoid redundancies, the appropriate paragraphs of the General Materials and Method Chapter are referred.

3.2.1 Biological samples

The human brain samples listed in Table 2.1 (Section 2.2.1), homogenized to 10% w/v as described in Section 2.2.1.2, were used for all the experiments presented in this Chapter.

3.2.1.2 Evaluation of PrP^{res} content in PMCA and RT-QuIC seeds

The levels of PrP^{res} present in each sCJD and vCJD 10% BH used to seed RT-QuIC or PMCA were evaluated by WB with mAb 3F4 as described in Sections 2.4.1 and 2.4.2 (see Appendix III for raw data)

3.2.2 RT-QuIC reaction: standard conditions

The general RT-QuIC protocol is described in Section 2.5. All the RT-QuIC experiments presented in this Chapter were performed in the FluoSTAR Optima plate reader (BMG Labtech, see Table 2.8 for the conditions used). Unless otherwise specified, the input of different CJD seeds was normalized to 100 fg of PrP^{res} by diluting the 10%BH in PBS prior to RT-QuIC. The input of the non-CJD seed was normalized by diluting the sample in PBS prior to RT-QuIC to the mean average dilution factor used to dilute all the other CJD seeds. The volume of seed used was always 2 µL irrespective of it being a dilution of sCJD, vCJD, non-CJD 10%BH or PBS.

3.2.3 PMCA reaction

3.2.3.1 Buffers and materials required for PMCA

All buffers and materials required to perform the PMCA reaction are listed in Table 3.1.

3.2.3.2 PMCA substrate preparation: humanized mice 10% brain homogenate

As mentioned in Section 2.2, transgenic mouse brains, used as PMCA substrate, were kindly provided by Dr Abigail Diack, Roslin Institute, University of Edinburgh, UK. The three lines of humanized transgenic mice expressing a single copy of the human *PRNP* gene that were used in this thesis, differed only for the *PRNP* codon 129 genotypes (MM, MV or VV). The limited availability of this material affected the number of PMCA technical and biological replicates performed.

Whole mouse brains stored at -80 °C were washed from frozen in Dulbecco modified PBS (DPBS w/o $CaCl_2$ and $MgCl_2$) to remove traces of blood. Working on ice under MSC II, washed mice brains were homogenized to 10% w/v in pre-chilled PMCA buffer supplemented with Complete® protease inhibitor cocktail (Roche) before use (see Table 3.1 for buffer composition). Homogenization was achieved by means of tissue grinder (Kimble Chase). The homogenate was transferred to a fresh 15 mL tube and centrifuged at 2000 rpm for 40 seconds in a refrigerated centrifuge (4 °C). After centrifugation, supernatant was retained as PMCA substrate and stored at -80 °C in 0.6 mL aliquots until use.

3.2.3.3 PMCA seed preparation: human sCJD and vCJD 10% brain homogenates

The PMCA seeds used were human sCJD and vCJD 10% BHs (Table 2.1) in PMCA Buffer (Table 3.1). PMCA buffer was supplemented with Complete® protease inhibitor cocktail (Roche) prior to use. Tissue samples homogenization was achieved with

plastic mini-pestles (Eppendorf) and thorough vortexing. Homogenates were clarified at 2000 rpm for 40 seconds in a refrigerated centrifuge (4 °C), supernatant retained as PMCA seed and stored at -80 °C until use.

	Composition	Supplier
PMCA Homogenization buffer	1% Triton-X 100	Sigma-Aldrich (t9-284) 500 mL
	150 mM NaCl	Powder VWR Chemicals (27810 295)
	1XDPBS	Dulbecco modified 1XPBS w/o $CaCl_2$ and $MgCl_2$ Sigma-Aldrich (D8537) 500 mL
Seed	See Section 3.2.3.2	Human sCJD and vCJD 10%BH
Substrate	See Section 3.2.3.3	10%BH of transgenic mice expressing human *PRNP*
PMCA reaction buffer	PMCA homogenization buffer added with protease inhibitor	Complete® Protease Inhibitor Cocktail w/o EDTA Roche (000000011697498001)
	5 mM EDTA	Sigma-Aldrich (03690 100)
	1 µg/mL low molecular weight heparin	Sigma-Aldrich (H3149)
Reaction tubes		Thermo-Scientific (AB-0337) 0.2 mL thin-walled
Tube caps		Thermo-Scientific (AB-0851) flat
Sonicator		Qsonica Q700
		Equipped with titanium horn

Table 3.1 List of buffers and materials needed to perform PMCA reaction

Catalogue numbers are reported in parenthesis following the name of the brand.

.

3.2.3.5 Standard PMCA reaction: general experimental design

The standard PMCA reaction was a 0.2 mL PCR tube based reaction consisting of a dilution of PMCA seed directly into PMCA substrate (hereafter referred to as PMCA dilution) with a minimum of one further serial dilution into substrate. Seed and substrate were always matched for having the same genotype at codon 129 of *PRNP* (Ritchie et al. 2017; Barria 2014). A minimum of two technical replicates per sample were run in an individual PMCA reaction. The final reaction volume was always 101 µL. Unless otherwise indicated, all the PMCA reactions were run for 48 hours divided in 30 minute long cycles. PMCA cycles consisted of a 20 seconds long sonication pulse in the ultrasound frequency range followed by incubation at constant temperature for 29 minutes and 40 seconds. Table 3.2 lists the equipment and the settings used for all the PMCA reactions presented in this Chapter. The detection method for the PMCA reaction products consisted of a standardized WB analysis with mAb 3F4 following PK digestion.

3.2.3.5.1 Definition of "Frozen" and "Sonicated" samples and PMCA signal

For each initial PMCA dilution and serial dilution thereof, volumes were calculated to obtain a final volume of 120 µL in each tube. At this stage, before starting the cycles of sonication/incubation of the PMCA reaction, 19 µL were sampled from each reaction tube obtaining the final reaction volume of 101 µL. The 19 µL of PMCA dilution were moved to fresh 0.5 mL tubes and stored at -80°C. These 19 µL, that did not enter the sonication/incubation cycles of the PMCA reaction, are termed "Frozen" samples as opposite to the PMCA treated samples termed "Sonicated". The PMCA signal resulted from the ratio of the PrP^{res} densitometric signal as detected by standardized WB analysis with mAb 3F4 following PK treatment in each Sonicated sample over the respective Frozen sample.

Sonicator	Qsonica Q-700 equipped with titanium microplate horn
Temperature	37 °C
Amplitude	Set at 37% generating ≈290 W per sonication
Cycle structure	20 s/1180 s (pulse-ON/pulse-OFF)
Reaction time	48 h

Table 3.2 PMCA sonicator settings for standard PMCA reaction condition.

3.2.3.5.2 Criteria for the normalization of the PMCA seed input using different seeds

Different PMCA seeds were diluted at different dilution factors in the initial PMCA dilution. Because vCJD 10% BH consistently shows seeding activity in PMCA (Barria 2014; Moda et al. 2014; Concha-Marambio et al. 2016; Cali et al. 2019) for all the PMCA reactions seeded with vCJD seeds the initial PMCA dilution factor was always $1x10^{-2}$. Also, based on the NCJDRSU expertise in performing PMCA (Barria 2014), $1x10^{-2}$ was as well the initial PMCA dilution factor for reactions seeded with sCJD subtype VV2. Therefore, the PMCA reactions seeded with vCJD or sCJD subtype VV2 were normalized for the input of 10% BH irrespective to the levels of PrP^{res}.

For all the other sCJD seeds, the initial PMCA dilution factor was selected based on the levels of PrP^{res} found in each 10% BH. These PMCA seeds dilutions were calculated to achieve a seed-dilution at which PrP^{res} was faintly detectable before amplification (*i.e.* in the Frozen samples) in order to clearly see the increased signal after PMCA.

3.2.3.6 PMCA reaction preparation 1: substrate manipulation

PMCA reactions were assembled working on ice, in 0.2 mL PCR tubes (Thermo Scientific) with a minimum of two technical replicates per sample. PMCA substrate aliquots were flash-thawed in distilled H_2O. Working on ice, under MSC I, 12 µL from each 0.6 mL aliquot of PMCA substrate were discarded and substituted with 6 µL of EDTA 0.5 M (5 mM final concentration) and 6 µL of 100 µg/mL low molecular weight heparin (1 µg/mL final concentration). The mixture obtained was carefully mixed by inversion and pipetting. When more than one PMCA substrate aliquot of a certain codon 129 genotype was required to prepare a PMCA reaction, individual aliquots were pooled together following addition of EDTA and heparin. The required volume of PMCA substrate was then aliquoted in each 0.2 mL PMCA reaction tube.

3.2.3.7 PMCA reaction preparation 2: dilution of seed into substrate and generation of Frozen samples

PMCA reaction tubes containing the required volume of PMCA substrate were moved under MSC II while kept on ice. The PMCA seeds were added to the respective substrate matching the codon 129 genotype and serial dilutions were performed. At the end a volume consisting of PMCA reaction mixture was disposed as waste to obtain the final 120 µL of PMCA reaction mixture in the last tube. At this stage, 19 µL were moved from each PMCA reaction to fresh 0.5 mL tubes to be stored at -80 °C as Frozen samples.

3.2.3.8 PMCA reaction: standard sonication conditions

The PMCA reaction tubes, now containing 101 µL of PMCA reaction mixture, were placed in a tube rack on top of the sonicator's microplate horn. To favour an even distribution of soundwaves, 300 mL of water, pre-heated at 37°C, were poured in the sonicator's horn. Such volume ensured that reaction tubes were submerged for half of their length. As the sonicator is kept inside an incubator, temperature is under control and set at 37 °C throughout the reaction time. PMCA reaction consisted of cycles of 20 seconds long sonication every 29 minutes and 40 seconds for a total of 48 hours. Sonicator settings for standard PMCA reaction are listed in Table 3.2.

3.2.3.9 PK digestion and WB analysis for PMCA signal detection

At the end of the PMCA reaction time (*i.e.* 48 hours, unless otherwise indicated), PMCA tubes were moved out of the sonicator and spun for 1 minute at 2000 rpm. Working under MSC I, 19 µL of the PMCA reaction were moved to a fresh 0.5 mL tubes as Sonicated samples. The Sonicated and the respective Frozen samples were always processed in parallel. Each Sonicated and Frozen sample was added with 1 µL of 1 mg/mL PK yielding a final digestion volume of 20 µL and a final concentration

of 50 µg/mL PK. Samples were then incubated for 1 hour at 37 °C. Digestion was stopped by adding 10 µL of LDS4X. Samples were immediately incubated at 100 °C for 10 minutes and analysed by SDS-PAGE and WB using mAb 3F4 as described in Sections 2.3 and 2.4. All the samples from an individual PMCA reaction were always blotted on an individual PVDF membrane.

3.2.3.10 Densitometric analysis of the WB for PMCA signal detection

The densitometric values of the PrP^{res} signals detected for each pair of Frozen and Sonicated samples by WB analysis with mAb 3F4, were taken with the ChemiDoc XRS+ ImageLab 4.1 software (BioRad) as described in Section 2.4.2. The data were exported to Microsoft Excel and the ratio of the densitometric values of each Sonicated over the respective Frozen sample for each individual pair (*i.e.* S/F ratio) was calculated.

3.2.3.10.1 The PMCA signal: the fold increase of PrP^{res} after PMCA

The S/F ratio is a measure of the increase of PrP^{res} after PMCA. Therefore, the mean average of the S/F ratio calculated on each technical replicate of an individual sample run in an individual PMCA were used to estimate the fold increase of PrP^{res} after PMCA and hence to score the seeding activity of different seeds in PMCA.

3.2.4 PMCA for the observation of PMCA reaction kinetics

The experiments to observe the PMCA reaction kinetics were performed as follows; for each sample tested, aliquots of PMCA substrate were thawed, supplemented with EDTA as well as low molecular weight heparin and pooled together as described in Section 3.2.3.6. From the PMCA substrate preparation, 118.8 µL were aliquoted into 0.2 mL PCR reaction tubes and individual reactions were seeded with 1.2 µL of the PMCA seed to be assayed. At this stage, each PMCA reaction tube contained 120 µL of PMCA dilution with a seed concentration of $1x10^{-2}$. From each reaction tube, 19 µL

where moved to fresh 0.5 mL tubes and stored at -80°C as Frozen samples. The PMCA reaction tubes, now containing 101 µL of seeded PMCA reaction, were placed in a tube rack on top of the sonicator's microplate horn. Standard PMCA reaction conditions, as the one described in Section 3.2.3.8, were used except for the reaction time that was extended to 54 hours. The PMCA reactions were sampled at time interval of t = 1, 6.5, 24, 30.5, 48 and 54.5 hours by moving three reaction tubes from the sonicator to -80°C. Selection of the time intervals was based on the NCJDRSU Laboratory Code of Practice that limit access to the containment level 3 laboratory to 8 hours a day. Three technical replicates per each time point were considered. At the end of the 54.5 h reaction time, all the reaction tubes were thawed, spun for 1 minute at 2000 rpm and 19 µL moved to fresh 0.5 mL tubes as Sonicated samples. The Frozen and the respective Sonicated samples where then treated in parallel with PK and analysed as described in Section 3.2.3.9 and 3.2.3.10.

3.3 Results

For sake of clarity, the PMCA results are summarized in graphs reporting the average means calculated on all the technical and biological replicates tested. The complete PMCA raw data set can be found in Appendix II.

3.3.1 Evaluation of sCJD and vCJD seeding activity in PMCA

To evaluate the seeding activity of sCJD and vCJD samples in PMCA, three vCJD cases as well as three cases of sCJD subtypes MM1, MV1, MM2c, MV2, VV2 and two cases of sCJD subtype VV1 (Table 2.1) were homogenized to 10% w/v in PMCA homogenization buffer and assayed in three independent PMCA experiments. In each PMCA experiment, a set of samples including one case of each type (*i.e.* vCJD and individual sCJD subtypes) was assayed. All the seeds were assayed in PMCA using substrates matching for the respective codon 129 status. Figure 3.1 shows the results obtained, summarized by seed (*i.e.* vCJD and individual sCJD subtypes).

On (mean) average, the vCJD samples assayed showed a 60-fold increase of PrP^{res} signal when diluted at $1x10^{-2}$ and a 27-fold increase when diluted at $1x10^{-3}$ (Figure 3.1 A). The sCJD subtype VV2 samples, showed a 32-fold increase of PrP^{res} signal when diluted at $1x10^{-2}$ and an 11-fold increase when diluted at $1x10^{-3}$ (Figure 3.1 B).

Overall, the sCJD subtypes MM1, MV1, MM2c, VV1 and MV2 showed a very weak seeding activity in PMCA (Figure 3.1C). Across these sCJD samples, the sCJD subtype MV2 showed the highest seeding potency with an 11-fold increase of the PrP^{res} signal following PMCA at the lower dilution used (Figure 3.1C).

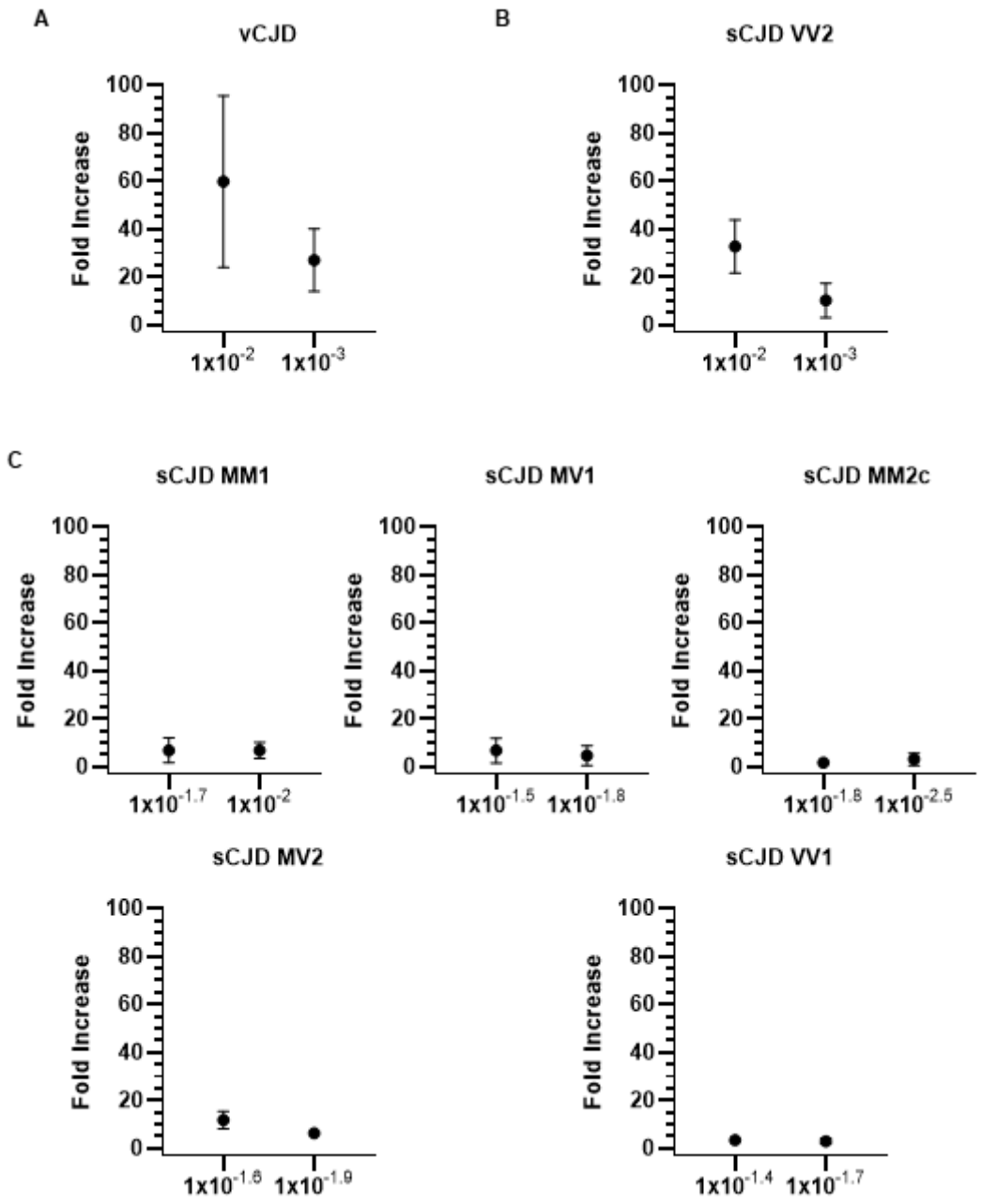

Figure 3.1 Evaluation of vCJD and sCJD subtypes seeding activity in PMCA

Each data point represents the mean average fold increase in PrP^{res} signal and standard deviation calculated across two technical replicates run for each of the three 10%BHassayed for each sample type. Each 10%BH was assayed once. Fold Increase values are the ratio of the densitometric signal detected by WB with mAb 3F4 in the Sonicated samples over the respective Frozen samples (S/F ratio). The identification of the type of sample is shown on top of each graph. The mean average dilution factor used to seed the PMCA reaction with different seed of the same type is shown at the bottom of each graph. The raw data and WB pictures can be found in Appendix II.

3.3.2 Evaluation of sCJD and vCJD seeding activity in RT-QuIC

To evaluate the seeding activity of sCJD and vCJD samples in RT-QuIC, small pieces of tissue were sampled from the same frozen brains used for the PMCA experiments presented in Section 3.3.1. The samples comprised three cases of vCJD as well as three cases of sCJD subtypes MM1, MV1, MM2c, MV2, VV2 and two examples of sCJD subtype VV1 (Table 2.1). The tissue samples were homogenized to 10% in RT-QuIC homogenization buffer as described in Section 2.5.2 and the levels of PrP^{res} content was evaluated by WB analysis as described in Section 2.4.1. The seed input in RT-QuIC of different sCJD and vCJD samples was normalized to 100 fg of PrP^{res} (see Section 2.5.2.1). An individual batch of FLHa-rPrP was purified and used as substrate (see Section 2.5.1). The samples were assayed in three independent RT-QuIC experiments with the same layout, comprising one case of each seed type (*i.e.* one vCJD sample and one sCJD sample per each of the six subtypes) a negative control (*i.e.* a non-CJD 10%BH) and a control for the spontaneous aggregation of the substrate without any seed (*i.e.* PBS). The spontaneous aggregation of the substrate was never observed, and no signal was observed from reactions seeded with the negative control. All the sCJD samples assayed consistently showed true positive signals (see Section 2.5.4) in at least 50% of the technical replicates tested in an individual RT-QuIC experiment. This result allowed for the further calculation of the lag time (t_{Lag}) per each sample. No signal was observed for reactions seeded with vCJD samples. Figure 3.2 summarizes the results obtained per each type of seed across the three experiments. The statistical analysis of the t_{Lag} values grouped by sCJD subtype was performed using the unpaired T test (two-tailed) and revealed no statistically significant differences.

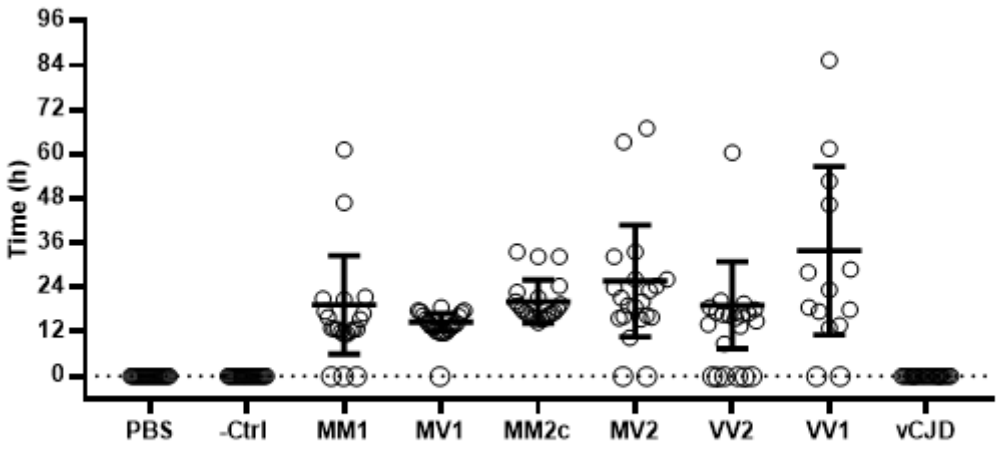

Figure 3.2 Evaluation of vCJD and sCJD subtypes seeding activity in RT-QuIC

The graph shows the RT-QuIC results obtained from three independent experiments. In each experiment, one example of each sample type (*i.e.* vCJD and sCJD subtypes) was tested in seven technical replicates. Two biological replicates of sCJD subtype VV1 were analysed in RT-QuIC due to unavailability of tissue at time of study. Seed input from different samples was normalized to 100 fg of PrP^{res}. Each data point represents the time to threshold (t_{Thr}) of individual reaction wells. Horizontal bars indicate the mean average (*i.e.* t_{Lag}) and standard deviation calculated across all the data points that crossed threshold. No signal was observed in vCJD, PBS (unseeded reaction wells) and -Ctrl (reaction wells seeded with a dilution of non-CJD 10% BH) seeded wells. These data points are shown for comparison.

3.3.3 Evaluation of sCJD and vCJD seeds in PMCA and RT-QuIC reaction: comparative analysis

Grouping together the results obtained for the three vCJD seeds assayed in the PMCA reactions showed that the average increase of PrP^{res} was 60-fold at dilution $1x10^{-2}$ and 27-fold at dilution $1x10^{-3}$ (Figure 3.1 A). Notwithstanding the large standard deviation on the means observed for these values, which can be ascribed to the minimal sample size (N = 3), vCJD seeds appeared to have the highest seeding activity among all the seeds evaluated by PMCA. When assayed in RT-QuIC, however, the vCJD samples prepared from the same brain material as the one tested in PMCA, showed no seeding activity at all. This is in line with previous observation regarding the seeding activity of vCJD samples assayed in RT-QuIC using the FLHa-rPrP (Peden *et al.*, 2012; Orrú *et al.*, 2015). In the same work Peden *et al.* also showed that vCJD samples in RT-QuIC showed limited or null seeding activity even when using other recombinant substrates such as human rPrP (FLHu-rPrP) and truncated form of hamster rPrP (90-231Ha-rPrP) (Peden et al. 2012).

The sCJD seeds showed seeding activity in both PMCA and RT-QuIC. However, different results were obtained with these seeds in the two CFC systems. Indeed, while in RT-QuIC all the sCJD samples tested presented seeding activity with no apparent subtype-specific difference (Figure 3.2), this was not observed for PMCA. The sCJD subtype VV2 showed the highest seeding activity in PMCA when compared to the other sCJD samples tested. On average, PMCA reactions seeded with $1x10^{-2}$ and $1x10^{-3}$ dilutions of sCJD subtype VV2 resulted in a 32-fold and 10-fold increase of PrP^{res} signal respectively (Figure 3.1 B). In RT-QuIC no statistically significant difference was observed when comparing the t_{Lag} values grouped by sCJD subtype.

These data suggest that the *in vitro* seeding activity of a CJD sample is affected by the conditions used to observe it (*e.g.* PMCA or RT-QuIC reaction conditions). The

same data also indicate that the sCJD subtype VV2 showed a robust seeding activity in both PMCA and RT-QuIC. For this reason, sCJD subtype VV2 was selected as the benchmark to further compare PMCA and RT-QuIC reaction kinetics.

3.3.4 Evaluation of the impact of PMCA homogenization buffer on the seeding activity of sCJD subtype VV2 in RT-QuIC

To validate further the use of sCJD subtype VV2 as benchmark seed for the comparison of PMCA and RT-QuIC reaction kinetics, the effect of the different homogenization buffer on sCJD subtype VV2 seeding activity was evaluated in RT-QuIC. In this test, the RT-QuIC reaction time was limited to 48 h to equal the PMCA reaction time. Brain samples used to seed PMCA and RT-QuIC were homogenized to 10% w/v using two protocols for the preparation of the seed material (see Table 2.2). The same sCJD subtype VV2 brain tissue was homogenized to 10% in PMCA (*i.e.* VV2BH1P) or RT-QuIC (*i.e.* VV2BH1R) homogenization buffer and then used to seed RT-QuIC. Seed input was normalized to 100 fg of PrP^{res}. The results obtained are shown in Figure 3.3. Both the seeds generated true positive (TP) signals in more than 50% of the technical replicates. The comparison of the t_{Lag} showed no statistical difference (unpaired t test) between the sample prepared in PMCA homogenization buffer and the one prepared in RT-QuIC homogenization buffer. Hence, sCJD subtype VV2 10% BH samples prepared in PMCA homogenization buffer were further used to compare PMCA and RT-QuIC reaction kinetics.

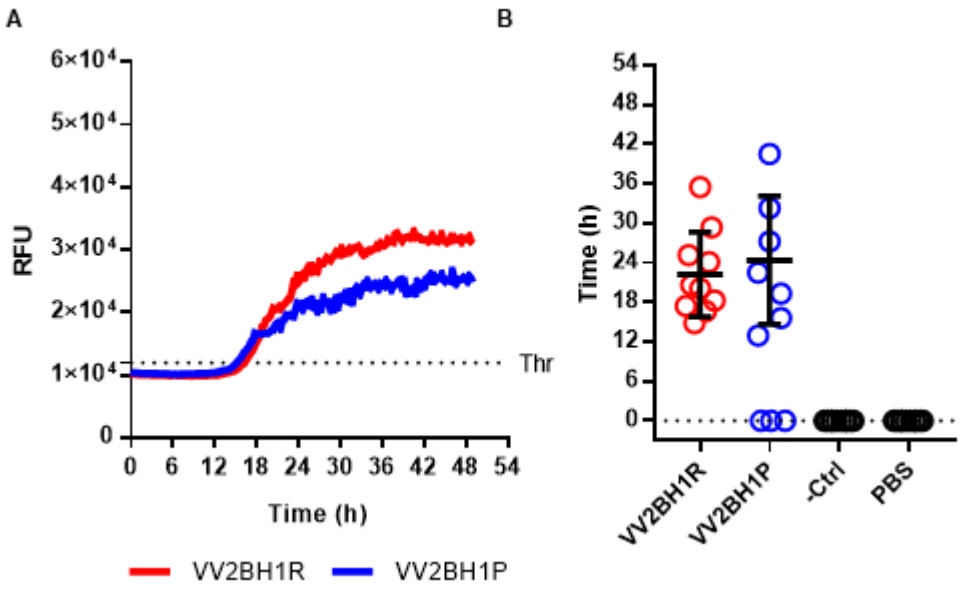

Figure 3.3 Evaluation of the impact of PMCA homogenization buffer on the sCJD subtype VV2 seeding activity in RT-QuIC

Figure A: RT-QuIC results showing the mean average increase in fluorescence emission in Relative Fluorescence Unit (RFU) against time calculated across all the technical replicates (N = 10) run per sample. The dotted line represent the fluorescence threshold for positivity (Thr). Figure B: analysis of the results shown in A. The data points represent the t_{Thr} of the individual technical replicates that crossed Thr. Horizontal bars indicate t_{Lag} (*i.e.* mean average) and standard deviation calculated across all the data points that crossed Thr. PBS: unseeded reaction wells. -Ctrl: reaction wells seeded with a dilution of non-CJD 10% BH.

3.3.5 Comparison of standard PMCA and standard RT-QuIC reactions kinetics seeded with sCJD subtype VV2

To compare PMCA and RT-QuIC reaction kinetics, brain tissue from three examples of sCJD subtype VV2 cases were homogenized to 10% w/v in PMCA homogenization buffer and used to seed both PMCA and RT-QuIC reactions. The seed input from different samples, was normalized by the dilution factor used to dilute the 10% BH in either PMCA substrate or PBS prior to RT-QuIC. The limited availability of PMCA substrate, allowed investigating the standard PMCA reaction kinetics in a restricted number of conditions regarding the dilution of seed into substrate.. Based on the analysis of the PMCA results when seeded with sCJD subtype VV2, the $1x10^{-2}$ dilution was selected. Indeed, higher dilutions appeared to seed the reaction less consistently (Figure 3.1 B and Figure II.2 in Appendix II). Nonetheless, in contrast with previous results, sample VV2BH2P did not show any seeding activity when tested in the PMCA kinetics assay at a $1x10^{-2}$ dilution (see Appendix II). Therefore, it was excluded from further analysis.

The PMCA kinetics assay consisted of sampling the PMCA at fixed time intervals of t = 1, 6.5, 24, 30.5, 48 and 54.5 hours (hereafter referred to as t_1, $t_{6.5}$, t_{24}, $t_{30.5}$, t_{48}, $t_{54.5}$ respectively). Figure 3.4 A, shows the mean average fold increase in PrP^{res} signal calculated across each time point. No substantial increase in PrP^{res} signal was detected at t_1 and $t_{6.5}$. At t_{24} a mean average 20-fold increase in PrP^{res} signal was observed that further increased to a 38-fold increase at $t_{30.6}$. At t_{48}, a 47-fold increase was observed followed by a 43-fold increase at $t_{54.5}$. The statistical analysis of the data (unpaired t test) showed that the differences between the fold increase values observed at $t_{30.6}$, t_{48} and $t_{54.5}$ was not statistically significant (Figure 3.4 A).

When diluting the sCJD subtype VV2 seeds to $1x10^{-2}$, none of the three sCJD subtype VV2 samples tested showed true positive (TP) signals in RT-QuIC. By further diluting

the seeds to $1x10^{-3}$, over the three samples tested, TP signals were observed in less than 50% of the technical replicates. When higher dilutions (*i.e.* $1x10^{-4}$, 10^{-5} and 10^{-6}) were used, on mean average, 98% of the technical replicates showed TP signals. The t_{Lag} appeared to increase with the increase of the dilution factor with $1x10^{-4}$ showing a t_{Lag} of 7.14 h, dilution $1x10^{-5}$ showing a t_{Lag} of 10.06 hours and dilution $1x10^{-6}$ showing a t_{Lag} was 14.55 hours (Figure 3.4 C).

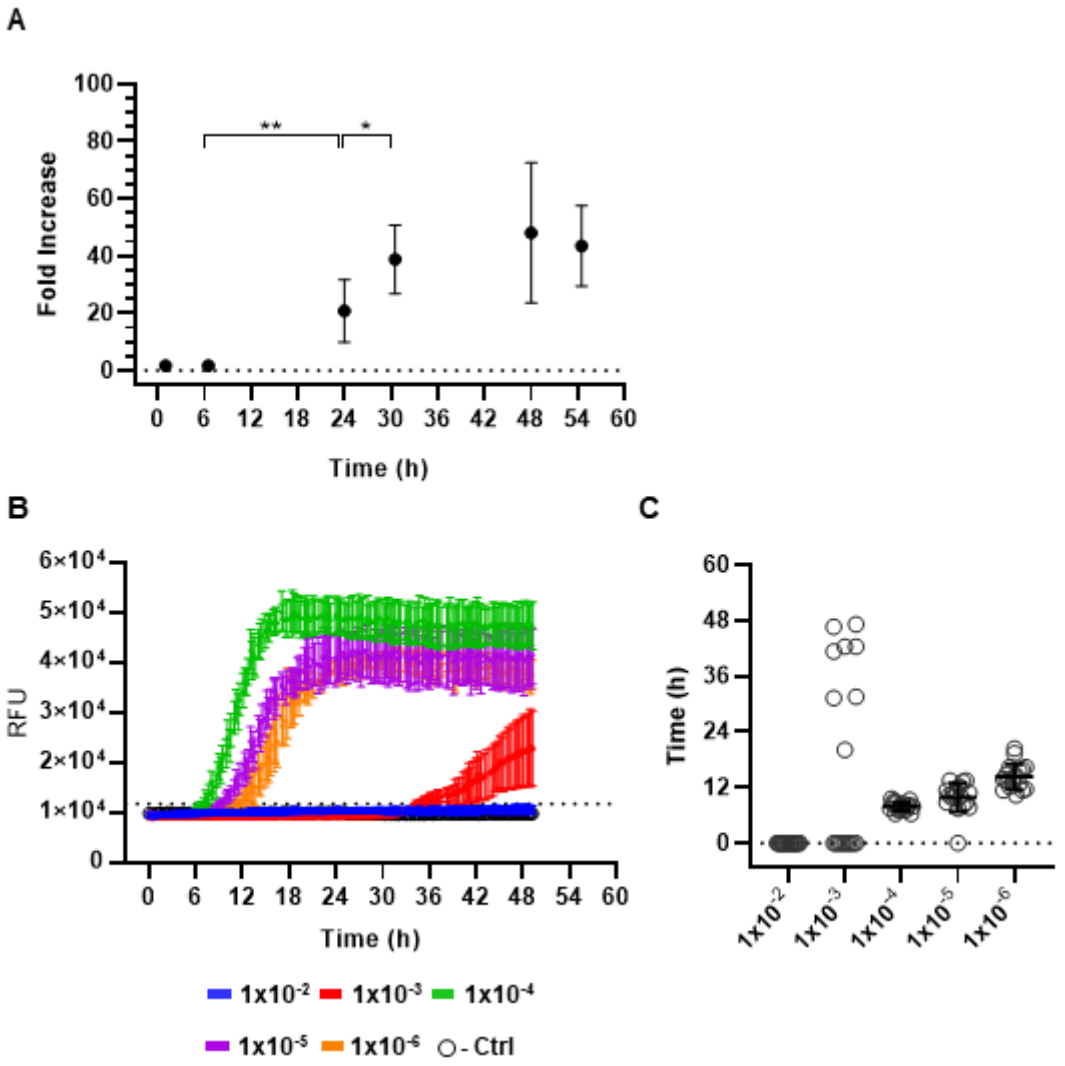

Figure 3.4 Comparison of PMCA and RT-QuIC reaction kinetics

Figure A; PMCA reaction kinetics when seeded with sCJD VV2 diluted $1x10^{-2}$. Each data point represents the mean average fold increase with standard deviation calculated across all the samples tested. Two technical replicates were tested per each of the three sCJD subtype VV2 10%BH. * = p value 0.03; ** = p value 0.003. Figure B; RT-QuIC results showing the mean average increase in fluorescence emission in Relative Fluorescence Unit (RFU) against time calculated across all the technical replicates run per sample. The dotted line represent the fluorescence threshold for positivity (Thr) Figure C; analysis of the results shown in B. The data points represent the t_{Thr} of the individual technical replicates. Six technical replicates were tested per each of the three sCJD subtype VV2 10%BH. Horizontal bars indicate t_{Lag} (*i.e.* mean average) and standard deviation calculated across all the data points.

3.4 Discussion

As mentioned in the introduction to this Chapter (see Section 3.1), the investigation of the hypothesis that PMCA and RT-QuIC reaction kinetics differ when seeded with the same seed was articulated in four aims;

1 To evaluate the *in vitro* seeding activity of sCJD samples by PMCA and RT-QuIC.
2 To evaluate the *in vitro* seeding activity of vCJD samples by PMCA and RT-QuIC.
3 To evaluate the effect of differences in sample preparations between PMCA and RT-QuIC (*e.g.* different homogenization buffers).
4 To design and implement a specific protocol for the observation of PMCA reaction kinetics.

For the sake of clarity, the discussion of the results has been divided in subsections.

3.4.1 Seeding activity of vCJD and sCJD in PMCA

The results obtained regarding aim 1 can be summarised as follows:

- When assayed in PMCA, the vCJD samples showed a more robust seeding activity compared to the seeding activity of sCJD samples. Among the sCJD samples, sCJD VV2 showed the highest seeding activity.

The characteristic observed for the seeding activity of vCJD and sCJD samples in PMCA, appears to be a generalized feature of the method, irrespective to the specific set-up used (*e.g.* different substrate, seed and sonication condition) (Cali et al. 2019; Moda et al. 2014; Concha-Marambio et al. 2016; Barria et al. 2018). No specific molecular mechanism has been agreed upon that explains this phenomenon. Only recently, Camacho and colleagues have produced evidence showing that the glycosylation of the PrP^C substrate, in combination with the codon 129 status, might

be a major factor shaping PMCA amplification abilities (Camacho et al. 2019). The observation regarding the seeding activity of sCJD subtype VV2 is also in line with previous data obtained at the NCJDRSU with the same PMCA set-up used in this thesis (Barria 2014) and by other researchers using a slightly different PMCA set-up (Camacho et al. 2019). The mechanistic explanation for this is not clear at this point in time. Interestingly, however, the inoculation of cases of sCJD subtype VV2 in the same transgenic mouse line used in this thesis to produce the PMCA substrate (*i.e.* expressing *PRNP* with codon 129 genotypes VV, see Section 3.3.3.2), produced clinical signs with the shorter incubation time when compared to the other five sCJD subtypes inoculated in the same host (*i.e. PRNP* with codon 129 genotypes VV) as well as in mice expressing *PRNP* with codon 129 genotypes MM or MV (Bishop, Will, and Manson 2010). In *in vivo* models, the length of the incubation time, is often related to the rate of PrP^{Sc} formation and accumulation following inoculation. Within this theoretical framework, a short incubation time *in vivo* suggests a fast rate of PrP^{Sc} formation. The robust seeding activity of sCJD subtype VV2 observed in PMCA, might then be determined by the same factors influencing the rapid rate of PrP^{Sc} formation observed *in vivo* when sCJD VV2 was inoculated into the transgenic mouse line used to produce the PMCA substrate.

3.4.2 Seeding activity of vCJD and sCJD in RT-QuIC

The results obtained regarding aim 2 can be summarised as follows:

- When assayed in RT-QuIC using the FLHa-rPrP substrate, the vCJD samples did not show any seeding activity while the sCJD samples showed a robust seeding activity irrespective of the sCJD subtype.

The characteristic observed for the seeding activity of vCJD and sCJD samples in RT-QuIC seems to be influenced by the specific set-up used (*e.g.* substrate, seed, shaking and incubation condition). For instance, in term of substrate selection, the

use of rPrP from bank vole (*i.e.* FLBV-rPrP), allowed the detection of the *in vitro* seeding activity of vCJD samples as well as sCJD samples (Orrù et al. 2015a; 2017). The natural propensity of the bank vole PrP sequence to misfold and aggregate (Kobayashi et al. 2019) may perhaps provide some insights regarding the ability of the derived rPrP to act as universal substrate in RT-QuIC (Orrù et al. 2015b). Adding to this, the misfolding propensity of the Bank vole prion protein appear to match with the *in vivo* transmission studies performed for this model (Watts et al. 2014; Pirisinu et al. 2013). Similarly, using second generation RT-QuIC (Orrù et al. 2015a), Foutz and colleagues (Foutz et al. 2017), reported the discrimination of sCJD subtypes on the basis of the shape of the RT-QuIC reaction kinetics seeded with human sCJD CSF samples.

Nonetheless, based on the experimental results obtained for this thesis, the selectivity for sCJD over vCJD appears to characterize the RT-QuIC set-up used. Notably, such selectivity appears to be in line with previous observations obtained with RT-QuIC reactions using FLHa-rPrP, 90-231Ha-rPrP and a SHa-rPrP as reaction substrates seeded with sCJD and vCJD samples (Peden et al. 2012; Orrù et al. 2015b; Peden et al. 2014). This evidence suggests that the use of the hamster PrP might be a major determinant of the selectivity for sCJD over vCJD. It might be premature, however, to propose a molecular description of this phenomenon as it has only been reported in RT-QuIC. Indeed, even though the hamster *in vivo* model has been extensively used to characterize scrapie, there is a scarcity of data regarding inoculation of hamster with sporadic or variant CJD. In one study (Thomzig et al. 2006), hamster inoculated with mouse-adapted BSE showed accumulation of PrP^{res} in brain and muscle. This evidence suggest that the hamster PrP^{C} could be susceptible to conversion *in vivo* to the PrP^{Sc} form by BSE prion. Such evidence, when combined with existing knowledge regarding the link between BSE and vCJD (see Section 1.5.1.2), allow to speculate

that the hamster recombinant PrP could be converted *in vitro* in a specific RT-QuIC set-up which has yet to be defined.

3.4.3 Comparative study of PMCA and RT-QuIC reaction kinetics

Based on the results obtained, sCJD subtype VV2 was selected as benchmark seed for the comparison of PMCA and RT-QuIC reaction kinetics as it showed seeding potency in both the methods. The selection of the sCJD subtype VV2 as benchmark seed was further validated by addressing the issue regarding the different sample preparation in PMCA and RT-QuIC (*i.e.* aim 3, see Section 3.4). Indeed, as described in the general materials and method Chapter (see Section 2.2.1.2 and Table 2.2), PMCA and RT-QuIC seeds were prepared in slightly different homogenization buffer (*i.e.* different detergent concentration and ionic strength) and tissue homogenization was achieved by two different methods (*i.e.* automated for RT-QuIC and manual for PMCA). To assess if these differences affected the seeding activity of sCJD subtype VV2, a direct comparison of the two preparative method was performed. Specifically, a sCJD subtype VV2 seed prepared for PMCA was assayed in RT-QuIC along with the same seed prepared for RT-QuIC. The results showed that no significant difference could be detected between the seeding activities of the two preparations with the experimental conditions used. This result allowed the use of samples prepared for PMCA as seeds for the RT-QuIC reaction.

To study the kinetics of the PMCA reaction in comparison with the RT-QuIC one (*i.e.* aim 4, see Section 3.4), a specific PMCA protocol was designed and implemented involving a selection of the dilution of sCJD subtype VV2 into substrate (*i.e.* $1x10^{-2}$) and the sampling of the PMCA reaction at selected time intervals. The seed dilution selected for the PMCA kinetics, however, showed no seeding activity in RT-QuIC. The RT-QuIC reaction appear to be inhibited when seeded with a $1x10^{-2}$ dilutions of seed and showed poor seeding activity at dilution $1x10^{-3}$. A similar inhibition effect

has been previously reported with this, as well as other RT-QuIC set-ups, so that it appears to be a general feature of the method (Wilham et al. 2010; Orrù et al. 2012). The inhibition of the RT-QuIC reaction with concentrated seeds marks a difference with PMCA for which such an effect has never been reported.

The results obtained for the PMCA reaction kinetics showed no increase of PrP^{res} signal (*i.e.* PMCA signal) at t_1 and $t_{6.5}$ while a significant increase was detected at t_{24} further increasing at $t_{30.5}$. There were not statistically significant differences in the values obtained after $t_{30.5}$, suggesting the conversion reaction had plateaued. Notably, the trend designed by the data, resembled a sigmoidal shape characterized by an initial lag-phase (t_1 and $t_{6.5}$) followed by a steep increase (t_{24} and $t_{30.5}$) reaching a plateau (t_{48} and $t_{54.5}$) which is typical of protein misfolding and aggregation (Cohen et al. 2013). The sigmoidal profile is in fact much more apparent in the shape of the RT-QuIC reaction which is a kinetic observation of the seeded misfolding and aggregation of the recombinant substrate.

The qualitative comparison of the two reactions kinetics, shows that the RT-QuIC reaction, even at the lowest seed dilution tested (*i.e.* $1x10^{-6}$), appear to be much quicker than PMCA. Specifically, the RT-QuIC kinetics when seeded with seed dilutions in between $1x10^{-4}$ to 10^{-6} reached the plateau phase well within the 24 hours. According to the data, PMCA kinetics was within the raising phase at t_{24} and $t_{30.5}$. Beyond this point, the RT-QuIC reaction reached a plateau phase where no significant variation in signal could be discriminated.

PMCA signal is given by the WB detection of PrP^{res}. The latter derives from the limited proteolysis of samples known to contain PrP^{Sc}. As mentioned in the introduction, PrP^{Sc} is thought to have a fibrillary amyloid-like structure (see Section 1.2). Hence, the PMCA kinetics follows the formation PrP^{Sc} fibrillary conformation(s) that when, subjected to limited proteolysis, yield PrP^{res}. RT-QuIC signal consists of readings of

fluorescence at a specific wavelength emitted by the dye Thioflavin T (ThT) when it binds to amyloid and amyloid-like structures (Wilham et al. 2010). The structure(s) assumed by the rPrP during the RT-QuIC, under conditions similar to the one used here, resemble naturally occurring PrP^{Sc} as they assume resistance to limited proteolysis, however their limited proteolysis yield a product with different structural and biochemical characteristics to PrP^{res}(Atarashi, Satoh, *et al.*, 2011b; McGuire *et al.*, 2012; Piconi *et al.*, 2019). It is conceivable that the difference in timing between PMCA and RT-QuIC reaction kinetics when seeded with the same seed, might results from a combinatorial effects of the differences in the misfolding landscapes of the two different substrates (*i.e.* a highly purified rPrP lacking post-translational modification as opposite to the much more complex composition of a 10% BH containing fully formed PrP^{C}) and the sensitivity and linear range of the different detection systems. The data presented in this Chapter suggest that, despite the methodological differences argued for the two cell-free conversion systems, the use of a specific subtype of sCJD (*i.e.* sCJD VV2) might allow an approximation to perform additional comparative studies for these two methods in the future.

Chapter 4: Molecular characterization of RT-QuIC products

Hypothesis: the epitope mapping analysis of the RT-QuIC protease resistant products allows discrimination between sCJD subtypes.

4.1 Introduction

As described in the introduction, sCJD subtypes are defined by the PrP^{res} type found in brain samples in combination with the genetic status of *PRNP* at codon 129. The sCJD subtypes loosely correlate with different disease presentation and clinical course and are currently most often discriminated at *post mortem*. The rate of *post mortem* examination, however, is falling in the United Kingdom (The National CJD Research & Surveillance Unit 2017). This may potentially impact on the ability of the laboratories specialized in CJD surveillance to confirm the different types of prion disease, particularly in cases where the clinical presentation is atypical or where prion disease may not have been considered. A possible aid to sCJD classification may come from RT-QuIC. Theoretically, a sCJD diagnostic RT-QuIC test informative of the sCJD subtype would provide valuable information regarding the disease course. Such information would be useful to caregivers, to the clinicians managing affected individual and possibly to stratify patients recruited in future clinical trials (Piconi et al. 2019). A strategy to approach this search of information is to study the structure of the RT-QuIC reaction products. Recently, evidence has been produced showing that the molecular characteristics of different prion seeds exert detectable, seed-discriminating effects on the RT-QuIC reaction outcomes. Such effects are apparent either in term sCJD subtype-specific variation of the second generation RT-QuIC reaction kinetics (Foutz et al. 2017) or in the structural characteristics (as detected by IFTR spectroscopy and conformational stability assay) of the products of the RT-QuIC reaction seeded with mouse adapted prion strains (Sano et al. 2014; Sano, Atarashi, and Nishida 2015).

The hypothesis formulated in this Chapter stems from these observations. To investigate it, the same methodological principles used for the typing of the naturally occurring PrP^{res} were applied to the analysis of the RT-QuIC reaction products. Namely, the products of RT-QuIC reaction, using FLHa-rPrP and seeded with sCJD BH and CSF samples, were assayed for their resistance to limited proteolysis and the length of the resistant fragments was investigated via epitope mapping using a panel of six commercially available antibodies, including those usually employed for sCJD molecular typing of *post mortem* brain tissue as part of the molecular diagnosis. This approach, even with low resolution when compared with biophysical methods, is informative of the structural conformation assumed by the recombinant substrate (Silva et al. 2015).

The methodology was initially optimized by analysing the products of RT-QuIC reactions seeded with a set of 10%BH including the six most common sCJD subtypes. Preliminary observations were then validated on three biological replicates per sCJD subtype (except for sCJD subtype VV1, because no tissue was available at the time of study). Next, the method for the analysis of the RT-QuIC reaction products was applied to the products of the RT-QuIC reaction seeded with sCJD CSF samples (*i.e.* diagnostic RT-QuIC reaction).

4.2 Materials and Methods

4.2.1 Biological samples CJD and non-CJD brain and CSF samples

For information regarding the human sCJD and non-CJD brain and CSF samples used, refer to the paragraphs 2.2.1 and 2.2.2 (Tables 2.2 and 2.3). Brain samples were homogenized to 10% w/v in RT-QuIC homogenization buffer (Table 2.2) as described in 2.5.2.

4.2.3 RT-QuIC reaction seeded with 10%BH

All the RT-QuIC reaction seeded with 10%BH presented in this Chapter were performed as described in 2.5.

4.2.4 Diagnostic RT-QuIC reaction seeded with CSF samples

When RT-QuIC (see Section 2.5) was seeded with 15 µL of undiluted CSF it was configured as in the diagnostic RT-QuIC protocol currently employed internationally for the diagnosis of sCJD (McGuire *et al.* 2016).

4.2.4.1 Criteria for the analysis of the diagnostic RT-QuIC reaction results

According to the RT-QuIC diagnostic criteria, a CSF sample is deemed a true positive if at least two technical replicates of that sample in the same RT-QuIC run, cross the fluorescence threshold of 10000 RFU by 90 h using the BMG LabTech Optima FLUOstar plate reader (McGuire et al. 2016).

4.2.5 Standard RT-QuIC untreated controls: the “Mix” samples

For all the RT-QuIC experiments presented in this Chapter, a volume of PBS accounting for the absence of seed (15 µL of CSF or 2 µL of a 10% BH dilution) was added to the excess of reaction mixture prepared each time. These mock reaction mixtures were then stored in 1.5 mL polypropylene tubes (APEX® NoStick™ Alpha Laboratories) at -20°C. These samples, termed “Mix”, were used as RT-QuIC untreated controls in subsequent immunochemical analyses of the RT-QuIC reaction products.

4.2.6 RT-QuIC reaction products collection

At the end of each RT-QuIC run, the sealed plate was removed from the plate reader and allowed to equilibrate at room temperature in MSC I. Condensation was spun down with 1 min centrifugation at 4500 rpm in a SIGMA 3-16K (rotor sigma 11240

337/F). Working in the MSC I, sealing tape was removed and the contents of the wells collected by carefully scraping the wells internal surfaces with a disposable pipette tip. Samples were stored in 1.5 mL polypropylene tubes (APEX® NoStick™ Alpha Laboratories) at -20°C until use.

4.2.7 SDS-PAGE and WB analysis to assess the efficiency of the collection of RT-QuIC reaction products

To estimate the amount of RT-QuIC reaction products collected, densitometry following WB with mAb 3F4 was performed on the collected RT-QuIC reaction products. SDS-PAGE analysis was performed as described paragraph 2.3 with a specific modification in the method used for sample preparation: namely, 6 µL of neat RT-QuIC reaction products were diluted 1:1 in 0.1%SDS and LDS Sample Buffer (NuPAGE) was added to 2X. Samples were incubated for 10 minutes at 100 °C and then loaded onto the gel along with FLHa-rPrP dilutions of known concentrations. Electrophoretic run conditions were 200 V constant for 40 minutes. At the end, gels were blotted as described in Section 2.4 using mAb 3F4 as primary antibody. Densitometric analysis of the WB signals were performed as described in 2.4.2.

4.2.7.1 Coomassie staining

Coomassie Brilliant Blue R250 (Thermo-Fisher Scientific) was purchased as powder and solution prepared fresh monthly (Table 4.1). Following SDS-PAGE, gels were incubated overnight in 50 mL Coomassie solution at room temperature with gentle shaking. The following day, stained gels were removed from Coomassie solution, rinsed with distilled water and incubated for at least 1 h in destaining solution at room temperature with gentle shaking. Images of the de-stained gels were taken with ChemiDoc XRS+ (BioRad) built-in function.

	Composition
Staining solution	0.1% w/v Coomassie R250 10% v/v Glacial acetic acid 40% v/v Methanol in distilled water
Destaining solution	10% v/v Glacial acetic acid 40% v/v Methanol in distilled water

Table 4.1 Coomassie staining and destaining solutions composition

4.2.8 PK digestion of RT-QuIC reaction products

For each digestion experiment, PK (Merck Millipore) was diluted fresh on the day from a glycerol stock to working stock in cell culture grade water. PK working stock concentrations were calculated to digest RT-QuIC reaction products with different amounts of PK using the same final digestion volume of 80 µL. The final digestion volume included 76 µL of sample and 4 µL of the appropriate PK working stock dilution to obtain the desired final concentration of protease. Digestions were carried out in 0.5 mL propylene tubes at 37 °C for 1 hour and stopped by placing the tubes on ice. PK activity was irreversibly inhibited by adding Pefabloc® SC (Sigma-Aldrich) to 1.25 mM.

4.2.9 Methanol precipitation of PK digested RT-QuIC reaction products

Products of PK digestion were methanol precipitated with 10 volumes of - 20°C 99.9% pure methanol (Fisher Chemicals). Samples, with added methanol, were thoroughly vortexed and incubated overnight at -20 °C. The following day, the samples were centrifuged for 35 minutes at 18200 x g (Eppendorf 5417R, rotor 06/09 HL128), the supernatant was discarded, and residual methanol evaporated by incubating the open tubes at 100°C in MSC II. Pellets were resuspended in 42 µL of 0.1%SDS/PBS, half of the volume was moved to a fresh tube and added to an equivalent volume of either LDS4X/2%βMA (reduced samples) or LDS4X with no βMA (non-reduced samples).

4.2.10 SDS-PAGE of PK treated and PK untreated RT-QuIC reaction products

The PK treated samples were prepared as described in 4.2.6 and .7, while for PK untreated samples 15 µL were diluted 1:1 in 0.1%SDS/PBS (final volume 30 µL), split in two fresh 0.5 mL tubes as 15 µL aliquots and combined with LDS4X/2%βMA or LDS4X to 2X, thus generating reduced and non-reduced samples, respectively. Samples were incubated at 100 °C for 10 minutes before loading on a 10% Bis-Tris

gel. The volume of sample loaded in each lane of an individual gel was always 10 µL, irrespective of being PK treated or untreated. The SDS-PAGE analysis was performed as described in 2.3.

4.2.11 WB analysis of the PK treated and PK untreated RT-QuIC reaction products

The general WB method used is described in paragraph 2.4. Additionally, at the end of the SDS-PAGE described in 4.2.8, the gels were blotted on the same PVDF membrane. Following transfer (see Section 2.4 for conditions), the PVDF membrane was split into Sections corresponding to individual gels, each Section being incubated with a different primary antibody. Performing the WB analysis with different primary antibodies on samples that had been transferred together increased the reliability of this comparison by reducing the variation in transfer efficiency.

4.2.12 Primary antibodies used and selection criteria

The criteria used to select the monoclonal antibodies for this project were the following:

- Being routinely employed for PrP^{res} typing.
- Monoclonality and known epitope sequence.
- Binding to an epitope encompassed in the PrP^{C} folded domain that is known to be involved in the re-folding that generates PrP^{Sc}.
- Ideally, but not exclusively, raised against hamster PrP antigens. Indeed, the main component of RT-QuIC reaction products is the RT-QuIC substrate FLHa-rPrP. This component is present in large excess compared to the seed. However, as PrP sequences are highly conserved among mammals (ref to intro), antibodies raised against PrP from other species were considered as well.

Table 4.2 lists the antibodies used while the diagram in Figure 4.1 shows the position of the epitope of each antibody on the PrP primary structure.

mAb	Supplier	Epitope (hamster sequence)	Dilution in TBST	T of incubation	Reducing Agent
12B2	Wageningen University CVI	89-93	1:10000	RT	Yes
3F4	Millipore	106-112	1:10000	RT	Yes
6H4	Prionics	144-152	1:1000	37 °C	No
SAF70	Bertin Pharma	155-161	1:1000	RT	Yes
8H4	Abcam	175-185	1:2000	37 °C	No
94B4	Wageningen University CVI	186-192	1:1000	37 °C	No

Table 4.2 Monoclonal antibodies used

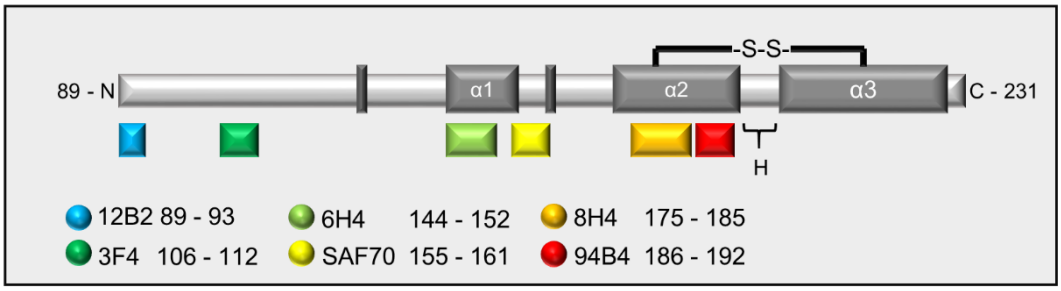

Figure 4.1 Diagram of Syrian golden hamster PrP^C primary sequence truncated at position 89 indicating relevant features as well as positions of the mAbs epitopes

Coloured boxes indicate positions of the epitopes recognised by each mAbs. Each box is colour coded to an individual mAb. For each mAb, epitope position in indicated. Dark grey boxes indicate positions of α-helices. The α-helix 2 and α-helix 3 are linked by the disulphide bridge (S-S) between cysteine residues 179 and 214 forming a hairpin loop. H: hinge.

4.3 Results

4.3.1 Preliminary validation of the selected monoclonal antibodies used

Each monoclonal antibody was individually tested to confirm its ability to bind the RT-QuIC untreated FLHa-rPrP in a WB assay. The concentration of a sample of the FLHa-rPrP batch used as substrate in all the RT-QuIC experiment was measured and serial dilution of known concentration prepared in reducing conditions. The generated standard stock was used to initially test the reactivity of all the selected mAb (Figure 4.2). The results of this preliminary analysis showed that 12B2, 3F4 and SAF70 consistently detected 2 to 10 ng of RT-QuIC untreated FLHa-rPrP (Figure 4.2 A, B and D) while 8H4 and 94B4 weakly detected 50 ng and 6H4 did not bind to the recombinant PrP at all under the conditions used (Figure 4.2 C, E and F).

The results obtained using 6H4, 8H4 and 94B4 highlighted the need to modify the protocol to increase the detection limit of these mAbs to levels comparable to those presented by 12B2, 3F4 and SAF70. The results showed that the binding of 6H4, 8H4 and 94B4 was negatively affected by the presence of the reducing agent β-mercaptoethanol (Figure 4.3). Therefore, this component was excluded from the preparation of samples to be probed with these mAbs. With the appropriate reducing or non-reducing conditions all the antibodies were able to detect 2 to 10 ng of FLHa-rPrP.

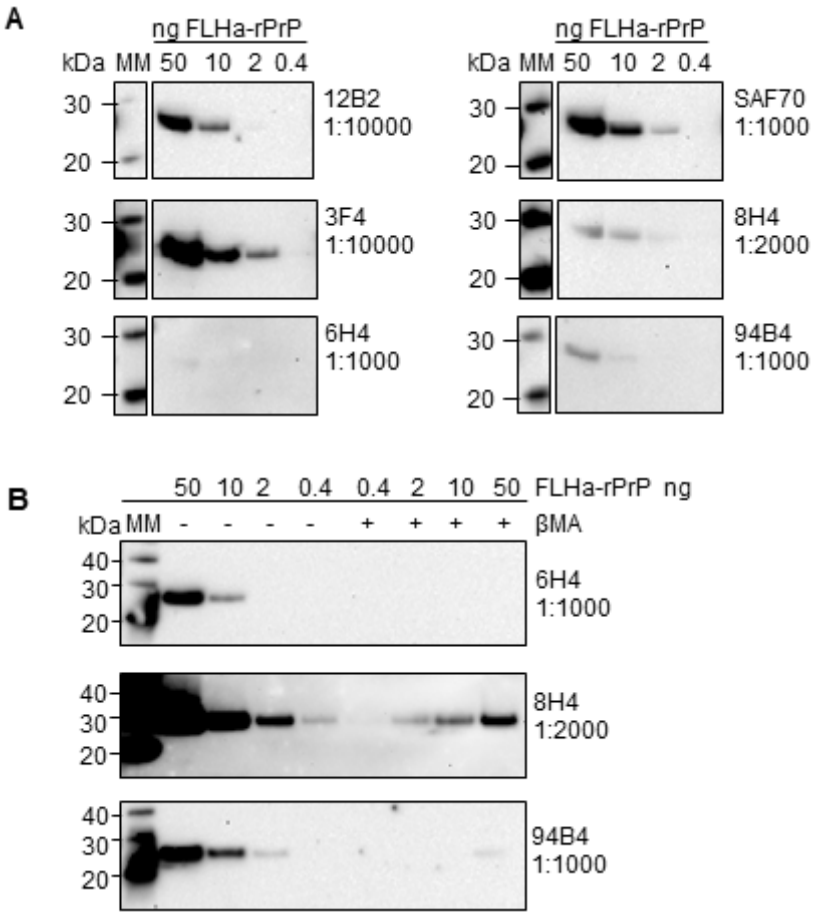

Figure 4.2 Validation of the monoclonal antibodies used and effect of the reducing agent β-mercaptoethanol

A) Testing mAbs ability to bind RT-QuIC untreated FLHa-rPrP in WB. FLHa-rPrP dilutions of known concentration were prepared in presence of 1% reducing agent β-mercaptoethanol. The same FLHa-rPrP was used to test all the mAbs. B) RT-QuIC untreated FLHa-rPrP dilutions were prepared with (+) or without (-) reducing agent β-mercaptoethanol (βMA), run on the same gel and probed with 6H4, 8H4 or 94B4. The dilution used for each mAb are indicated beside each blot. kDa: kiloDalton; MM: Molecular weight Marker.

4.3.2 Assessing the efficiency of RT-QuIC reaction products collection method

Preserving the integrity of the misfolded conformation assumed by the recombinant substrate during RT-QuIC was a prerequisite to investigate the hypothesis that the conformation(s) of the RT-QuIC reaction products were dependent on seed subtype. To achieve this, the RT-QuIC reaction products were collected from the plate wells without using any detergent or denaturant.

A preliminary analysis of the samples collected in this way from individual reaction wells showed, however, that the amounts of recombinant protein collected was not reproducible (Figure 4.3 A and B). This was considered an issue because samples that contained very low amounts of FLHa-rPrP might introduce bias into the analysis. Low recovery of FLHa-rPrP following a limited treatment with PK, might produce PK resistant fragments, below the limit of detection of the selected antibodies.

To address this problem, the replicated wells were pooled together upon collection from the plate, which reduced the differences in FLHa-rPrP content between samples, minimising bias (Figure 4.4 A). Washing the wells with a mild denaturant solution (*i.e.* 0.1%SDS/PBS) and analysing the generated samples by WB with mAb 3F4 showed that the missing substrate was, at least in part, adherent to the well walls (Figure 4.4 B). This material was not analysed further as it was collected in a buffer containing a denaturing agent (*i.e.* SDS) that could be expected to modify the structural features under analysis.

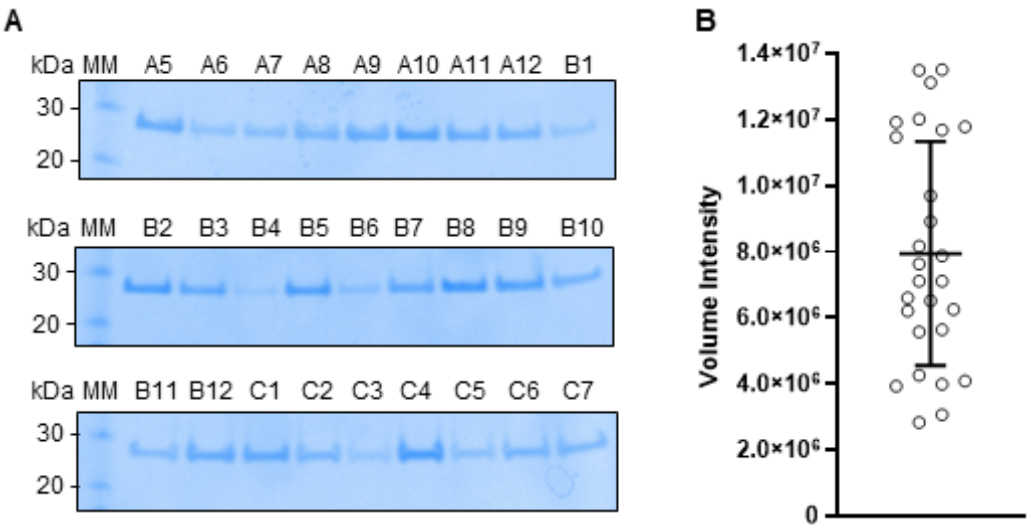

Figure 4.3 Efficiency and reproducibility of RT-QuIC end-product collection from individual reaction wells

[A] Coomassie staining of RT-QuIC products collected from individual reaction wells. Samples are coded according to well position on the 96-well plate. [B] Densitometric analysis of gels in A. As no standard was used, Volumes Intensity values measured by the Image Lab software (BioRad) are reported. Mean average and standard deviation were calculated showing that the data points were normally distributed.

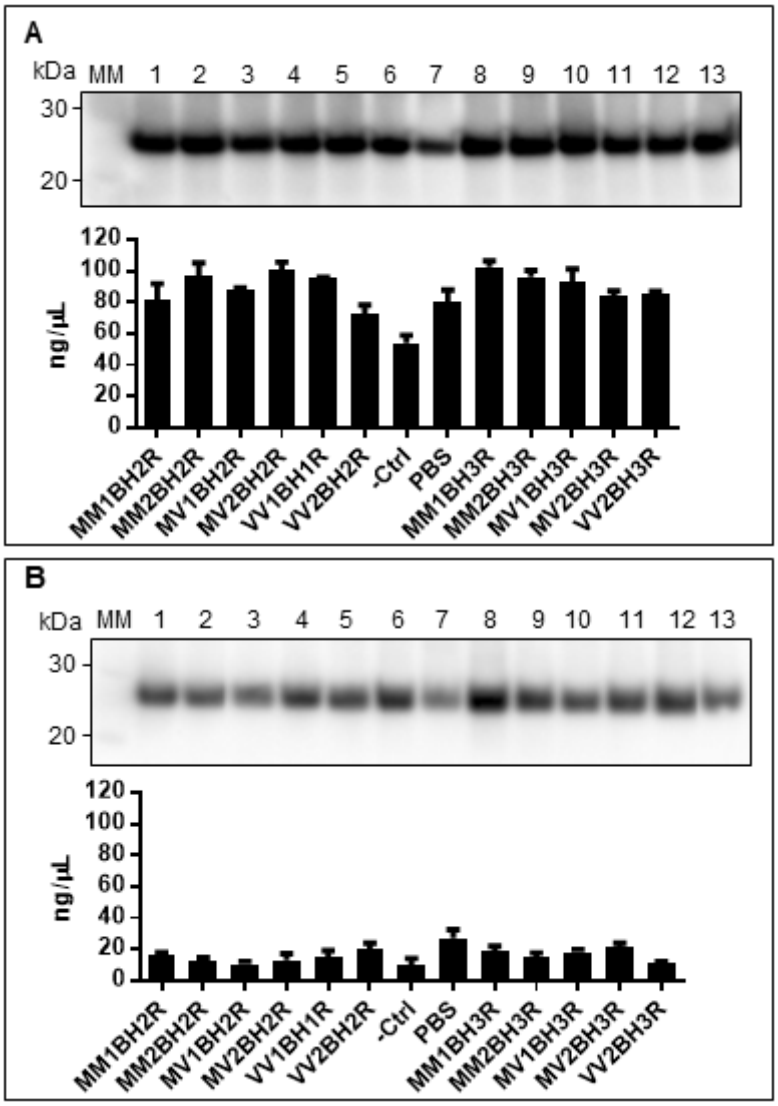

Figure 4.4 WB analysis of pooled RT-QuIC technical replicates and wells washes

The pictures show one representative blot of two technical replicates. Histograms report the mean average and standard deviation of the densitometric signal measured on the two technical replicates of the blot. [A] WB of the RT-QuIC reaction products pooled by technical replicates and densitometric analysis of the signals [B] WB of the well washes pooled by technical replicates and densitometric analysis of the signals. WBs gels layout is mirrored in the arrangement of the histogram columns; samples are named after the seed content. 1) MM1BH1R; 2) MM2cBH2R; 3) MV1BH2R; 4) MV2BH2R 5) VV1BH1R 6) VV2BH2R 7) -Ctrl 8) PBS; 9) MM1BH3R; 10) MM2cBH3R; 11) MV1BH3R; 12) MV2BH3R 13) VV2BH3R. kDa: kiloDalton; MM: Molecular weight Marker. Immunodetection was with mAb 3F4 1:10000

4.3.3 Detection the PK untreated RT-QuIC reaction products with the selected monoclonal antibody

The optimization of the method for collecting the RT-QuIC reaction products (4.3.2), showed that this material was readily detected by mAb 3F4 as an individual band an apparent molecular mass corresponding to the RT-QuIC untreated FLHa-rPrP. The same observation was repeated for each of the mAbs in the panel. The samples analysed were from an individual RT-QuIC experiment in which the reaction was seeded with a dilution of a 10% BH for each sCJD subtype and included a negative control and an unseeded control for the spontaneous aggregation of the substrate. Samples were prepared as describe in 4.2.9. The results showed that all the antibodies in the panel detected the PK untreated RT-QuIC reaction products. Indeed, irrespective of the antibody used and whether RT-QuIC product was seeded, unseeded or from an RT-QuIC untreated control (*i.e.* mix), PK untreated RT-QuIC reaction products were invariably detected as an individual band running at the same molecular weight as the RT-QuIC untreated FLHa-rPrP (Figure 4.5). Taken together these results indicated as well that the sample preparation was effective in disrupting aggregates and in linearizing the protein, exposing all the epitopes probed.

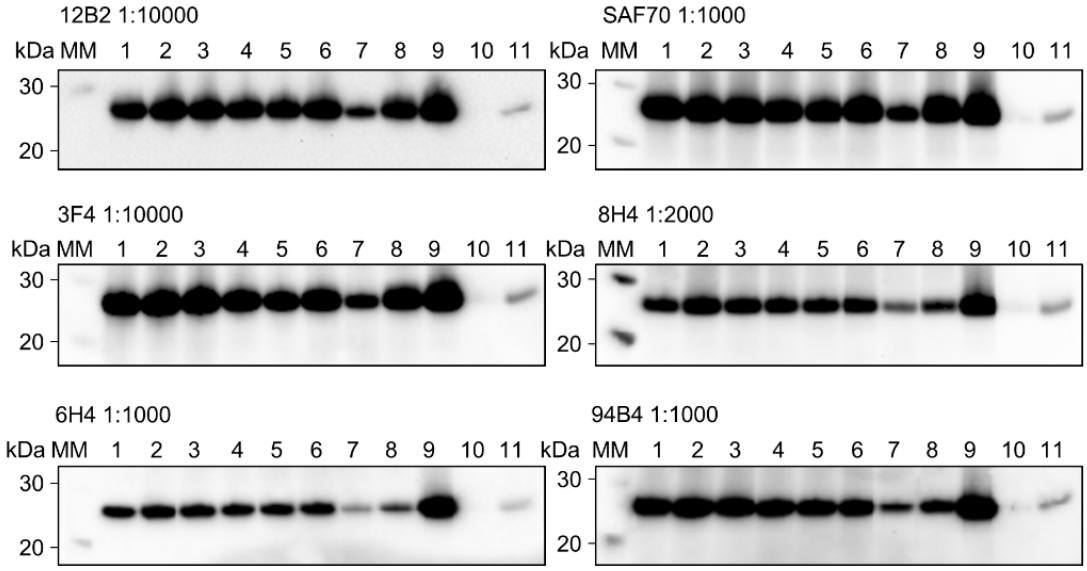

Figure 4.5 Epitope map of PK untreated RT-QuIC reaction products

The six gels were transferred on an individual PVDF membrane which was subsequently split in Sections. Individual membrane Sections were incubated with different primary antibodies. The mAbs and dilutions used are indicated on top of each WB picture. RT-QuIC reaction products are identified by the seed content 1) MM1BH1R; 2) MM2cBH1R; 3) MV1BH1R; 4) MV2BH1R; 5) VV1BH1R; 6) VV2BH1R; 7) -Ctrl; 8) PBS; 9) Mix; 10) 2 ng FLHa-rPrP; 11) 10 ng FLHa-rPrP. kDa: kiloDalton; MM: molecular weight marker.

4.3.4 Limited proteolysis of RT-QuIC reaction products with low PK concentration and epitope mapping of the resistant fragments

Treating the same RT-QuIC reaction products previously analysed in 4.3.3 with PK at 10 µg/mL, dramatically reduced and, in some instance, abolished the signal from all the mAbs except SAF70, which in contrast detected additional bands (Figure 4.6). Signals at an apparent molecular mass corresponding to the PK untreated FLHa-rPrP were clearly detected by mAbs SAF70, 3F4, 8H4 and 94B4 (Figure 4.6 B, C, D and F) with the highest intensity detected in the RT-QuIC untreated mixture sample.

Such a high intensity was very likely due to the higher concentration of FLHa-rPrP present in the RT-QuIC untreated mixture sample. Indeed, this sample was not affected by the loss of material due to the prolonged contact with wells surfaces of the RT-QuIC plate in contrast to the other RT-QuIC reaction products. Furthermore, the signals at an apparent molecular mass corresponding to the PK untreated FLHa-rPrP suggested that, with the conditions adopted, the amount of PK used produced a limited digestion of the FLHa-rPrP present in solution.

Regarding the additional bands detected by SAF70, a new band was detected at ~ 22 kDa as well as a prominent band at ~10 kDa (Figure 4.6 B). This latter band was not detected by SAF70 in the RT-QuIC reactions seeded with the negative control or PBS suggesting that it was specific to the sCJD seeded RT-QuIC reaction products. Indeed, even though the RT-QuIC untreated mixture sample showed a signal between ~5 to 15 kDa, it was smeared. Such a smeared signal was most likely the result of partially digested FLHa-rPrP rather than the sign of resistance to the proteolytic treatment.

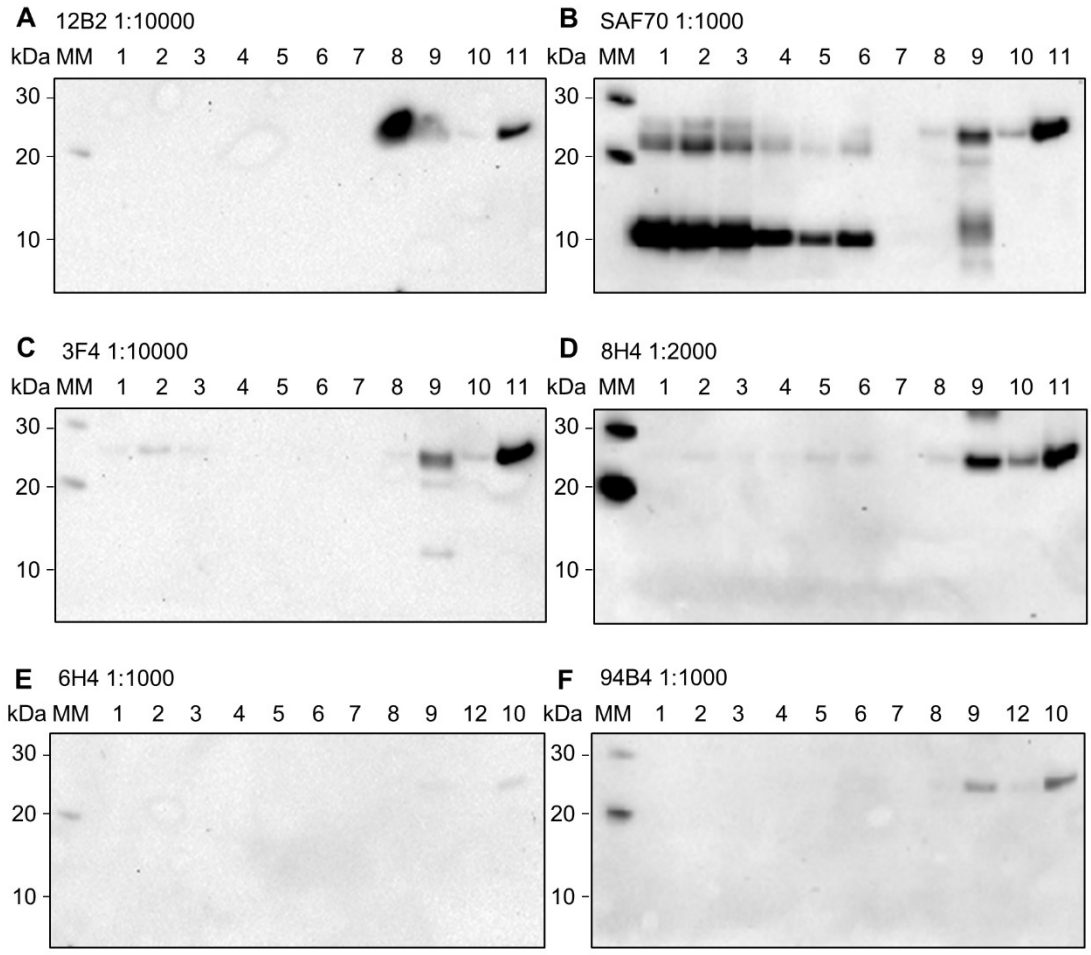

Figure 4.6 Epitope map RT-QuIC reaction products treated with 10 µg/mL PK

The six gels were transferred on an individual PVDF membrane subsequentially split in patches. Individual membranes were incubated with different primary antibodies. The mAb and dilution used are indicated on top of each WB picture. RT-QuIC reaction products are identified by the seed content 1) MM1BH1R; 2) MM2cBH1R; 3) MV1BH1R; 4) MV2BH1R; 5) VV1BH1R; 6) VV2BH1R; 7) -Ctrl; 8) PBS; 9) Mix; 10) 10 ng FLHa-rPrP; 11) 50 ng FLHa-rPrP; 12) 2 ng FLHa-rPrP. kDa) kiloDalton; MM: molecular weight marker.

4.3.5 Limited proteolysis of RT-QuIC reaction products with higher concentrations of PK and the epitope mapping of resistant fragments

To further investigate whether the ~10 kDa band, detected by SAF70, was indeed due to the FLHa-rPrP acquiring PK resistance during the sCJD seeded RT-QuIC reaction, or resulted from the incomplete digestion of the FLHa-rPrP, the same samples analysed in 4.3.4 were treated with increased concentration of PK. The limited proteolytic treatment was carried out with 30 or 50 µg/mL PK. The latter enzyme concentration corresponds to the one routinely used when screening 10% BH samples for the presence of PrP^{res}. This amount of PK is considered enough to achieve the digestion of most if not all the PK sensitive PrP isoforms in solution allowing for the unhindered immunodetection of PrP^{res}.

When the RT-QuIC reaction products treated with 30 or 50 µg/mL PK were probed with SAF70, no signal was detected from the negative control seeded sample, the unseeded sample and the RT-QuIC untreated mixture sample. An intense signal at ~10 kDa was instead clearly detected in all the sCJD seeded RT-QuIC products samples irrespective of the sCJD subtype (Figure 4.7 B and C).

All the other antibodies in the panel failed to detect, in the same samples, signals of intensities comparable to the one detected from SAF70. However, occasionally, very faint bands were detected by mAbs other than SAF70 at a molecular weight corresponding to the intact FLHa-rPrP and more rarely at 22 kDa (see S1 Figure in Appendix I). Notably, however, the signal detected by SAF70 at ~22 kDa appeared to reduce progressively with the increase of PK (Figure 4.7 A, B and C) suggesting that it resulted from the incomplete digestion of the FLHa-rPrP rather than representing a fragment resistant to proteolytic treatment.

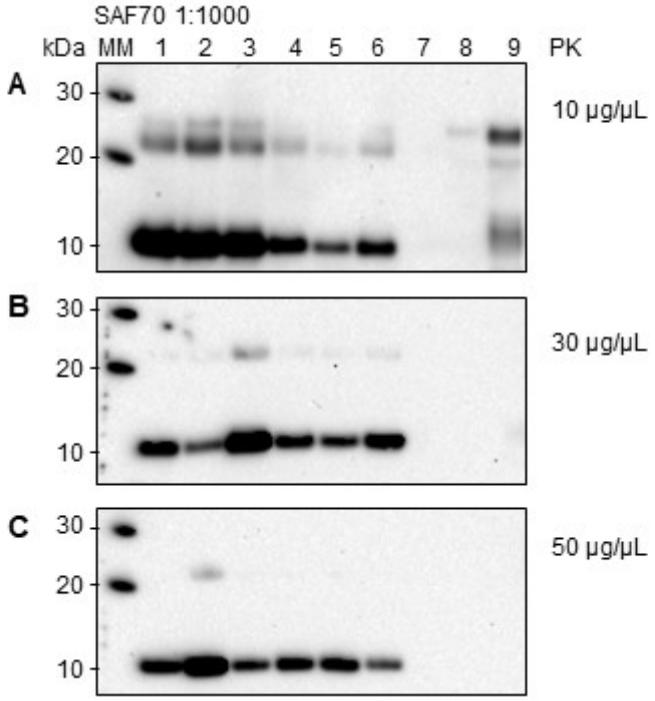

Figure 4.7 RT-QuIC products treated with 10, 30 or 50 µg/mL PK and probed with mAb SAF70 1:1000

The figure summarises the results obtained with mAb SAF70 for the RT-QuIC end-products treated with PK at A 10, B 30 and C 50 µg/mL PK. RT-QuIC reaction products obtained from the same RT-QuIC experiment and used in A, B, C are identified by the seed content 1) MM1BH1R; 2) MM2cBH1R; 3) MV1BH1R; 4) MV2BH1R; 5) VV1BH1R; 6) VV2BH1R; 7) -Ctrl; 8) PBS; 9) Mix; kDa: kiloDalton; MM: molecular weight marker. The results obtained when probing these samples with the other mAbs in the panel, can be found in Appendix C.

4.3.6 Preliminary conclusions and validation of the observed banding profile of the PK treated RT-QuIC reaction products

The preliminary optimization of the method used for the epitope mapping analysis following limited PK treatment of the RT-QuIC products seeded with sCJD 10%BH, indicated that:

- RT-QuIC products seeded with a sCJD seed were characterised by resistance to limited proteolytic treatment up to 50 µg/mL PK.
- The core of the protease resistant conformation assumed by the FLHa-rPrP during the RT-QuIC reaction encompasses the SAF70 epitope, and no sCJD subtype-specific difference, in term of electrophoretic mobility or abundance, were apparent.

To validate these observations, biological replicated samples of RT-QuIC reaction products were produced and analysed. Two additional examples of sCJD 10%BH subtypes MM1/MV1, MM2c, MV2, VV2 and one example of sCJD subtype VV1 were assayed in RT-QuIC (Figure 4.8 A). The RT-QuIC products were collected by pooling together replicated wells and the samples obtained were treated with 50 µg/mL PK in parallel with the same samples used during the optimization phase (BH1R sample set). Following PK treatment, the samples were analysed by WB with mAb SAF70.

The results of this analysis are shown in Figure 4.8 B. In line with the previous results, a band at MW ~10 kDa was clearly detected by SAF70 in all the samples analysed, irrespective to the sCJD subtype. A weaker signal was also detected with an apparent molecular mass of ~22 kDa in most of the analysed samples, but with no apparent correlation to the sCJD subtype. It should be noted that a similar, if not identical, ~22 kDa signal was detected in the RT-QuIC products seeded with MM2cBH1R analysed in Figure 4.7, but not in the same sample analysed in 4.8.

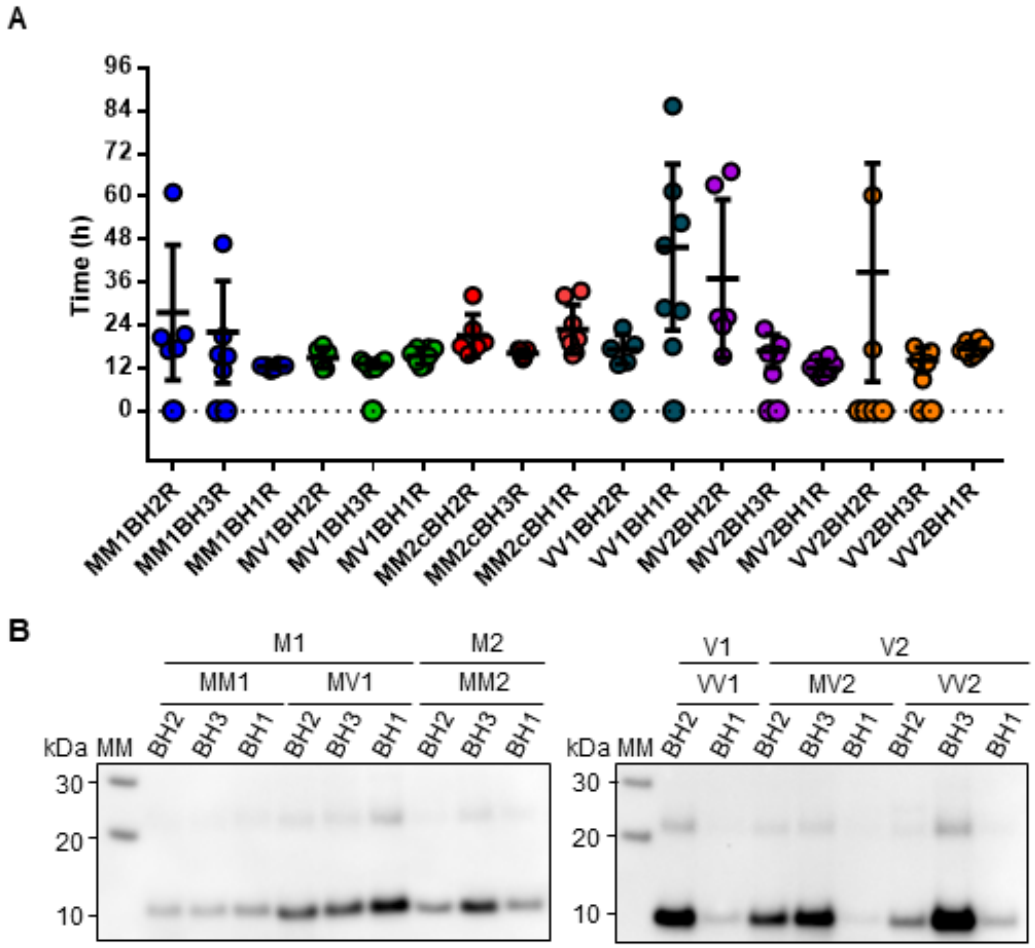

Figure 4.8 Comparative analysis of RT-QuIC reaction products seeded with 10%BH dilutions

[A] Three examples of sCJD 10%BH subtype MM1/MV1, MM2c, MV2, VV2 and 2 examples of subtype VV1 were run in standard RT-QuIC. The BH1 sample set was run in eight technical replicates per sample whereas BH2 and BH3 sample set were run in six technical replicates per sample. For each sample, the time to threshold of individual technical replicates that crossed Thr is shown. Bars indicates the mean average and standard deviation calculated on each group of technical replicates that crossed Thr. [B] The products of the RT-QuIC reactions presented in A were collected, treated with 50 µg/mL PK and analysed in WB with mAb SAF70 1:1000. In both A and B samples are arranged in the same order and grouped according to putative strains of prions as defined in Bishop *et al.* 2010.

4.3.7 Analysis of the products of RT-QuIC reaction seeded with CSF samples

CSF samples from all the different sCJD subtypes except sCJD VV1 were assayed in three independent RT-QuIC analyses. The results of the RT-QuIC analysis showed, as expected based on the sample selection criteria, that all the different CSF samples assayed satisfied the diagnostic criteria for positivity (McGuire et al. 2016). Even though spontaneous aggregation of the substrate was observed in two out of 20 unseeded reaction wells, none of the negative controls showed aggregation-associated fluorescence increase. The t_{Thr} of individual diagnostic RT-QuIC reaction wells are reported in Figure 4.9 A.

Following the same experimental design as with 10%BH, the diagnostic RT-QuIC reaction products were collected by pooling replicated wells together. The samples were subsequently treated with 50 µg/mL PK and analysed by WB with mAb SAF70. No signals were apparent from the PK treated RT-QuIC products seeded with the negative control (*i.e.* non-CJD CSF sample) or from the unseeded RT-QuIC reactions. All the sCJD seeded RT-QuIC reaction products instead, showed a similar if not identical banding pattern characterised by two prominent signals at around 10 and 22 kDa irrespective of the sCJD subtype of the CSF sample used to seed the reaction (Figure 4.9 B).

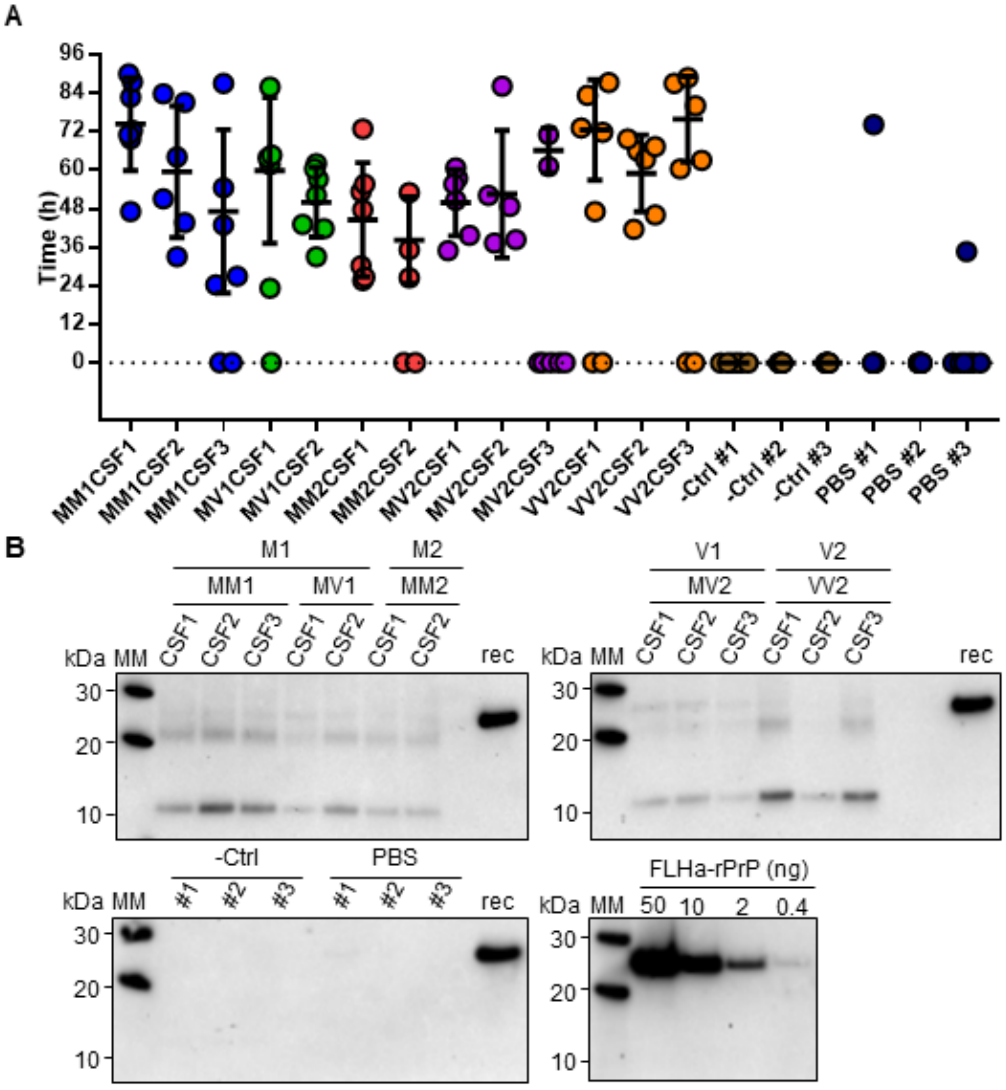

Figure 4.9 Comparative analysis of diagnostic RT-QuIC reaction products

[A] Time to threshold of individual reaction wells that crossed Thr is reported with mean average and standard deviation. CSF samples from all the different sCJD subtypes except sCJD VV1 were assayed in seven technical replicates in three independent RT-QuIC analysis using the same non-CJD CFS and negative control. -Ctrl) negative control; PBS) unseeded control for the spontaneous aggregation of the substrate. [B] The products of the RT-QuIC reactions presented in A were collected, treated with 50 µg/mL PK and analysed in WB with mAb SAF70 1:1000 along with FLHa-rPrP dilutions of known concentration. rec) 10 ng of FLHa-rPrP. In both A and B samples are arranged in the same order and grouped according to putative strains of prions as defined in Bishop et al 2010.

4.4 Discussion

The generation of PK resistant material from the prion seeded conversion of a recombinant substrate was first reported by Kocisko and co-workers (Kocisko et al. 1994) and has been subsequently exploited in different CFCs as a detectable sign of the prion seeded conversion of PrP^C, or of recombinant PrP substrates along with, or instead of, alterations in ThT fluorescence (Atarashi et al. 2008). More recently, Sano and co-workers used two different rodent adapted prion strains and mouse rPrP as reaction substrates and showed that RT-QuIC reaction products retain some of the strain specific biochemical properties such as the conformational stability and β-sheet structure (Sano et al. 2014; Sano, Atarashi, and Nishida 2015). However, the same authors were unable to discriminate strain-specific structural differences by epitope mapping of PK digested RT-QuIC reaction products using the mAb ICSM35 (epitope 93-102) and the polyclonal PrP antiserum R20 (epitopes 218-231). These results were in line with previous findings obtained with sCJD seeds, showing that the conformation acquired by the seeded RT-QuIC reaction products confers PK-resistance to a C-terminal domain encompassing the R20 epitopes (Wilham et al. 2010). In addition, the banding profile detected with R20 by Sano and colleagues was specific to prion seeded RT-QuIC reaction products but independent of the rodent prion strain used as seed. Similar results have been obtained with R20 by McGuire and colleagues (McGuire et al. 2012) on a limited number of PK-treated RT-QuIC reaction products generated with human 10%BH and CSF sCJD seeds and employing FLHa-rPrP as a reaction substrate. In both these studies only very mild PK treatments using 10 and 6 μg/mL PK respectively were performed, prior to western blotting. The present study expands on these observations by systematically investigating the extent of PrP primary structure that is encompassed by the RT-QuIC PK resistant reaction products generated by sCJD seeds, by employing six

commercially available monoclonal antibodies and harsher proteolytic conditions that are discriminatory for subtyping sCJD brain tissue itself.

The initial assessment of the sensitivity of the selected mAbs towards the RT-QuIC substrate FLHa-rPrP in WB, showed that the binding of mAbs 6H4, 8H4 and 94B4 to their respective epitopes was negatively affected when the reducing agent β-mercaptoethanol was added to the sample loading buffer (Figure 4.2). The reducing agent was added to reduce and thereby break the one disulphide bond in PrP (cysteine 179- cysteine 214, Figure 4.10 A), favouring the linearisation of the protein structure by LDS and preventing the rPrP intermolecular dimerisation while in the denatured state. The fact that reducing conditions suppressed the binding of mAbs 6H4, 8H4 and 94B4 suggests that the correct presentation or availability of the epitopes recognised by these mAbs may depend on the local secondary structure of the protein, *i.e.* specific amino acid residues at the epitopes must be spatially arranged in a specific conformation. The disruption of the 6H4 epitope by reduction and alkylation has been reported previously (Yuan et al. 2005). The data presented here, however, show that reducing conditions and the consequent disruption of the disulphide bond distal to the 6H4 epitope, is enough to reduce or suppress 6H4 binding. No previous report was found instead regarding of the negative effect of sample reduction on 8H4 and 94B4 binding. However, in the latter case, the supplier (Central Veterinary Institute at Wageningen University, Netherlands, EU) states in the product information sheet that the 94B4 epitope is “assumed to be conformation dependent”, hence its binding may be susceptible to the conformational modifications determined by the reducing agent.

The cysteine at position 179 that forms one half of the disulphide bridge, is part of 8H4 epitope (Zanusso et al. 1998; Li et al. 2000) and the latter is followed on the C-terminal side by the 94B4 epitope (Yull et al. 2006). Hence, the 8H4 and 94B4

epitopes are contiguous and map on one arm of the hairpin loop that may remain intact when the protein is denatured, and the disulphide bond is oxidised. It is therefore conceivable that the disruption of the hairpin loop by reduction of the disulphide bridge may lead to a conformational rearrangement that in turn negatively affects the 8H4 and 94B4 epitopes.

In the absence of reducing conditions and when no PK treatment was used, all the antibodies used detected both the FLHa-rPrP substrate prior to RT-QuIC and the FLHa-rPrP recovered from the plate following RT-QuIC (Figure 4.2 and 4.5). The treatment of the RT-QuIC reaction products with 10 µg/mL PK, was enough to negate the signal detected by all the selected antibodies apart from SAF70 (Figure 4.6). The fragment detected by SAF70 was specific to sCJD seeded RT-QuIC reactions and has an apparent molecular weight of around 10 kDa (Figure 4.10 B). The latter estimate was made on the basis of the migration distance on western blot and is therefore only approximate. Nevertheless, the SAF70-detected band was observed irrespective of the sCJD subtype or whether brain or CSF was used to seed the reaction (Figures 4.8 B and 4.9 B). Moreover, the fragment detected with SAF70 was unaffected by the harsher PK treatment used (*i.e.* 50 µg/mL PK,). Taken together these observations indicate the fragment detected by SAF70 represents the PK resistant conformational core generated during sCJD seeded RT-QuIC reactions.

The negative results obtained after PK digestion using mAbs that recognise more N-terminal epitopes, namely 12B2 and 3F4, indicate that these parts of FLHa-rPrP are digested by even the mildest PK treatment used in this study. This observation is in line with previously published evidence regarding RT-QuIC reaction products generated with human and non-human prion seeds, indicating that in the conformation generated during RT-QuIC the C-terminal region of the recombinant

substrate acquires PK resistance (Wilham et al. 2010; McGuire et al. 2012; Sano et al. 2014; Sano, Atarashi, and Nishida 2015)

The apparent molecular weight of the fragment detected by SAF70 cannot be reconciled easily with the lack of detection by 6H4 and 8H4 because the region of hamster PrP between 6H4 and 8H4 epitopes has a much smaller molecular mass (~2.7 kDa) than the apparent molecular mass of 10 kDa (Figure 4.10 B). Taking into consideration the observed susceptibility of the 6H4 epitope to distal conformational changes (Figure 4.10 B), it is possible that the structural integrity of this epitope was affected by the proteolytic digestion of either or both the N-terminal and C-terminal domains, rather than by a direct effect of the PK. It is also possible that the observed loss of 8H4 and 94B4 signals might arise from a secondary conformational effect resulting from PK exerting its activity on distal domains so that the sequence encompassing these epitopes may contribute to the observed molecular weight of ~10 kDa. In particular, PK activity may determine an outcome similar to the one determined by the reducing agent (*i.e.* the disruption of the hairpin loop between α2 and α3), by exerting its activity on the hinge between the arms of the hairpin loop (Figure 4.10 A). The digestion of the hinge may lead to a topological change in the local sequence that negatively affects 8H4 and 94B4 binding without destroying the peptide sequence encompassing their epitopes.

The results presented here show that the RT-QuIC reaction products, generated by seeding the reaction with either sCJD brain samples or sCJD CSF samples, are partially resistant to PK digestion. The PK digestion of the sCJD seeded RT-QuIC reaction products yields a fragment that is detected by mAb SAF70 at a molecular weight of ~10 kDa. The epitope mapping analysis showed that the same banding profile is observed irrespective of the sCJD subtype used to seed the RT-QuIC reaction and irrespective to seed being a sCJD brain or CSF samples. These results

suggest that all the sCJD seeds have induced the same conformational change in the FLHa-rPrP irrespective of PrP^{res} type or sCJD subtype of the seed.

This conclusion allows to speculate that the sCJD brain and CSF samples share a similar if not identical component capable of inducing the generation of similar RT-QuIC reaction products. Alternatively, the selection of the conformation(s) assumed by the substrate might be entirely due to the purified FLHa-rPrP conformational uniformity and RT-QuIC reaction conditions. The highly purified recombinant FLHa-rPrP might offer a limited conformational landscape (too much order) that does not allow the selection of specific conformational pathways within the time frame of the RT-QuIC reaction kinetics. More complex and sensitive molecular methodologies or a different set of mAb, directed towards the domains surrounding of SAF70 epitope, may be able to better characterise the products of the protein misfolding events taking place during RT-QuIC. These data may eventually permit this technique to discriminate sCJD subtypes *intra vitam*.

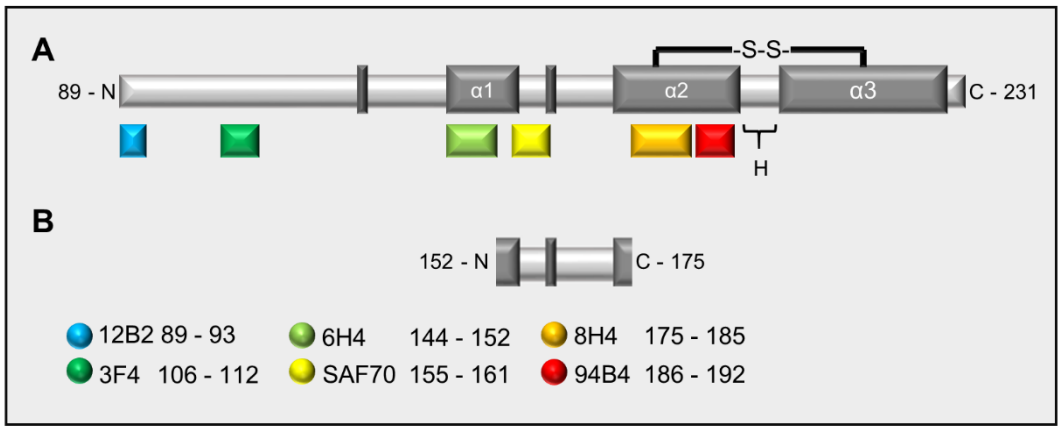

Figure 4.10 Diagram of Syrian golden hamster PrP^C primary sequence truncated at position 89 and putative sequence of the PK resistant core of RT-QuIC products

[A] Coloured boxes indicate positions of the epitopes bind by the mAbs used. Each box is colour coded to an individual mAb. For each mAb epitope position in indicated. Dark grey boxes indicate positions of α-helices. The α-helix 3 and α-helix 2 are juxtaposed by the disulphide bridge (S-S) between cysteine residues 179 and 214 forming a hairpin loop. H: hinge. [B] Minimal extent of the fragment detected by SAF70 following PK digestion of sCJD seeded RT-QuIC products.

Chapter 5: RT-QuIC seeding activity in sCJD urine samples

Hypothesis RT-QuIC reaction can discriminate sCJD from non-CJD urine samples

5.1 Introduction

The investigations regarding the shedding of prions in urine of humans and of other animals, has been traditionally hampered by the lack of methodologies capable of reliably detecting direct or indirect markers of prions in this easily accessible biological fluid. Shaked and colleagues, firstly reported the immunodetection by WB analysis of protease resistant prion protein isoforms in urine samples from patient affected by genetic prion disease (Shaked et al. 2001). Following studies on larger sample sets showed, however, that the detection of protease-resistant material with the method used by Shaked and collaborators resulted from antibodies cross-reacting with aggregated fragments of light-chain immunoglobulins (Head et al. 2005; Kariv-Inbal et al. 2006; Dabaghian et al. 2008). Prion infectivity has been observed by bioassay, in urine from prion infected mice affected by concomitant nephritis (Seeger 2005) and, at very low titre, in urine of hamsters experimentally inoculated with hamster adapted scrapie strain (Kariv-Inbal et al. 2006; Gregori et al. 2008). However, early transmission studies in primates (Brown et al. 1994) and a more recent bioassay investigation (Notari et al. 2012) did not detected infectivity in urine samples of humans affected by sCJD.

The introduction of CFC systems for the ultrasensitive detection of prions represented a major technology change in this field. Moda and colleagues (Moda et al. 2014) demonstrated, for the first time, that urine samples from vCJD patients seed the PMCA reaction when using humanized transgenic mouse 10%BH as substrate and multiple round of PMCA. In contrast, sCJD and gCJD urine samples gave a negative result when tested using the same conditions. The PMCA method used by Moda and collaborators, in spite of technical differences when compared to the PMCA method

discussed in Chapter 3, is similarly poorly seeded by sCJD brain samples (Cali et al. 2019). Hence, the authors could not reject the hypothesis that the lack of seeding activity observed in sCJD and gCJD urine samples was in fact due to the analytical limitations of the method used.

The hypothesis addressed in this Chapter is that RT-QuIC can detect prion-related seeding activity if it is present in sCJD urine. RT-QuIC analysis of urine samples has been successfully applied to follow disease progression in rodents experimentally inoculated with a mouse-adapted scrapie strain (Shi et al. 2015). In addition, a CWD diagnostic RT-QuIC test, based on urine analysis (as well as saliva and faeces), has been optimized and adopted in laboratories involved in the surveillance of CWD (John, Schatzl, and Gilch 2013; Henderson et al. 2015a; 2015b; Denkers et al. 2016). Additionally, the sCJD diagnostic RT-QuIC test based on CSF analysis demonstrate the ability of RT-QuIC to detect prion related seeding activity in a biological fluid characterized by very low titre of infectivity and by inference low amount of prions (Brown et al. 1994).

The existing literature suggests that, in order to detect prion related seeding activity by either PMCA or RT-QuIC in urine samples, they need to be concentrated by centrifugation (Moda et al. 2014) or fractionated by chemical and physical treatments (Denkers et al. 2016; Shi et al. 2015). In this Chapter, two methods to prepare urine samples, before RT-QuIC, are derived from the relevant literature and tested on an artificial sCJD urine reference standard as well as on actual sCJD urine samples. The first method, based on the work by Moda and collaborators (Moda et al. 2014), entails pelleting urine samples by ultracentrifugation and using the resuspended pellets to seed RT-QuIC. The second method, termed Iron Oxide Magnetic Extraction (IOME), is derived from Denkers *et al.*, 2016 and exploits the known affinity of prions for metal surfaces (Zobeley et al. 1999).

5.2 Materials and methods

5.2.1 Biological samples

For information regarding the human sCJD and non-CJD urine samples used, refer to paragraphs 2.2.3 and Table 2.4. The sCJD subtype MM1 10%BH, used as positive control to the RT-QuIC reaction as well as to generate the model of sCJD urine, was MM1BH1R (see 2.2.3 and Table 2.1).

5.2.1.2 Artificial sCJD urine reference standard

In a preliminary analysis, it was observed that the RT-QuIC reaction was inhibited when neat urine spiked with sCJD 10%BH was used as seed. Such inhibition was abolished when spiked urine were dialysed against 1XPBS. Therefore, to model the shedding of prions in urine, sCJD 10%BH MM1BH1R was serially diluted in 1XPBS. The dilutions (hereafter referred to as spikes) were used as surrogates for actual sCJD urine samples. Following preparation, spikes were frozen at -80 °C to simulate storage conditions of the actual urine samples.

5.2.2 RT-QuIC reaction

All the RT-QuIC reactions presented in this Chapter were performed as described in Section 2.5 on a FLUOstar Omega (BMG Labtech) plate reader (Table 2.8). Seed volume was always 2 µL irrespective to sample preparation.

5.2.2.1 Preparation of urine samples: pelleting by ultracentrifugation

Urine samples were cleared by centrifugation for 5 min at 2000 rpm generating supernatant S_1 and pellet P_1. A 3 mL volume of S_1 was loaded in Slide-A-Lyzer™ Dialysis Cassette (7 kDa membrane cut-off, Thermo-Fisher) and dialysed at RT against 100 volumes 1XPBS (pH 7.4). The dialysate was changed after 1 h and dialysis continued overnight. The sample was then retrieved from the dialysis cassette generating DS_1 samples. The DS_1 samples were further ultra-centrifuged at 100,000

g for 1h at 4 °C generating supernatant S_2 and pellets P_2. Table 5.1 lists the ultracentrifuge equipment and conditions used. Supernatants S_2 were discarded whereas pellets P_2 were resuspended in 20 µL of PBS and 2 µL of this used to seed individual RT-QuIC reaction wells. The sCJD urine reference standard (5.2.1.2) was treated as if it were a DS_1 sample, namely, 3 mL were pelleted as described above and the resuspended pellets used to seed RT-QuIC (Figure 5.1).

Ultracentrifuge	Optima Max, Beckman Coulter
Rotor	MLS-50, swinging bucket, Beckman Coulter
Tubes	Open-top thick-wall, Beckman Coulter
Conditions	40,000 rpm 1 h at 4 °C

Table 5.1 Ultracentrifuge equipment and settings

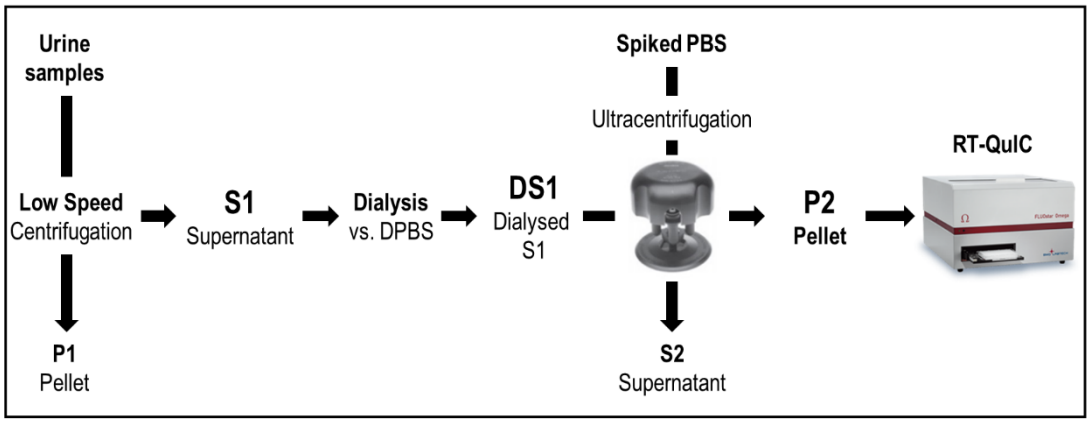

Figure 5.1 Pelleting by ultracentrifugation (PBU)

Diagram depicting the method used to pellet urine samples

5.2.2.2 Preparation of urine samples: Iron Oxide Magnetic Extraction, IOME

Superparamagnetic iron oxide beads (~ 9 µm in diameter) were purchased from Bang Laboratories (Indiana, US) as a suspension at 49 ng/µL. Using a magnetic separation rack, 2 µL of beads per sample were washed twice in 500 µL of 1XPBS. Washed beads were incubated overnight at RT on a head-to-head rotator with 800 µL of urine supernatant S_1 (generated as described in 5.2.2.1) or an equal volume of sCJD urine reference standard (5.2.1.2). The following day, using a magnetic separation rack, samples were removed, beads were resuspended in 20 µL of 1XPBS and 2 µL used to seed individual RT-QuIC reaction wells (Figure 5.2).

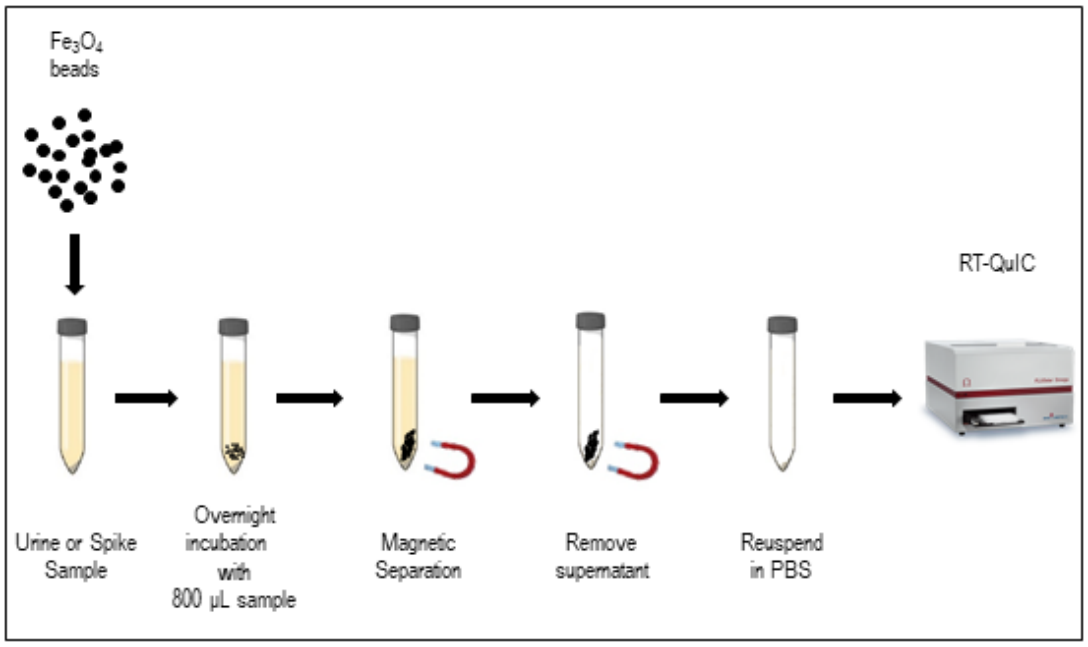

Figure 5.2 Iron oxide magnetic extraction (IOME)

Diagram depicting the iron oxide magnetic extraction method

5.3 Results

5.3.1 RT-QuIC analysis of urine following PBU

Preliminary evaluation of ultracentrifugation as a means of concentrating seeding activity from sCJD urine samples was conducted using the sCJD 10%BH sample MM1BH1R serially diluted from $1x10^{-3}$ to $1x10^{-12}$ in 1XPBS. Following ultracentrifugation, the pellets were resuspended in PBS and assayed in RT-QuIC along with a standard positive control for the RT-QuIC reaction, (*i.e.* 2 µL of dilution of MM1BH1R containing 100 fg of PrP^{res}) and a negative control constituted by reactions seeded with 1XPBS (Figure 5.3 A).

One out of 5 technical replicates of the negative control showed a TP signal at around 80 hours. According to the criteria for positivity applied in this thesis (see Section 2.5.4) the control was considered negative. Overall the results showed that, by means of pelleting by ultracentrifugation, it was possible to reliably retrieve seeding activity in spikes diluted from $1x10^{-3}$ to $1x10^{-6}$ with lag times increasing with the increasing dilution of the reference standard. True positive signals were also observed in individual wells seeded with spikes diluted at $1x10^{-7}$, 10^{-8}, 10^{-10}, 10^{-11}. As these signals occurred in less than 50% of the replicated wells, the samples were considered negative.

The pelleting procedure was then applied to actual urine samples. In this instance one non-CJD urine samples (*i.e.* -Ctrl 1) and three sCJD urine samples (*i.e.* U1, U2, U3) were assayed along with a standard positive control and unseeded samples (Figure 5.3 B). TP signals were observed in two out of six PBS seeded wells while no signals were observed in the negative control and the positive control presented with a t_{Lag} of 8.49±0.24 hours. Of the three sCJD urine samples assayed, only one out of six reaction wells seeded with sample U1 showed TP signal while exactly 50% of the

wells seeded with sample U2 or U3 did. Therefore, none of the sCJD urine samples tested fulfilled the criteria for positivity used in this thesis (see Section 2.5.4).

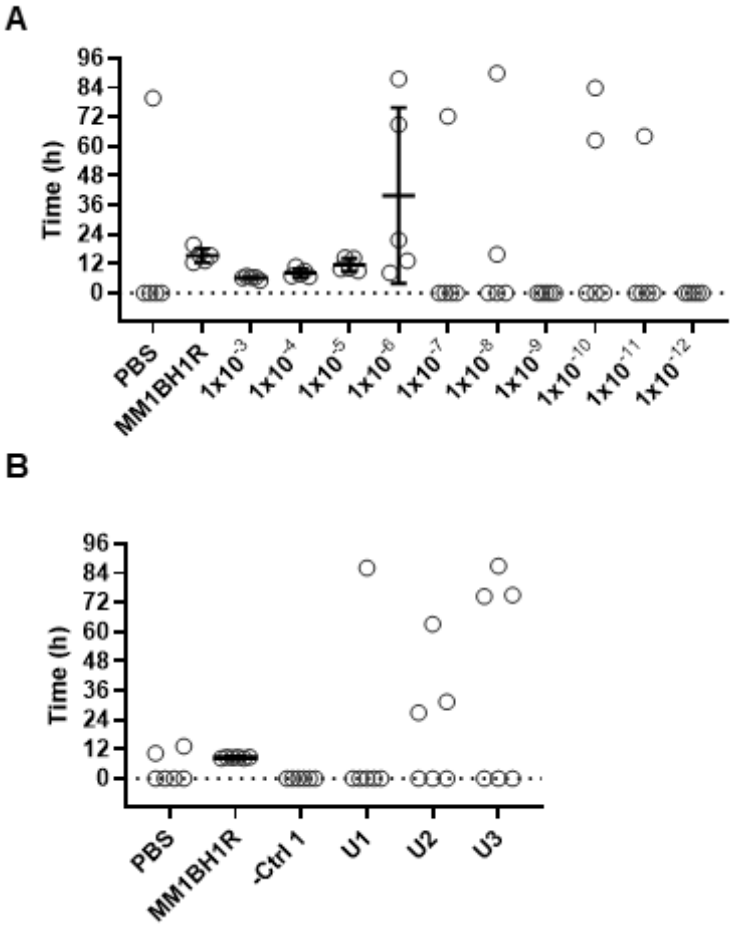

Figure 5.3 RT-QuIC analysis of urine following PBU

Data points indicate the time to threshold for each technical replicate (N = 6) per individual sample. Bars indicate the mean average (*i.e.* t_{Lag}) and standard deviation calculated for those samples showing signals in more than 50% of the technical replicates. In [A] PBS spiked with sCJD 10%BH MM1BHR from 10^{-3} to 10^{-12}, pelleted by ultracentrifugation and used to seed RT-QuIC. In [B] three sCJD urine samples (*i.e.* U1, U2, U3) and one non-CJD urine sample (*i.e.* –Ctrl 1). PBS) unseeded sample; MM1BH1R) positive control.

5.3.2 RT-QuIC analysis of urine following IOME

The ability of the paramagnetic iron oxide beads to bind and extract prion seeding activity from samples during Iron Oxide Magnetic Extraction (IOME) was tested on PBS spiked with sCJD 10%BH MM1BH1R at dilutions ranging from 10^{-1} to10^{-12}. Beads incubated overnight with PBS only (*i.e.* IOME PBS) were also assayed in the experiment. The IOME PBS sample had a double function, to act as negative control to the spikes and, when compared with the unseeded sample (*i.e.* PBS), to assess whether the presence of the beads effected the spontaneous aggregation of the reaction substrate. A standard positive control (*i.e.* 2 µL of dilution of MM1BH1R containing 100 fg of PrP^{res}) was tested as well (Figure 5.4 A).

No TP signals were observed in the unseeded sample, whereas two wells out of five seeded with PBS IOME did show TP signals. The PBS IOME sample was deemed negative because TP signals were detected in less than 50% of the technical replicates, however, this result suggested that the iron oxide beads did promote the misfolding and aggregation of the unseeded reaction substrate (Figure 5.4 A).

The results obtained from reaction wells seeded with beads that were incubated with sCJD urine reference standard, showed that by means of IOME it was possible to extract RT-QuIC detectable seeding activity from dilutions of 10% BH ranging from $1x10^{-1}$ to $1x10^{-6}$. Seeding activity was also detected in reactions seeded with beads incubated $1x10^{-8}$ to $1x10^{-11}$ dilution of sCJD 10% BH (Figure 5.4 A). Next, three non-CJD urine samples and seven sCJD urine samples were treated with IOME and the beads used to seed the RT-QuIC reaction (Figure 5.4 B). Adopting the criteria for positivity used in this thesis (see Section 2.5.4) the RT-QuIC analysis of these samples resulted in one false positive out of three negative controls and four false negatives out of seven sCJD urine samples. Based on these results, the RT-QuIC

analysis of IOME treated urine samples show a sensitivity of 42.9% and a specificity of 66.6% in discriminating sCJD from non-CJD urine samples.

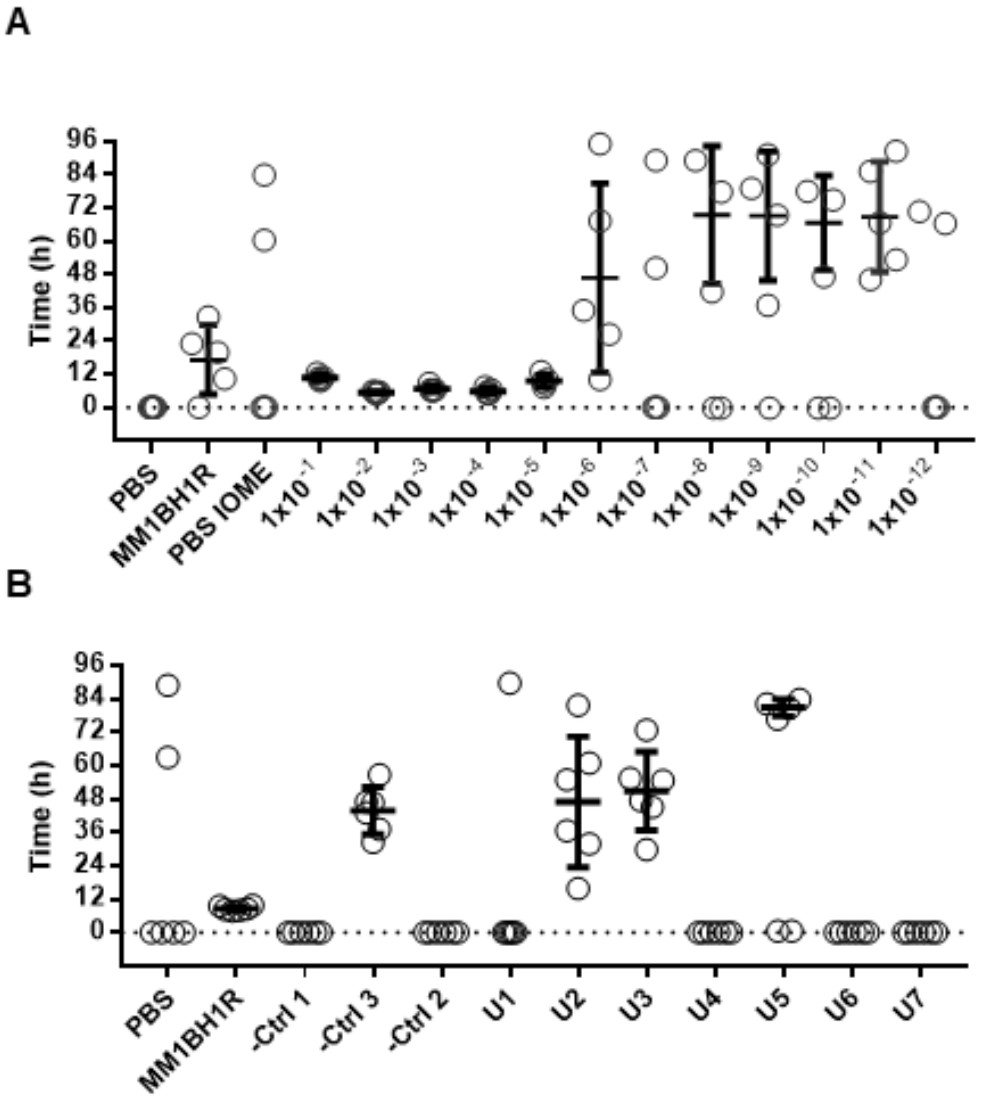

Figure 5.4 RT-QuIC analysis of IOME treated samples

Data points indicate the time to threshold for each technical replicate per individual sample that crossed the Thr. Bars indicate the mean average (*i.e.* t_{Lag}) and standard deviation calculated on the replicated wells that crossed the Thr for each samples showing TP signals in more than 50% of the technical replicates (N = 5). In [A] PBS samples spiked with sCJD 10%BH MM1BHR from 10^{-1} to 10^{-12} were incubated with iron oxide beads and the beads used to seed RT-QuIC. PBS IOME) RT-QuIC reaction seeded with beads incubated with PBS only. In [B] three non-CJD urine samples (-Ctrl 1, 2 and 3) and 7 sCJD urine sample (U1-U7) were treated iron oxide beads and the beads used to seed RT-QuIC. PBS) unseeded sample; MM1BH1R) positive control.

5.4 Discussion

The results presented in this Chapter represent a first attempt at investigating the use of RT-QuIC to discriminate sCJD from non-CJD urine samples. With respect to the RT-QuIC conditions employed when seeding the reaction with sCJD brain material or CSF, no modifications were introduced in the RT-QuIC reaction in terms of temperature, shaking frequency, reaction buffer and reaction substrate, while two different methods were investigated to prepare the samples to be tested. These methods were deployed with the aim of concentrating (*i.e.* pelleting) or extracting (*i.e.* IOME) seeding activity from the samples prior to RT-QuIC analysis.

Both methods were first tested on reference standard sCJD urine generated by diluting a sCJD 10%BH in PBS and the two methods produced different results. When using the pelleting method, seeding activity was detected at dilutions down to $1x10^{-6}$ with individual reaction wells presenting with TP signals beyond this dilution point (Figure 5.3 A). In contrast, the iron oxide beads used for IOME, were able to extract seeding activity from samples diluted down to $1x10^{-11}$ (Figure 5.4 A). There was an anomaly at the dilution 10^{-7} where, TP signals in two out of five technical replicates were observed. In addition, judging from the results observed for the PBS IOME sample, the presence of the beads appeared to increase the spontaneous aggregation propensity of the substrate.

The low sensitivity achieved with the pelleting method was also observed upon analysis of actual urine samples. Of the three sCJD urine samples tested, none tested positive using the criteria adopted in this thesis. It is to be noted, however, that for two out three of the sCJD urine samples tested (*i.e.* U2 and U3) exactly 50% of the technical replicates showed TP signals (Figure 5.3 B). This result suggests that less stringent criteria for positivity might be better suited to analyse the results of this test.

Similarly, the characteristics of the IOME method deduced from the analysis of the sCJD urine reference standard (*i.e.* high sensitivity and positive effect on the spontaneous aggregation of the substrate) were confirmed upon analysis of actual urine samples. When using the IOME method, seeding activity was detected in three out seven of the sCJD urine samples, but also in one out three of the negative controls (Figure 5.4 B). Interestingly, of the three sCJD urine samples that tested positive, two (*i.e.* U2 and U3) showed TP signals in 50% of the technical replicates when the pelleting method was used. Considering the small sample size, the IOME method coupled with RT-QuIC appears to be 42.9% sensitive and 66.6% specific in discriminating sCJD urine samples from non-CJD ones.

Taken together, these data suggest that coupling RT-QuIC with specific sample preparation strategies and a *post hoc* study for the selection of specific criteria for positivity, may have the potential to achieve the discrimination of sCJD from non-CJD urine samples. In particular, the IOME method used in this study appears to be more promising than the one based on urine samples pelleting. Further experiments are needed to confirm these results and to explore the possibility of achieving levels of sensitivity and specificity that will allow the development of a sCJD diagnostic test based on urine analysis by RT-QuIC.

Chapter 6: General Discussion

6.1 Overview of the results obtained

The overarching aim of this thesis was to describe and compare the *in vitro* human prion amplification by PMCA and RT-QuIC and to extend the diagnostic applicability of the latter, which is currently employed for the diagnosis of sCJD. The results presented in Chapter 3 show that vCJD samples, when assayed in PMCA, showed a more robust seeding activity compared to the seeding activity of sCJD samples and that, among the sCJD samples, sCJD subtype VV2 showed the highest seeding activity. Conversely, when assayed in RT-QuIC using the FLHa-rPrP substrate, the vCJD samples did not show any seeding activity while the sCJD samples showed a robust seeding activity irrespective of the sCJD subtype. Moreover, for the first time, PMCA and RT-QuIC reaction kinetics were compared using a specifically designed protocol and the same benchmark seed (*i.e.* sCJD VV2). In Chapter 4, a biochemical analysis of the RT-QuIC reaction products obtained by seeding the reaction with sCJD brain and CSF samples was presented. The results show that in term of the extent, abundance and electrophoretic mobility of the PK resistant core of the RT-QuIC products no sCJD subtype- or seed-specific differences were apparent (Piconi et al. 2019). Moreover, the RT-QuIC reaction was optimised and deployed to investigate the possibility of developing a clinical diagnostic test for sCJD based on the analysis of patient urine samples. The results of the latter study are presented in Chapter 5 and show that coupling RT-QuIC with specifically designed sample preparation and data analysis methods may allow the discrimination of sCJD urine samples.

6.2 Molecular characterization of human prion amplification in cell-free systems

As discussed in Chapter 3, PMCA preference for vCJD over sCJD appears to be a general feature of the method, irrespective of the set-up used (Moda *et al.*, 2014; Concha-Marambio *et al.*, 2016; Barria *et al.*, 2018; Cali *et al.*, 2019). Likewise, the

efficient amplification of sCJD VV2 by PMCA, has been reported by other authors (Barria 2014; Jones et al. 2008) and appears to be in line with the results obtained from transmission studies using the transgenic mouse line which was the source of the PMCA substrate for the experiments presented in this thesis (Bishop, Will, and Manson 2010). The results obtained with RT-QuIC instead appear to be specific to the RT-QuIC set-up based on the substrate FLHa-rPrP (used in this thesis) as well as of the RT-QuIC set-ups based on substrates 90-231Ha-rPrP, FLHu-rPrP and hamster sheep chimeric rPrP (Peden et al. 2012; Orrù et al. 2015b; Levavasseur et al. 2017). The evidence indicating that the symmetry between PMCA and RT-QuIC in amplifying variant or sporadic CJD prions can be overcome by modification of the PMCA (*i.e.* deglycosylaton) and RT-QuIC (*i.e.* use of FLBV-rPrP) reaction substrates, suggests a pivotal role for this component in both the methods (Orrù et al. 2015b; Camacho et al. 2019).

However, the idea that the substrate is the only major factor shaping PMCA and RT-QuIC *in vitro* amplification of human prions might be simplistic as there is evidence indicating that the two *in vitro* reactions utilize their respective substrate in different ways. Specifically, in RT-QuIC sequence homology between seed and substrate is not mandatory to obtain amplification, while in PMCA, it is a key factor influencing the efficiency of amplification (Barria 2014; Jones et al. 2008; Camacho et al. 2019).

Therefore, other factors should be taken into account to attempt a mechanistic description of the observed differential amplification preferences of PMCA and RT-QuIC for vCJD or sCJD. Among these factors are the molecular characteristics of the seeds. Indeed, sCJD and vCJD can be discriminated, at a molecular level, based on the different glycotype of the respective PrP^{res}. The PrP^{res} found in sCJD, irrespective of being type 1 or type 2, typically presents, upon standardized WB analysis, a relative over-representation of the monoglycosylated form (termed pattern A) while

the PrP^{res} found in the vCJD cases analysed so far is typically of type 2 and shows a relative over-representation of the diglycosylated form (termed pattern B) (Head 2013). The latter pattern is also typical of the classical BSE (Hill et al. 1997; Bruce et al. 1997), while it has been suggested that the former (*i.e.* pattern A) characterizes rarer, atypical forms of BSE (Casalone et al. 2004; Biacabe et al. 2004). Interestingly, PMCA amplification preference for vCJD over sCJD is mirrored by its preference for classical BSE over the atypical forms of BSE (Barria et al. 2014). Remarkably, several RT-QuIC set-ups (*i.e.* those using full-length and truncated forms of hamster rPrP or FLHu-rPrP) show a symmetrical trend, being more efficient than PMCA at amplifying sCJD and the atypical forms of BSE (Levavasseur et al. 2017; Masujin et al. 2016). Collectively, this evidence appears to suggest that PMCA preferentially amplifies pattern B seeds while RT-QuIC preferentially amplifies pattern A. This observation allows speculation regarding the role of seed glycosylation in shaping prion *in vitro* amplification. Specifically, it appears that less heavily glycosylated seeds (*i.e.* pattern A) are amplified more efficiently by an unglycosylated substrate (*i.e.* a rPrP or deglycosylated PrP^{C} as in Camacho *et al.*, 2019), while more heavily glycosylated seeds (*i.e.* pattern B) are amplified more efficiently by a glycosylated substrate (*i.e.* the typical PMCA substrate). As above-mentioned, results presented in Chapter 3, show for the first time a comparative analysis of PMCA and RT-QuIC reaction kinetics when amplifying the same seed. Notably, both the reaction kinetics show a sigmoidal shape, with an initial lag phase followed by a rise to reach a plateau phase, that is typical of protein misfolding and aggregation. However, as discussed in Chapter 3, the systematic comparison of PMCA and RT-QuIC reaction kinetics is limited by the technical differences between the detection systems of the two methods as well as by the biochemical characteristics of the substrates used. Nonetheless, the identification of the sCJD subtype VV2 as benchmark seed amplified by both methods, offers the possibility to further compare the two methods and possibly

elucidate the role of seed glycosylation and substrate modifications in PMCA and RT-QuIC.

PMCA and RT-QuIC also differ in regard to the characteristics of the respective amplification products. The experimental inoculation of the products of PMCA reaction seeded with animal and human prion strains, suggest that the material generated *in vitro* is able to reproduce the disease phenotype of the original prion strain (Castilla et al. 2008; Cali et al. 2019). In contrast, Scrapie-seeded RT-QuIC reaction products do not appear to be infectious upon experimental inoculation into animal models (Groveman et al. 2017). Moreover, the amplification by PMCA of vCJD and sCJD samples, generate products, which, upon PK digestion and standardized WB analysis, present with the same PrP^{res} type of the original seed (Jones et al. 2008; Barria et al. 2014). Conversely, it is not clear, at this point in time, to what extent the characteristics of the original seed are retained in the RT-QuIC reaction products (Sano et al. 2014; Piconi et al. 2019). The results presented in Chapter 4 suggest that the RT-QuIC set-up using the FLHa-rPrP, when seeded with sCJD 10%BH or CSF samples, generates products that resemble naturally occurring PrP^{Sc} in being resistant to limited PK treatment. Nonetheless, no sCJD subtype-specific differences in terms of the electrophoretic mobility, abundance or extent of the PK resistant core were observed *via* the epitope mapping analysis of the protease resistant products presented in the same Chapter (Piconi et al. 2019). In this framework of evidence, it is plausible that the above-mentioned differences in PMCA and RT-QuIC reactions products might be explained, at least in part, by the different composition of PMCA and RT-QuIC reaction environments. On the one hand, PMCA reaction environment seems to resemble the cellular environment more closely and, therefore, allows PMCA to more accurately model the complete set of properties (*i.e.* biochemical properties, infectivity, species barrier, strain phenomenon) that the natural prion

replication mechanism reproduces each time prions replicate. On the other hand, the RT-QuIC reaction environment is much simpler and appears to be a distillation of the basic elements (*i.e.* seed, substrate, energy input) needed for reproducing prion replication process. It is also to be noted that the RT-QuIC reaction environment, in spite of being seeded with brain material, might not contains, at an high enough concentration, the cofactors known to be needed in order to produce infectious preparations *in vitro* from rPrP (Noble and Supattapone 2015) In this way, RT-QuIC appears to model basic functional properties of prions, specifically the ability to induce the misfolding of homologous proteins (*i.e.* seeding activity). The idea that the prion defining properties, such as seeding activity and infectivity, may exist independently from one another is at the basis of the deployment of the prion concept to proteins other than PrP. The successful design and deployment of RT-QuIC set-ups based on prion-like proteins (*i.e.* proteins characterized by certain prion defining properties) appears to sustain this idea (Fairfoul et al. 2016; Groveman et al. 2018; Saijo et al. 2017).

6.3 Diagnostic application of human prion amplification in cell-free systems

The diagnosis of sCJD has significantly improved in the last 20 years, thanks to technological advancements in brain imaging, the development of biomarker assays including the CSF analysis by RT-QuIC and improved knowledge of the disease phenotypic spectrum (reviewed in Zerr and Parchi, 2018). However, the *post mortem* examination of brain tissue remains the gold standard method for confirming a sCJD diagnosis as well as for the identification of sCJD subtypes. In this context, the development of diagnostic tests based on the analysis of body fluid more accessible than CSF and/or able to discriminate sCJD subtypes *intra vitam*, represent desirable further improvements. Although no treatment is currently available for sCJD, the definition of the sCJD subtype *intra vitam* would inform patient and caregivers more

precisely on the disease outlook, as well as aid the stratification of patients upon recruitment in future clinical trials. The hypothesis investigated in Chapter 4 addresses the discrimination of sCJD subtypes by systematically investigating the resistance to limited proteolysis and the length of the PK resistant fragments of the RT-QuIC products generated when seeding the reaction with brain or CSF samples of the six most common sCJD subtypes. The results showed that, for the characteristics investigated, no subtype-specific differences were apparent. As discussed in Chapter 4, this evidence allows speculation that sCJD brain and CSF samples may share a component that induces the misfolding and aggregation of the rPrP substrate into structurally similar aggregates. Indeed there is evidence indicating that sCJD CSF samples may contain disease-specific PrP aggregates (Bieschke et al. 2000). However, these aggregates have not been further characterized and, therefore, cannot be unequivocally related to the PrP^{Sc} found in sCJD brain samples. An alternative explanation for the results obtained might be that the highly ordered conformational landscape of the purified FLHa-rPrP substrate does not allow the selection of subtype-specific conformational pathways within the time frame of the reaction kinetics. Applying the RT-QuIC product analysis method developed here to the products of the second generation RT-QuIC (Orrù et al. 2015a), might possibly address this latter point. In fact, second generation RT-QuIC uses 90-231Ha-rPrP instead of the FLHa-rPrP as reaction substrate and there is evidence indicating that, the shape of the second generation RT-QuIC reaction kinetic seeded with sCJD CSF samples are subtype-specific (Foutz et al. 2017) therefore might represent structural differences in the generated aggregates.

The possibility of using olfactory mucosa (OM) samples from sCJD patients to seed RT-QuIC is a promising alternative or complementary option to CSF. OM can be sampled with relatively non-invasive methods (*i.e.* nasal brush or swab) and it has

been shown that its analysis *via* RT-QuIC has diagnostic value for sCJD (Bongianni et al. 2017; Orrù et al. 2014). The hypothesis addressed in Chapter 5, instead, represents a first step in extending RT-QuIC diagnostic applicability to urine, one of the more easily sampled human biological fluids. The results obtained showed for the first time that the application of specifically designed sample preparation procedures, allow to observe seeding activity in sCJD urine samples by RT-QuIC. However, the levels of specificity and sensitivity achieved were not high enough to confer reliable diagnostic power to the assay. While these data can be considered a proof of concept, it is important to remark that the seeding activity observed in the sCJD urine samples examined should not raise public health concerns. In fact, it cannot be unequivocally assigned to the presence of a prion-specific seeding active component. Moreover, even in the case that a prion-specific seeding active component is responsible for the observed seeding activity in sCJD urine, it would be present at very low concentration and very likely be unable to transmit the disease. Indeed, as already shown by other authors, experimental inoculation of sCJD urine samples does not elicit disease transmission (Brown et al. 1994; Notari et al. 2012).

Nonetheless, these data demands further investigation to ascertain the presence or the complete absence of seeding activity in sCJD urine would be valuable information. On the one hand, the complete absence of prion-specific seeding activity in sCJD urine would further refine the description of this disease and highlight another difference with vCJD. Indeed, it has been shown that vCJD urine samples can seed the PMCA reaction (Moda et al. 2014) and, therefore, be discriminated from non-CJD urine samples. On the other hand, the reliable detection of seeding activity in sCJD urine may represent a further reduction of the invasiveness of the diagnostic sampling for the most common form of human PrD.

6.4 General conclusions

The *in vitro* human prion amplification by PMCA and RT-QuIC represents an invaluable tool for prion research and clinical diagnosis of PrD. Through the research performed for this thesis, it has been possible to: (i) systematically evaluate PMCA and RT-QuIC amplification of vCJD and sCJD, (ii) compare for the first time the kinetics of the two reactions, (iii) investigate the possible discrimination of sCJD subtype by RT-QuIC, and (iv) assess the possibility of generating a sCJD diagnostic test based on the RT-QuIC analysis of patient urine samples. In summary, the work presented in this thesis provide insights into the molecular mechanisms of the *in vitro* amplification of human prions and highlights its diagnostic applicability.

Appendix I

Part of the data presented in this thesis were published in a scientific journal. The article is reproduced in this appendix.

Piconi G., Peden A.H., Barria M.A., Green A.J.E. (2019) Epitope mapping of the protease resistant products of RT-QuIC does not allow the discrimination of sCJD subtypes. PLoS ONE 14(6): e0218509. https://doi.org/10.1371/journal.pone.0218509

PLOS ONE

RESEARCH ARTICLE

Epitope mapping of the protease resistant products of RT-QuIC does not allow the discrimination of sCJD subtypes

Gabriele Piconi*, Alexander H. Peden, Marcelo A. Barria, Alison J. E. Green

The National CJD Research & Surveillance Unit, Centre for Clinical Brain Sciences, University of Edinburgh, Edinburgh, Scotland, United Kingdom

* s1576892@ed.ac.uk

OPEN ACCESS

Citation: Piconi G, Peden AH, Barria MA, Green AJE (2019) Epitope mapping of the protease resistant products of RT-QuIC does not allow the discrimination of sCJD subtypes. PLoS ONE 14(6): e0218509. https://doi.org/10.1371/journal.pone.0218509

Editor: Ina Maja Vorberg, Deutsches Zentrum fur Neurodegenerative Erkrankungen, GERMANY

Received: April 4, 2019

Accepted: June 4, 2019

Published: June 17, 2019

Data Availability Statement: All relevant data are within the manuscript and its Supporting Information files.

Funding: This work was funded by the Department of Health and Social Care Policy Research Programme and the Scottish Government (PR-ST-0614-00008; GP, AHP, MAB and AJEG); the funders had no role in study design, data collection and analysis, decision to publish or preparation of manuscript.

Abstract

Sporadic Creutzfeldt-Jakob disease (sCJD) is a transmissible, rapidly progressive and fatal neurodegenerative disease. The transmissible agent linked to sCJD is composed of the misfolded form of the host-encoded prion protein. The combination of histopathological and biochemical analyses has allowed the identification and sub-classification of six sCJD subtypes. This classification depends on the polymorphic variability of codon 129 of the prion protein gene and the PrP^{res} isotype, and appears to be associated with neuropathological and clinical features. Currently, sCJD subtyping is only fully achievable *post mortem*. However, a rapid and non-invasive method for discriminating sCJD subtypes *in vita* would be invaluable for the clinical management of affected individuals, and for the selection of participants for clinical trials. The CSF analysis by Real Time Quaking Induced Conversion (RT-QuIC) reaction is the most sensitive and specific *ante mortem* sCJD diagnostic test available to date, and it is used by a number of laboratories internationally. RT-QuIC takes advantage of the natural replication mechanisms of prions by template-induced misfolding, employing recombinant prion protein as reaction substrate. We asked whether epitope mapping, of the RT-QuIC reaction products obtained from seeding RT-QuIC with brain and CSF samples from each of the six molecular subtypes of sCJD could be employed to distinguish them and therefore achieve *in vita* sCJD molecular subtyping. We found that it is possible to distinguish the RT-QuIC products generated by sCJD biological samples from the ones generated by spontaneous conversion in the negative controls, but that different sCJD subtypes generate very similar, if not identical RT-QuIC reaction products. We concluded that whilst RT-QuIC has demonstrable diagnostic value it has limited prognostic value at this point in time.

Introduction

Prions are the infectious agents associated with Transmissible Spongiform Encephalopathies (TSEs) or prion diseases. Prion diseases are transmissible, rapidly progressive and invariably fatal neurodegenerative diseases affecting humans and other mammals. According to the

Competing interests: The authors have declared that no competing interests exist.

protein only hypothesis [1,2], prions are constituted by the misfolded form of the host prion protein (PrP^{C}), a copper binding glycoprotein bound by a glycophosphastidyl-inositol (GPI) anchor to the outer leaflet of cell membranes, which is constitutively expressed in the central nervous system (CNS).

The misfolded PrP scrapie (PrP^{Sc}) isoforms, replicates inside a host by imposing their conformation on PrP^{C}. The conformational change of PrP^{C} to PrP^{Sc} makes the latter insoluble in non-denaturing detergents and partially resistant to proteases such as protease K (PK), a broad-spectrum serine and threonine protease. PK is routinely used in prion research because the product of the digestion of PrP^{Sc} with PK, referred to as resistant PrP (PrP^{res}), is used for the molecular characterisation of prion diseases [3].

In humans, the most common form of prion disease is sporadic Creutzfeldt-Jakob disease (sCJD) accounting for 85%-90% of all human prion disease cases. The remaining 10–15% of human prion disease cases are mainly due to genetic forms, linked to point or insertional mutations in the prion protein gene *PRNP*. Although of high concern to public health, acquired forms, due to inadvertent human-to-human transmission or zoonotic transmission, are the rarest [4,5].The clinical presentation and disease course of sCJD, broadly correlate with six molecular subtypes usually referred to as sCJD MM1/MV1, MM2c (c for cortical), MM2t (t for thalamic), MV2, VV1, and VV2. Currently, the biochemical identification of sCJD subtypes is achieved *post mortem*, as it requires the analysis of brain tissue samples. These sCJD biochemical subtypes are defined by the genotype at *PRNP* polymorphic codon 129 (encoding methionine [M] or valine [V]) in combination with the molecular weight of the unglycosylated PrP^{res} found in brain tissue samples and scored by western blot (WB) with an anti-PrP monoclonal antibody [6,7] (Type 1 = 19 kDa, Type 2 = 21 kDa). Animal studies have shown that these six sCJD subtypes comprise four major human strains of prions (M1, M2, V1, V2) as defined by the length of incubation time, susceptibility and disease phenotype in selected inbred strains of mice as well as the conservation of characteristic neuropathological lesion patterns upon serial passage in the same host [8,9].

To explain the phenotypic characteristic of different strains, it has been proposed that these are enciphered within a subset of all the possible PrP^{Sc} conformations and their interaction with the cellular milieu [10]. A corollary to this hypothesis, is that the two PrP^{res} types, the discrimination of which contribute to sCJD biochemical subtyping, might arise from different PrP^{Sc} conformations that in turn dictate which sites on the structure of PrP^{Sc} are available to PK activity.

Cell-free conversion (CFC) systems are methodologies that emulate prion replication *in vitro*. CFCs were originally developed to test the protein only hypothesis [11] and investigate prion biology [12,13] and have subsequently found application in clinical practice as an aid to prion disease diagnosis. The Real Time Quaking Induced Conversion reaction (RT-QuIC) is a 96-well plate-based CFC system. It is characterised by the use of bacterially expressed and purified recombinant prion protein as reaction substrate. Heat and intermittent shaking are the energy inputs and the registered output signal consists of fluorescence readings over time. The fluorescent signal output is provided by the amyloid-specific dye Thioflavin T (ThT), which is present in the reaction mixture. When a prion containing sample (termed seed) is present, it induces the recombinant substrate to alter its conformation and form ThT binding-competent aggregates. Ultimately, RT-QuIC signal output is an indirect observation of the kinetics of the prion induced misfolding and aggregation of the recombinant substrate.

Since its first introduction, RT-QuIC has been applied to human prion disease diagnosis [14–16]. To maximize RT-QuIC diagnostic specificity (i.e. minimize false positive), efforts have been put into optimising the RT-QuIC reaction conditions to increase the kinetic difference between sCJD and non-CJD seeded reactions as well as to avoid the spontaneous

aggregation of the recombinant substrate in unseeded reactions.These efforts resulted in the optimisation and international harmonisation of an *ante mortem* sCJD diagnostic RT-QuIC protocol, based on cerebrospinal fluid (CSF) analysis [17,18].

A widely used and characterised substrate for the sCJD RT-QuIC diagnostic protocol is the full-length hamster prion protein (a.a. 23–231) [19]. However, by adapting the reaction conditions, recombinant prion protein from other mammals have been used, highlighting the flexibility of RT-QuIC in its ability to detect human and non-human prions from different sources [20][21].

RT-QuIC has shown to be the most sensitive and specific *ante mortem* diagnostic test for sCJD available at this point in time, prompting researcher to ask whether it might be employed to discriminate sCJD subtypes. The discrimination of the sCJD subtypes by RT-QuIC would provide an outlook on the disease progressionas well as diagnostic information, which would inform the clinical management of affected individuals. Moreover, sCJD molecular subtypes ascertained *in vita* could be used as inclusion criteria for the recruitment of patients into future clinical trials.

Testing a limited number of sCJD brain samples, Peden and colleagues [22], firstly reported a lower RT-QuIC seeding potency for the rarer sCJD subtypes MM2 and VV1 when compared with the more common MM1 / MV1 subtype. In subsequent studies, however, the stratification of sCJD diagnostic RT-QuIC results (i.e. the RT-QuIC analysis of sCJD CSF samples) obtained from multiple laboratories, by either codon 129 genetic status, or sCJD subtype, showed little or no differences in terms of specificity and sensitivity [23–25]. In contrast, a recent adaptation of RT-QuIC, employing an N-terminally truncated form of the Hamster recombinant PrP (i.e. 90-231Ha-rPrP) as a reaction substrate, revealed sCJD subtype-specific kinetics of aggregation, when reactions were seeded with CSF samples [26]. Adding to this, there is evidence that the misfolded form(s) of recombinant PrP generated during the RT-QuIC reaction (herein referred to as RT-QuIC reaction products) can retain structural features of the prion seed that generated them allowing for their *in vitro* identification [27–29]. These findings suggest that sCJD subtypes may be discriminated by RT-QuIC based on the biochemical characteristics of the generated aggregates, however it is not clear at this point in time whether the commonly employed routine CSF analysis by RT-QuIC can be extended to subtype sCJD using the same criteria used for post-mortem PrP^{res} subtyping from brain tissue. Or to put the same point in more theoretical terms: whether conformational and perhaps even strain characteristics are conserved during quaking induced conversion.

By seeding the diagnostic RT-QuIC reaction with brain and CSF samples accounting for the most common sCJD subtypes (MM1/MV1, MM2, MV2, VV1, VV2), we have analysed the RT-QuIC reaction products for their resistance to limited proteolysis and investigated the length of the resistant fragments via epitope mapping using a set of six commercially available antibodies, including those usually employed for sCJD molecular typing.

Materials and methods

Biological samples and sample inclusion criteria

All the human biological samples were provided by the National CJD Research and Surveillance Unit (NCJDRSU) Brain and Tissue Bank in Edinburgh, UK (part of the MRC Edinburgh Brain Bank) ethical approval (Scotland A REC 05/MRE00/67, Edinburgh Brain Bank 16-ES-0084). The inclusion criteria for the sCJD and non-CJD samples used in this study were based on of the appropriate consent for research for each individual case and the availability of frozen tissue. The cases selected comprised three frozen brains each of sCJD subtypes MM1, MM2, MV1, MV2, VV2 and two of subtype VV1 (using the Parchi subtypes nomenclature; 6).

In addition, one case reported to the NCJDRSU with neurological symptoms but no signs of prion disease (non-CJD) following pathological investigation, was selected as negative control. Small pieces of frontal cerebral cortex were sampled from all the above-mentioned cases.

The collected tissue samples were homogenised to 10% weight/volume in Phosphate Buffered Saline (PBS) supplemented with 150 mM NaCl, 1 mM ethylene-diamine-tetra-acetic acid (EDTA), 0.5% Triton X-100 and Complete Protease Inhibitor (Roche) using a FastPrep-24 automated homogeniser (MPbio) and lysing matrix D.

The levels of PrP^{res} in each 10% brain homogenate (10% BH) was evaluated by densitometric analysis following Western blot (WB) analysis using purified recombinant PrP as a standard. The amounts of brain used to seed individual RT-QuIC reactions were normalised to 100 fg of PrP^{res}. All the 10%BH were diluted in PBS, the range of 10%BH dilution factors used after normalisation was from $10^{-3.8}$ to $10^{-5.7}$ and the mean of this dilution factor range was adopted as the dilution factor for the non-CJD 10%BH used as negative control. PBS was used in the unseeded samples as a control for the spontaneous aggregation of the substrate.

CSF samples were selected on the basis of volume availability, testing positive in a previous RT-QuIC analysis and being from patients with neuropathologically-confirmed sCJD with a known sCJD subtype. The selected CSF sample set included three examples of sCJD MM1, MV2 and VV2 and two examples of MV1 and MM2 (cortical rather than thalamic variant). Two additional CSF samples were selected as negative controls based on being assigned with diagnosis of a non-prion related neurological disease, sample volume availability and testing negative in a previous RT-QuIC analysis. A volume of 15 μL of neat CSF were used to seed individual reaction wells [17].

Recombinant full-length hamster prion protein purification

An individual batch of full-length Syrian Golden Hamster recombinant prion protein (FLHaPrP, residues 23–231) was purified and used in this study. Purification protocol was as previously described [11], in brief: Syrian Golden Hamster *PRNP* (accession K02234) expression and translation from transformed *Escherichia coli* Rosetta cells (Invitrogen), was obtained with Overnight Express Instant TB medium (Merck Novagen). Bacteria were collected and inclusion bodies (IB) isolated in pellets by means of Bug Buster Master Mix (Merck Novagen). IB pellets were resuspended and bound to Ni-NTA Superflow resin beads (Qiagen) in denaturing conditions. Protein was refolded on the column and subsequently eluted. Concentration was adjusted by means of Amicon Ultra-15 centrifugal Filter Units (Merck Millipore) and one millilitre aliquots were prepared, flash frozen and stored at -80˚C until use.

RT-QuIC reaction and collection of RT-QuIC reaction products

The RT-QuIC reaction was performed in a sealed 96 well plate with clear bottom (ThermoFisher) incubated at 42˚C for 90 h in a FLUOstar Optima (BMG Labtech) plate reader. During the incubation, the plate reader performed cycles of intermittent shaking (1 minute shake, 1 minute rest) and took fluorescence readings from the bottom of each well every 15 min (450 nm excitation, 480 nm emission, gain 2000) [17].

All the RT-QuIC reaction buffer components were purchased as concentrated stock solutions from Sigma-Aldrich and diluted in cell culture grade water. RT-QuIC reaction buffer composition was as follows: PBS (5 mM phosphate, 154 mM NaCl), 170 mM NaCl, 1 mM EDTA and 10 μM ThT. Because PBS contains NaCl, the final RT-QuIC reactions contained 324mM NaCl. Thioflavin T (ThT) solution was prepared monthly as a 10 mM solution which was syringe filtered through a 0.22 μm filter (Merck Millipore) and kept at +4˚C in the dark. Prior to use, ThT was diluted to 1 mM and used at a final concentration of 10 μM in the

RT-QuIC reactions. Recombinant FLHa-rPrP substrate was thawed (1 hour on ice followed by 30 minutes at room temperature) and filtered through a 100 kDa centrifuge filter (Nanosep, Pall). Following filtering, the concentration of the substrate was calculated from measures of absorbance at 280 nm taken on a dilution 1:2 in 0.1% sodium dodecyl sulphate in PBS (0.1% SDS/PBS) using a NanoDrop OneC (Thermo-Fisher), blanking with 0.05%SDS/PBS.

The FLHa-rPrP was then incorporated to the reaction buffer at 0.1 μg/μL, generating a bulk reaction mixture that was subdivided between reaction wells. The final reaction volume was 100 μL per well including seed. The RT-QuIC reactions were seeded with 15 μL of CSF or 2 μL of 10% BH serially diluted in PBS containing 100 fg of PrP^{res}. After preparing the RT-QuIC reaction plate, a volume of PBS accounting for the absence of seed (15 μL of CSF or 2 μL of 10% BH dilution) was added to the excess of reaction mixture. These mock reaction mixtures were then stored in 1.5 mL polypropylene tubes (APEX NoStick Alpha Laboratories) at -20˚C. These samples, termed "Mix", were used as RT-QuIC untreated controls in subsequent immunochemical analyses of the RT-QuIC reaction products.

At the end of each RT-QuIC, the sealed plate was extracted from the plate reader and left to equilibrate at room temperature. Condensation was spun down by centrifugation at 2505 x g for 1 min. The content of the wells was collected by carefully scraping the well surfaces with a disposable pipette tip, prior to transferring the liquid suspension to a storage tube. A minimum of six technical replicates per seed were prepared on an individual plate. Collected samples were stored in 1.5 mL polypropylene tubes (APEX NoStick Alpha Laboratories) at -20˚C until use.

SDS PAGE and Western blot

All SDS-PAGE analyses were performed using pre-cast 10% bis-tris gels (NuPAGE). Following preparation, samples were incubated at 100˚C for 10 minutes in sample loading buffer (LDS4X, NuPAGE) or in LDS4X supplemented with 2% volume/volume (v/v) 2-mercaptoethanol (LDS4XβMA) and loaded onto the gel. Electrophoretic separation was performed in MES-SDS buffer (NuPAGE) at 200V for between 35 and 45 minutes.

Gels were blotted on polyvinylidene fluoride membrane (BioRad Immun-Blot PVDF) by means of wet transfer (1 hour, 0.8 A constant) using Towbin buffer [30]. This system permitted the transfer of up to six gels onto one membrane [31]. Following transfer, PVDF membranes were blocked overnight in a 5% solution of non-fat dry milk in 0.1% Tween 20 Tris buffered saline (TBST). The following day, blocking solution was removed and at this stage, if multiple gels had been transferred onto the same membrane, the membrane was split into patches corresponding to individual gels. The membranes were incubated according to the conditions specific for the primary antibody of choice. Performing the analysis of primary antibodies on samples that had been transferred together increased the reliability of this comparison by eliminating any variation in transfer efficiency. At the end, each membrane was washed three times for 10 minutes with fresh TBST and subsequently incubated for 1 hour at RT and gentle shaking in a solution of horseradish peroxidase conjugated secondary antibody (Novex, Goat anti-Mouse IgG) 1:25000 in TBST. After one hour, the membrane was washed with two 10 minutes washes and two 5 minutes washes with TBST before applying enhanced chemiluminescence system (ECL Prime, Amersham). The signal was detected by digital imaging with ChemiDoc XRS+ (BioRad).

Monoclonal antibodies used

Anti-PrP monoclonal antibody (mAb) 3F4 (epitope 106–112, Hamster sequence) was purchased from Millipore as a 1 mg/mL solution and was used at a dilution of 1:10000. PrP^{res}

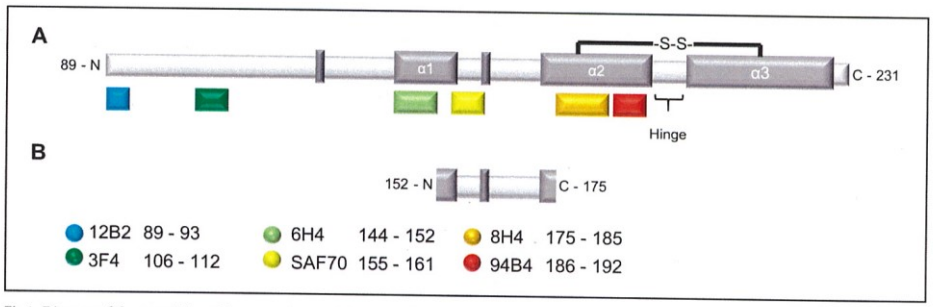

Fig 1. Diagram of the recombinant Hamster prion protein summarizing structural features and epitope locations. (A) diagram of the recombinant Hamster prion protein truncated at position 89. Dark grey boxes represent secondary structures. S-S indicates the disulphide bridge that connects alpha helix 2 (α2) to alpha helix 3 (α3) generating the hairpin loop. H indicates the hinge of the loop. Antibodies are listed and colour-matched with boxes indicating the location of the recognised epitope on the sequence. (B) Minimal extent of the fragment detected by SAF70 following PK digestion of sCJD seeded RT-QuIC products.

https://doi.org/10.1371/journal.pone.0218509.g001

Type 1 specific mAb 12B2 (epitope 89–93) and C-terminus specific 94B4 (epitope 186–192) were purchased from the Central Veterinary Institute at Wageningen University Netherlands, EU, as 1 mg/mL solutions and used at dilutions of 1:10000 and 1:1000, respectively. Monoclonal PrP specific mAb 8H4 (epitope 175–185, Abcam) was used at a dilution of 1:2000, while mAb 6H4 (epitope 140–152, Prionics) and mAb SAF70 (epitope 155–161, Bertin Pharma) were diluted 1:1000 (Fig 1A).

Limited proteolysis of RT-QuIC reaction products

For each digestion experiment, PK (Merck Millipore) was diluted fresh on the day from a glycerol stock to working stock in cell culture grade water. PK working stock concentrations were calculated to digest RT-QuIC reaction products with different amounts of PK. The final digestion volume included 76 μL of sample and 4 μL of a PK working stock solution. Digestions were carried out at 37˚C for 1 hour and stopped by placing the tubes on ice. PK activity was irreversibly inhibited by adding Pefabloc SC (Sigma-Aldrich) to 1.25 mM.

Products of PK digestion were methanol precipitated with 10 volumes of -20˚C 99.9% pure methanol (Fisher Chemicals). Samples, with added methanol, were thoroughly vortexed and incubated overnight at -20˚C. The following day samples were centrifuged for 35 minutes at 18200 x g (Eppendorf 5417R, rotor 06/09 HL128), the supernatant was discarded, and residual methanol evaporated by incubating the open tubes at 100˚C in a Class II microbiological safety cabinet. Pellets were resuspended in 42 μL of 0.1%SDS/PBS, half of the volume was moved to a fresh tube and added to an equivalent volume of either LDS4X/2%βMA (reduced samples) or LDS4X with no βMA (not reduced samples).

RT-QuIC data analysis

In experiments using 10%BH seeded RT-QuIC, in order to discriminate between fluorescence signal due to aggregation (signal) and the stochastic fluctuation of baseline fluorescence intrinsic to the RT-QuIC detection system (noise), a fluorescence threshold was calculated as equal to the average of the first fluorescence reading from each used well on a 96-well plate plus three standard deviations. Those reaction wells that produce three consecutive fluorescence readings equal or greater than threshold were deemed true positive signals and the time of the

third fluorescence reading equal or above threshold was termed Time to Threshold (TtoT). The CSF seeded RT-QuIC reaction results were analysed with reference to the diagnostic criteria as described in [17].

Results

Seeding RT-QuIC with sCJD brain homogenate dilutions: BH-RT-QuIC

Currently, the molecular typing of the different sCJD subtypes is based on the genotyping of *PRNP* polymorphic codon-129 and the evaluation of the electrophoretic mobility and glycoform ratio of PrP^{res} as is assessed by WB using mAb [6,7]. Broadly, the discrimination of two different unglycosylated PrP^{Sc} PK digestion products (i.e. PrP^{res} Type 1 21 kDa and Type 2 19 kDa) suggests that PK exerts its activity on, at the very least, two different PrP^{Sc} conformations that are generated and conserved during the prion replication process *in vivo*.

Our hypothesis was that if seeds from sCJD subtypes specifically induced different misfolded conformations of the recombinant substrate in the RT-QuIC reaction products, then we could detect these alternate conformations by means of proteolytic treatment (PK digestion) and WB.

To study this, we initially generated RT-QuIC reaction products using sCJD 10% brain homogenates (10%BH) as RT-QuIC seeds, and then analysed them for their resistance to PK digestion. In addition, the protease resistant regions of PrP in the RT-QuIC reaction products were assessed by means of epitope mapping. The selected sCJD and non-CJD controls (i.e. 10%BHs) seeds were assayed in two RT-QuIC experiments. The amount of material used to seed individual RT-QuIC reactions with different 10%BHs was normalised to 100 fg of PrP^{res} by diluting the 10% BHs in PBS and an individual batch of recombinant substrate was used. At least six replicate reactions were performed for each seed in the same experiment.

While the spontaneous aggregation of the substrate was never observed in the negative controls or in the unseeded reactions, all sCJD seeded reactions showed aggregation-associated fluorescence for at least two replicates, and 89.2% of all the sCJD seeded wells showed fluorescence above threshold. No significant subtype specific trend, however, was observed (Fig 2A).

To investigate our hypothesis that the conformation(s) of the RT-QuIC reaction products are dependent on seed subtype, we sought to preserve the integrity of the misfolded conformation assumed by the recombinant substrate during RT-QuIC. With this aim, we collected the contents of individual reaction wells without using any detergent or denaturant. Densitometric analysis following WB with anti-PrP monoclonal antibody (mAb) 3F4 showed that it was not possible to recover the totality of the input substrate from individual reaction wells (i.e. 10 μg of FLHa-rPrP per well) and that the efficiency of collection was highly variable. By washing the wells with 0.1%SDS/PBS, and performing densitometric analysis on the collected washes, it was possible to show part of the input substrate was adherent to the well surface. Pooling replicated wells together reduced collection variability and, on average, 60 to 70% of the input recombinant substrate per group of replicates per seed was recovered.

We then selected a panel of commercially available monoclonal antibodies to construct an epitope map of the RT-QuIC reaction products after proteolytic treatment with PK. The anti-PrP monoclonal antibodies (mAbs) sensitivity for detecting the RT-QuIC substrate (FLHa-rPrP) by WB was assessed. We found that the ability of mAbs 6H4, 8H4 and 94B4, (which are all directed towards PrP^{C} folded domains, Fig 1A), to detect of FLHa-rPrP was negatively affected by the presence of the reducing agent β-mercaptoethanol (Fig 3). Therefore, this component was excluded from the preparation of samples to be probed with these mAbs.

All the antibodies in our panel were able to detect the RT-QuIC reaction products prior to proteolytic treatment (S1A Fig). However, treating the RT-QuIC reaction products with PK at

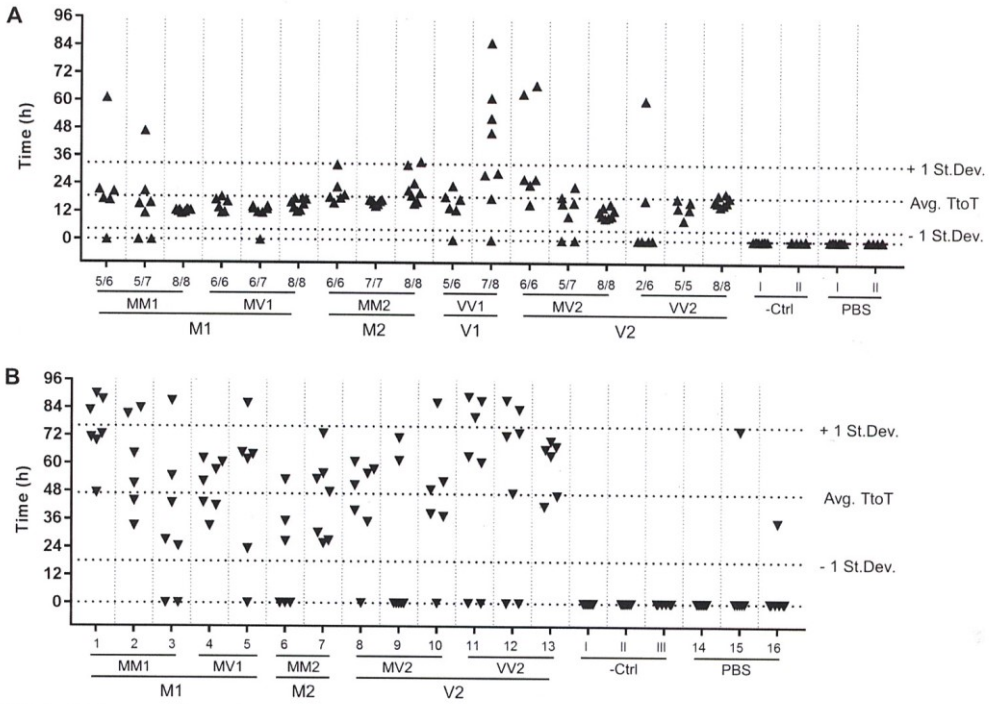

Fig 2. Graphical summary of the RT-QuIC reactions results. Each data point represents the time (in hours) at which an individual reaction well reached the threshold of fluorescence for positivity (Time to Threshold, TtoT). Technical replicates per individual seed are displayed in columns. Dashed lines mark the average TtoT +/- one standard deviation. (A) 10%BH seeded RT-QuIC (B) CSF seeded RT-QuIC. In both instances no subtype specific trend is observed.

https://doi.org/10.1371/journal.pone.0218509.g002

10 μg/mL abolished or dramatically reduced the detection signal from all of the mAbs except SAF70 (epitope 155–161, S1B Fig), which also showed readily detectable resistant prion protein fragments after treatment with higher concentrations of PK (Fig 4).

RT-QuIC reaction products treated with PK 10 μg/mL and probed with mAb SAF70, showed a reduction in the signal intensity of the band corresponding to the full-length RT-QuIC product as well as the appearance of additional bands. In particular, a new band was detected at ~ 22 kDa as well as a prominent band at ~10 kDa (Fig 4).

It should be noted that the 22 kDa band was also detected in the RT-QuIC untreated Mix samples, whereas the 10 kDa band was found to be specific to sCJD seeded reactions, as it was not observed in unseeded or non-CJD seeded reactions or in the RT-QuIC untreated Mix.

In addition, the 10 kDa band was detectable by SAF70 even following treatment with 30 and 50 μg/mL PK, whereas the 22 kDa band was eliminated with these treatments. When treating samples with 30 or 50 μg/mL PK, occasionally, very faint bands were detected by mAbs other than SAF70 at a molecular weight corresponding to the intact FLHa-rPrP and more rarely at 22 kDa and 17 kDa (S1C and S1D Fig). SAF70, however, detected a similar if not

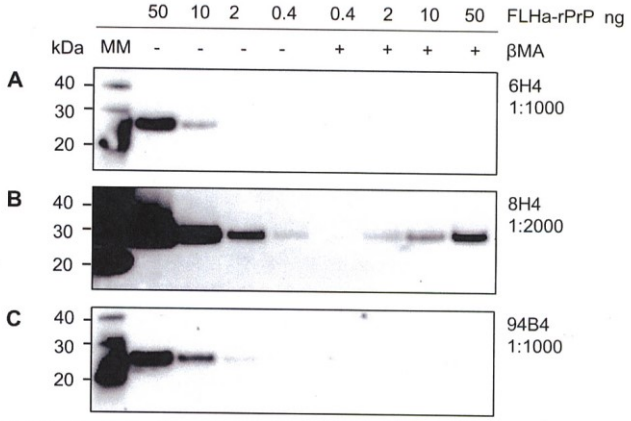

Fig 3. Sample reduction affects mAb reactivity. Dilutions of FLHa-rPrP of known concentration were boiled with (+) or without (-) 2% reducing agent β-mercaptoethanol. The dilution factor for each mAb is reported. All mAbs were diluted in TBST.

https://doi.org/10.1371/journal.pone.0218509.g003

identical banding pattern, characterised by a signal at 10 kDa, irrespective of the sCJD subtype used to seed the reaction (Fig 5).

Seeding RT-QuIC with sCJD CSF samples: CSF-RT-QuIC

Having established the WB methodology for the detection of RT-QuIC reaction products resulting from reactions seeded with 10%BH, we moved our study to the RT-QuIC reaction products resulting from seeding the reaction with CSF samples. Following a similar experimental design as with 10%BH, we assayed in three independent experiment the seeding activity of CSF samples from all the different sCJD subtypes except sCJD VV1. Upon testing by RT-QuIC, all the selected sCJD CSF samples satisfied the diagnostic criteria for positivity (17). Even though spontaneous aggregation of the substrate was observed in two out of 20 unseeded reaction wells, none of the negative controls showed aggregation-associated fluorescence. Treating CSF-RT-QuIC reaction products with 50 μg/mL PK and probing the digested material with mAb SAF70 in WB, resulted in a banding pattern characterised by two prominent signals at around 10 and 22 kDa irrespective of the sCJD subtype of the CSF sample used to seed the reaction. (Fig 6), consistent with the previous observation using sCJD brain homogenates.

Discussion

The generation of PK resistant material from the prion seeded conversion of a recombinant substrate was first reported by Kocisko and co-workers [11] and has been exploited in different CFCs as a detectable sign of the prion seeded conversion of the recombinant substrates along with, or instead of, alterations in ThT fluorescence [32]. More recently, Sano and co-workers used two different rodent adapted prion strains and mouse rPrP as reaction substrates and showed that RT-QuIC reaction products retain some of the strain specific biochemical properties such as the conformational stability and β-sheet structure [27,29]. However, the same authors were unable to discriminate strain-specific structural differences by epitope mapping

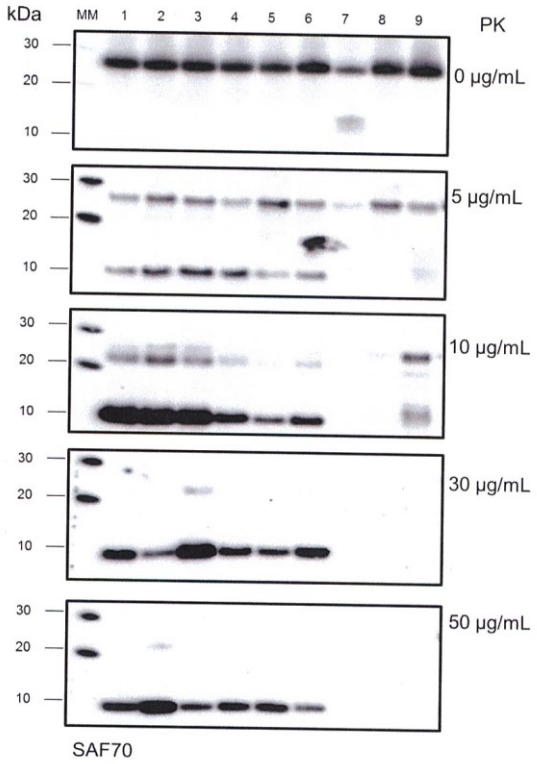

Fig 4. WB analysis with mAb SAF70 of RT-QuIC reaction products treated with increasing concentrations of PK. Lane 1–6: RT-QuIC reaction products from reactions seeded with sCJD subtypes MM1, MM2, MV1, MV2, VV1, VV2, respectively. Lane 7: products of RT-QuIC reactions seeded with non-CJD 10%BH. Lane 8: unseeded RT-QuIC reaction products. Lane 9: RT-QuIC untreated reaction mixture.

https://doi.org/10.1371/journal.pone.0218509.g004

of PK digested RT-QuIC reaction products using the mAb ICSM35 (epitope 93–102) and the polyclonal PrP antiserum R20 (epitopes 218–231). These results were in line with previous findings obtained with sCJD seeds, showing that the conformation acquired by the seeded RT-QuIC reaction products confers PK-resistance to a C-terminal domain encompassing the R20 epitope [16]. In addition, the banding profile detected with R20 was specific to prion seeded RT-QuIC reaction products but independent of the rodent prion strain used as seed. Similar results have been obtained with R20 by McGuire and colleagues [23] on a limited number of PK-treated RT-QuIC reaction products generated with human 10%BH and CSF sCJD seeds and employing FLHa-rPrP as a reaction substrate. In both these studies only very mild PK treatments using 10 or 6 µg/mL PK were used, prior to western blotting.

The present study expands on these observations by systematically investigating the extent of PrP primary structure that is encompassed by the RT-QuIC PK resistant reaction products

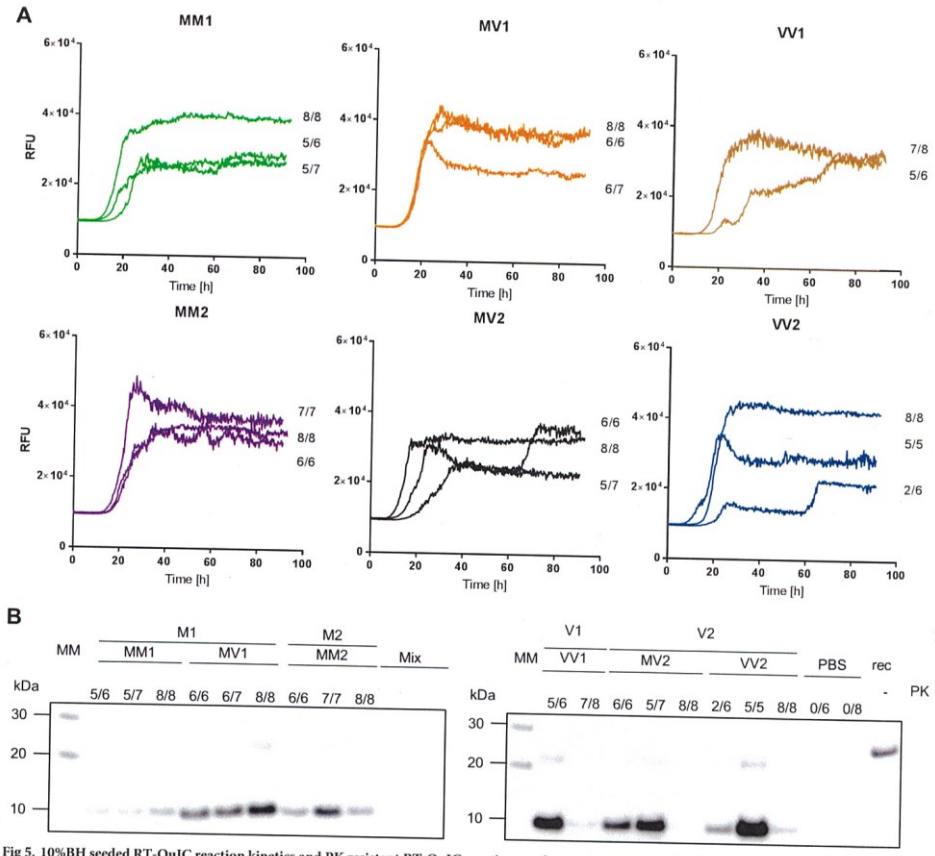

Fig 5. 10%BH seeded RT-QuIC reaction kinetics and PK resistant RT-QuIC reaction products. A) Averaged RT-QuIC traces per individual seed are displayed along with the number of replicates that reached the fluorescence threshold for positivity. (B) RT-QuIC reaction products from reactions displayed in (A) were digested with PK (50 ug/mL) and probed by WB with mAb SAF70 1:1000. Samples are grouped according to sCJD strain of prions as defined in [8] and sub-grouped according to sCJD subtype as defined in [6]. Lane MM: Molecular weight marked; lane rec: 10 ng of FLHa-rPrP; Lane PBS: unseeded reactions; Lane Mix: RT-QuIC untreated reaction mixture.

https://doi.org/10.1371/journal.pone.0218509.g005

generated by sCJD seeds, by employing six commercially available monoclonal antibodies and harsher proteolytic conditions that are discriminatory for subtyping sCJD brain tissue itself.

The initial assessment of the sensitivity of the selected mAbs toward the RT-QuIC substrate FLHa-rPrP in WB, showed that the binding of mAbs 6H4, 8H4 and 94B4 to their respective epitopes was negatively affected when the reducing agent β-mercaptoethanol was added to the sample loading buffer (Fig 3). The reducing agent was added to reduce and thereby break the one disulphide bond in PrP (cysteine 179- cysteine 214, Fig 1A), favouring the linearisation of the protein structure by LDS and preventing the rPrP intermolecular dimerisation while in the

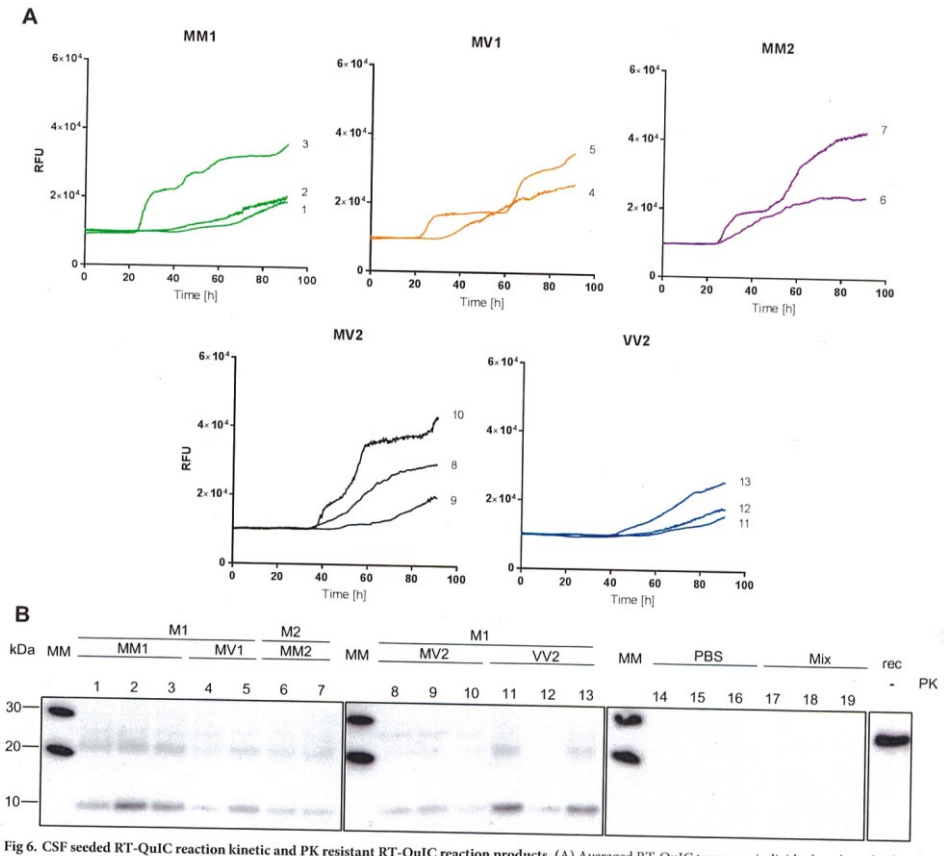

Fig 6. CSF seeded RT-QuIC reaction kinetic and PK resistant RT-QuIC reaction products. (A) Averaged RT-QuIC traces per individual seed are displayed (B) RT-QuIC reaction products from the reaction displayed in (A) were digested with PK 50 ug/mL and probed in WB with mAb SAF70 1:1000. Samples are grouped according to sCJD strain of prions as defined in (8) and sub-grouped according to sCJD subtype as defined in (6). Lane MM: Molecular weight marked; lane rec: 10 ng of FLHa-rPrP; Lane PBS: unseeded reactions; Lane Mix: RT-QuIC untreated reaction mixture.

https://doi.org/10.1371/journal.pone.0218509.g006

denatured state. The fact that reducing conditions suppressed the binding of mAbs 6H4, 8H4 and 94B4 suggests that the correct presentation or availability of the epitopes recognised by these mAbs may depend on the local secondary structure of the protein, i.e. specific amino acid residues at the epitopes must be spatially arranged in a specific conformation. The disruption of the 6H4 epitope by reduction and alkylation has been reported previously [33]. Our data, however, show that reduction, even if acting distal to the 6H4 epitope, is sufficient to reduce or suppress 6H4 binding.

To our knowledge, this is the first report of the negative effect of sample reduction on 8H4 and 94B4 binding. However, in the latter case, the supplier (Central Veterinary Institute at

Wageningen University, Netherlands, EU) states in the product information sheet that 94B4 epitope is "assumed to be conformation dependent" hence its binding may be susceptible to the conformational modifications determined by the reducing agent.

The cysteine at position 179 that forms one half of the disulphide bridge, is part of 8H4 epitope [34,35] and the latter is followed on the C-terminal side by the 94B4 epitope [36] (Fig 1A). Hence, the 8H4 and 94B4 epitopes are contiguous and map on one arm of the hairpin loop that may remain intact when the protein is denatured and the disulphide bond is oxidised. It is therefore conceivable that the disruption of the hairpin loop by reduction of the disulphide bridge may lead to a conformational rearrangement that in turn negatively affects the 8H4 and 94B4 epitopes.

In the absence of reducing conditions and when no PK treatment was used, all the antibodies in our panel detected both the FLHa-rPrP substrate prior to RT-QuIC and the FLHa-rPrP recovered from the plate following RT-QuIC (S1A Fig). The treatment of the RT-QuIC reaction products with 10 μg/mL PK, was sufficient to delete the signal detected by all the selected antibodies apart from SAF70 (S1 Fig). The fragment detected by SAF70 was specific to sCJD seeded RT-QuIC reactions and has an apparent molecular weight of around 10 kDa. The latter estimate was made on the basis of the migration distance on western blot, and is only therefore approximate. Nevertheless, the SAF70-detected band was observed irrespective of the sCJD subtype or whether brain or CSF was used to seed the reaction. Moreover, the fragment detected with SAF70 was unaffected by the harsher PK treatment used (i.e. 50 μg/mL PK, **Figs 5B and 6B**). Taken together these observations indicate the fragment detected by SAF70 represents the PK resistant conformational core generated during sCJD seeded RT-QuIC reactions.

The negative results obtained after PK digestion using mAbs that recognise more N-terminal epitopes, namely 12B2 and 3F4, indicate that these parts of FLHa-rPrP are digested by the mildest PK treatment used in this study. This observation is in line with previously published evidence regarding RT-QuIC reaction products generated with human and non-human prion seeds, indicating that in the conformation generated during RT-QuIC the C-terminal region of the recombinant substrate acquires PK resistance [16,22,29].

The apparent molecular weight of the fragment detected by SAF70 cannot be reconciled easily with the lack of detection by 6H4 and 8H4 because the region of hamster PrP between 6H4 and 8H4 epitopes has a much smaller molecular mass (~2.7 kDa) than the apparent molecular mass of 10 kDa (Fig 1B). Taking into consideration the susceptibility of 6H4 epitope to distal conformational changes that we have observed (Fig 3A), possibly the structural integrity of this epitope was affected by the proteolytic digestion of either or both the N-terminal and C-terminal domains, rather than a by direct effect of the PK.

It is also possible that the observed loss of 8H4 and 94B4 signals might also arise from a secondary conformational effect resulting from PK exerting its activity on distal domains so that the sequence encompassing these epitopes may contribute to the observed molecular weight of ~10 kDa. In particular, PK activity may determine an outcome similar to the one determined by the reducing agent (i.e. the disruption of the hairpin loop between α2 and α3), by exerting its activity on the hinge between the arms of the hairpin loop (Fig 1A). The digestion of the hinge may lead to a topological change in the local sequence that negatively affects 8H4 and 94B4 binding without destroying the peptide sequence encompassing their epitopes.

Our results show that the RT-QuIC reaction products, generated by seeding the reaction with either sCJD brain samples or sCJD CSF samples, are partially resistant to PK digestion. The PK digestion of the sCJD seeded RT-QuIC reaction products yields a fragment that is detected by mAb SAF70 at a molecular weight of ~10 kDa and the same banding profile is observed irrespective of the sCJD subtype used to seed the RT-QuIC reaction and irrespective to seed being a sCJD brain or CSF samples.

These results suggest that all the sCJD seeds have induced the same conformational change in the FLHa-rPrP as assessed by WB following PK digestion irrespective of PrP^{res} type or sCJD subtype of the seed and that the seeding mechanism is common to sCJD brain and CSF samples based on its effects on this particular commonly used substrate.

We cannot exclude the possibility that more complex and sensitive molecular methodologies, to the one used in this work, may be able to better characterise the products of the protein misfolding events taking place during RT-QuIC. These may eventually permit this technique to discriminate sCJD subtypes *in vita*. Nevertheless, our results do not support the hypothesis that there are distinctive misfolding pathways related to different sCJD subtypes that can be discerned using this commonly employed diagnostic RT-QuIC method. Therefore, whilst RT-QuIC has considerable diagnostic value, at present it has questionable prognostic value based on epitope mapping of reaction products.

Supporting information

S1 Fig. BH-RT-QuIC reaction products treated with increasing concentrations of PK and analysed by WB with panel of six commercially available mAs. Results from each individual mAb are displayed in columns, from left to right, 12B2 1:10000, 3F4 1:10000, 6H4 1:1000, SAF70 1:1000, 8H4 1:2000, 94B4 1:1000. This order mirrors the position on the FLHa-rPrP primary sequence of each mAbs epitope from the N- to the C-terminal. For each blot, Lanes (1–6): products of RT-QuIC reactions seeded with sCJD 10%BH subtypes MM1, MM2c, MV1, MV2, VV1, VV2, respectively. Lane (7): products of reaction seeded with non-CJD 10%BH. Lane 8: unseeded reaction products. Lane (9): RT-QuIC untreated reaction mixture. Row (A) RT-QuiC reaction products before proteolytic treatment, row (B) RT-QuIC reaction products treated with PK 10 μg/mL, row (C) PK 30 μg/mL, row (D) PK 50 μg/mL. Each row displays blots that were transferred on an individual PVDF membrane.
(TIF)

Acknowledgments

We thank Professor Colin Smith and Dr. D.L. Ritchie for the provision of the human brain tissue (MRC Edinburgh Brain Bank). We also thank Dr N. McKenzie from the National CJD Research and Surveillance Unit for his expert assistance during the recombinant protein purification. We are also most grateful to M.W. Head for his critical review of the manuscript. This report is independent research commissioned and funded by the Department of Health and Social Care Policy Research Programme and the Scottish Government. The view expressed in this publication are those of the authors and not necessarily those of the Department of Health or the Scottish Government.

Author Contributions

Conceptualization: Gabriele Piconi, Alexander H. Peden, Marcelo A. Barria.

Data curation: Gabriele Piconi.

Formal analysis: Gabriele Piconi.

Funding acquisition: Alison J. E. Green.

Investigation: Gabriele Piconi.

Methodology: Marcelo A. Barria.

Supervision: Alexander H. Peden, Marcelo A. Barria, Alison J. E. Green.

These results suggest that all the sCJD seeds have induced the same conformational change in the FLHa-rPrP as assessed by WB following PK digestion irrespective of PrP^{res} type or sCJD subtype of the seed and that the seeding mechanism is common to sCJD brain and CSF samples based on its effects on this particular commonly used substrate.

We cannot exclude the possibility that more complex and sensitive molecular methodologies, to the one used in this work, may be able to better characterise the products of the protein misfolding events taking place during RT-QuIC. These may eventually permit this technique to discriminate sCJD subtypes *in vita*. Nevertheless, our results do not support the hypothesis that there are distinctive misfolding pathways related to different sCJD subtypes that can be discerned using this commonly employed diagnostic RT-QuIC method. Therefore, whilst RT-QuIC has considerable diagnostic value, at present it has questionable prognostic value based on epitope mapping of reaction products.

Supporting information

S1 Fig. BH-RT-QuIC reaction products treated with increasing concentrations of PK and analysed by WB with panel of six commercially available mAs. Results from each individual mAb are displayed in columns, from left to right, 12B2 1:10000, 3F4 1:10000, 6H4 1:1000, SAF70 1:1000, 8H4 1:2000, 94B4 1:1000. This order mirrors the position on the FLHa-rPrP primary sequence of each mAbs epitope from the N- to the C-terminal. For each blot, Lanes (1–6): products of RT-QuIC reactions seeded with sCJD 10%BH subtypes MM1, MM2c, MV1, MV2, VV1, VV2, respectively. Lane (7): products of reaction seeded with non-CJD 10%BH. Lane 8: unseeded reaction products. Lane (9): RT-QuIC untreated reaction mixture. Row (A) RT-QuiC reaction products before proteolytic treatment, row (B) RT-QuIC reaction products treated with PK 10 μg/mL, row (C) PK 30 μg/mL, row (D) PK 50 μg/mL. Each row displays blots that were transferred on an individual PVDF membrane.
(TIF)

Acknowledgments

We thank Professor Colin Smith and Dr. D.L. Ritchie for the provision of the human brain tissue (MRC Edinburgh Brain Bank). We also thank Dr N. McKenzie from the National CJD Research and Surveillance Unit for his expert assistance during the recombinant protein purification. We are also most grateful to M.W. Head for his critical review of the manuscript. This report is independent research commissioned and funded by the Department of Health and Social Care Policy Research Programme and the Scottish Government. The view expressed in this publication are those of the authors and not necessarily those of the Department of Health or the Scottish Government.

Author Contributions

Conceptualization: Gabriele Piconi, Alexander H. Peden, Marcelo A. Barria.

Data curation: Gabriele Piconi.

Formal analysis: Gabriele Piconi.

Funding acquisition: Alison J. E. Green.

Investigation: Gabriele Piconi.

Methodology: Marcelo A. Barria.

Supervision: Alexander H. Peden, Marcelo A. Barria, Alison J. E. Green.

Writing – original draft: Gabriele Piconi.

Writing – review & editing: Gabriele Piconi, Alexander H. Peden, Marcelo A. Barria, Alison J. E. Green.

References

1. Bolton DC, Mckinley MP, Prusiner SB. Identification of a protein that purifies with the scrapie prion. Science. 1982; 218(4579):1309–11. PMID: 6815801
2. Prusiner SB. Novel proteinaceous infectious particles cause scrapie. Science. 1982; 216(4542):136–44. PMID: 6801762
3. Meyer RK, McKinley MP, Bowman KA, Braunfeld MB, Barry RA, Prusiner SB. Separation and properties of cellular and scrapie prion proteins. Proc Natl Acad Sci U S A. 1986; 83(8):2310–2.14. https://doi.org/10.1073/pnas.83.8.2310 PMID: 3085093
4. Ladogana A, Puopolo M, Croes EA, Budka H, Jarius C, Collins S, et al. Mortality from Creutzfeldt-Jakob disease and related disorders in Europe, Australia, and Canada. Neurology. 2005 May 10; 64(9):1586–91. https://doi.org/10.1212/01.WNL.0000160117.56690.B2 PMID: 15883321
5. World Health Organisation. WHO manual for surveillance of human transmissible spongiform encephalopathies including variant Creutzfeldt-Jakob disease. WHO. 2003.
6. Parchi P, Saverioni D. Molecular pathology, classification, and diagnosis of sporadic human prion disease variants. Folia Neuropathol. 2012; 50(1):20–45. PMID: 22505361
7. Head MW. Human prion diseases: Molecular, cellular and population biology. Neuropathology. 2013; 33(3):221–36. https://doi.org/10.1111/neup.12016 PMID: 23331517
8. Bishop MT, Will RG, Manson JC. Defining sporadic Creutzfeldt-Jakob disease strains and their transmission properties. Proc Natl Acad Sci. 2010; 107(26):12005–10. https://doi.org/10.1073/pnas.1004688107 PMID: 20547859
9. Moda F, Suardi S, Di Fede G, Indaco A, Limido L, Vimercati C, et al. MM2-thalamic Creutzfeldt-Jakob disease: Neuropathological, biochemical and transmission studies identify a distinctive prion strain. Brain Pathol. 2012; 22(5):662–9. https://doi.org/10.1111/j.1750-3639.2012.00572.x PMID: 22288561
10. Collinge J, Clarke AR. A General Model of Prion Strains and Their Pathogenicity. Science. 2007; 318 (5852):930–6. https://doi.org/10.1126/science.1138718 PMID: 17991853
11. Kocisko DA, JH C, SA P, B C, GJ R, PT L, et al. Cell free formation of protease resistant prion protein. Nature. 1994; 370(066/21):471.
12. Saborio GP, Permanne B, Soto C. Sensitive detection of pathological prion protein by cyclic amplication of protein misfolding. Nature. 2001; 411(June):1–4.
13. Colby DW, Zhang Q, Wang S, Groth D, Legname G, Riesner D, et al. Prion detection by an amyloid seeding assay. Proc Natl Acad Sci U S A. 2007; 104(52):20914–9. https://doi.org/10.1073/pnas.0710152105 PMID: 18096717
14. Atarashi R, Satoh K, Sano K, Fuse T, Yamaguchi N, Ishibashi D, et al. Ultrasensitive human prion detection in cerebrospinal fluid by real-time quaking-induced conversion. Nat Med. 2011; 17(2):175–8. https://doi.org/10.1038/nm.2294 PMID: 21278748
15. Atarashi R, Sano K, Satoh K, Nishida N. Real-time quaking-induced conversion: A highly sensitive assay for prion detection. Vol. 5, Prion. 2011. p. 150–3. https://doi.org/10.4161/pri.5.3.16893 PMID: 21778820
16. Wilham JM, Orrú CD, Bessen RA, Atarashi R, Sano K, Race B, et al. Rapid end-point quantitation of prion seeding activity with sensitivity comparable to bioassays. PLoS Pathog. 2010; 6(12).
17. McGuire LI, Poleggi A, Poggiolini I, Suardi S, Grznarova K, Shi S, et al. Cerebrospinal fluid real-time quaking-induced conversion is a robust and reliable test for sporadic creutzfeldt–jakob disease: An international study. Ann Neurol. 2016; 80(1):160–5. https://doi.org/10.1002/ana.24679 PMID: 27130376
18. Schmitz M, Cramm M, Llorens F, Müller-Cramm D, Collins S, Atarashi R, et al. The real-Time quaking-induced conversion assay for detection of human prion disease and study of other protein misfolding diseases. Nat Protoc. 2016; 11(11):2233–42. https://doi.org/10.1038/nprot.2016.120 PMID: 27735933
19. Green AJE. RT-QuIC: a new test for sporadic CJD. Pract Neurol. 2018 Oct 3; practneurol-2018-001935.
20. Franceschini A, Baiardi S, Hughson AG, McKenzie N, Moda F, Rossi M, et al. High diagnostic value of second generation CSF RT-QuIC across the wide spectrum of CJD prions. Sci Rep. 2017 Dec 6; 7 (1):10655. https://doi.org/10.1038/s41598-017-10922-w PMID: 28878311

21. Orrú CD, Hughson AG, Groveman BR, Campbell KJ, Anson KJ, Manca M, et al. Factors that improve RT-QuIC detection of prion seeding activity. Viruses. 2016; 8(5).

22. Peden AH, McGuire LI, Appleford NEJ, Mallinson G, Wilham JM, Orru CD, et al. Sensitive and specific detection of sporadic Creutzfeldt-Jakob disease brain prion protein using real-time quaking-induced conversion. J Gen Virol. 2012; 93(2):438–49.

23. McGuire LI, Peden AH, Orrú CD, Wilham JM, Appleford NE, Mallinson G, et al. RT-QuIC analysis of cerebrospinal fluid in sporadic Creutzfeldt- Jakob disease. Ann Neurol. 2012;

24. Cramm M, Schmitz M, Karch A, Zafar S, Varges D, Mitrova E, et al. Characteristic CSF Prion Seeding Efficiency in Humans with Prion Diseases. Mol Neurobiol. 2014; 51(1):396–405. https://doi.org/10.1007/s12035-014-8709-6 PMID: 24809690

25. Lattanzio F, Abu-Rumeileh S, Franceschini A, Kai H, Amore G, Poggiolini I, et al. Prion-specific and surrogate CSF biomarkers in Creutzfeldt-Jakob disease: diagnostic accuracy in relation to molecular subtypes and analysis of neuropathological correlates of p-tau and Aβ42 levels. Acta Neuropathol. 2017; 133(4):559–78. https://doi.org/10.1007/s00401-017-1683-0 PMID: 28205010

26. Foutz A, Appleby BS, Hamlin C, Liu X, Yang S, Cohen Y, et al. Diagnostic and prognostic value of human prion detection in cerebrospinal fluid. Ann Neurol. 2017; 81(1):79–92. https://doi.org/10.1002/ana.24833 PMID: 27893164

27. Sano K, Atarashi R, Nishida N. Structural conservation of prion strain specificities in recombinant prion protein fibrils in real-time quaking-induced conversion. Prion. 2015; 9(4):237–43. https://doi.org/10.1080/19336896.2015.1062201 PMID: 26284507

28. Orrú CD, Groveman BR, Raymond LD, Hughson AG, Nonno R, Zou W, et al. Bank Vole Prion Protein As an Apparently Universal Substrate for RT-QuIC-Based Detection and Discrimination of Prion Strains. PLoS Pathog. 2015; 11(6).

29. Sano K, Atarashi R, Ishibashi D, Nakagaki T, Satoh K, Nishida N. Conformational Properties of Prion Strains Can Be Transmitted to Recombinant Prion Protein Fibrils in Real-Time Quaking-Induced Conversion. J Virol. 2014; 88(20):11791–801. https://doi.org/10.1128/JVI.00585-14 PMID: 25078700

30. Towbin H, Staehelin T, Gordon J. Electrophoretic transfer of proteins from polyacrylamide gels to nitrocellulose sheets: procedure and some applications. Proc Natl Acad Sci U S A. 1979 Sep [cited 2018 Dec 6]; 76(9):4350–4. https://doi.org/10.1073/pnas.76.9.4350 PMID: 388439

31. Ritchie DL, Barria MA, Peden AH, Yull HM, Kirkpatrick J, Adlard P, et al. UK Iatrogenic Creutzfeldt–Jakob disease: investigating human prion transmission across genotypic barriers using human tissue-based and molecular approaches. Acta Neuropathol. 2017; 133(4):579–95. https://doi.org/10.1007/s00401-016-1638-x PMID: 27812793

32. Atarashi R, Wilham JM, Christensen L, Hughson AG, Moore RA, Johnson LM, et al. Simplified ultrasensitive prion detection by recombinant PrP conversion with shaking. Nat Methods. 2008; 5(3):211–2. https://doi.org/10.1038/nmeth0308-211 PMID: 18309304

33. Yuan J, Kinter M, McGeehan J, Perry G, Kneale G, Gambetti P, et al. Concealment of epitope by reduction and alkylation in prion protein. Biochem Biophys Res Commun. 2005; 326(3):652–9. https://doi.org/10.1016/j.bbrc.2004.11.088 PMID: 15596149

34. Zanusso G, Liu D, Ferrari S, Hegyi I, Yin X, Aguzzi A, et al. Prion protein expression in different species: analysis with a panel of new mAbs. Proc Natl Acad Sci U S A. 1998; 95(15):8812–6. https://doi.org/10.1073/pnas.95.15.8812 PMID: 9671761

35. Li R, Liu T, Wong BS, Pan T, Morillas M, Swietnicki W, et al. Identification of an epitope in the C terminus of normal prion protein whose expression is modulated by binding events in the N terminus. J Mol Biol. 2000; 301(3):567–73. https://doi.org/10.1006/jmbi.2000.3986 PMID: 10966770

36. Yull HM, Ritchie DL, Langeveld JPM, Van Zijderveld FG, Bruce ME, Ironside JW, et al. Detection of type 1 prion protein in variant Creutzfeldt-Jakob disease. Am J Pathol. 2006; 168(1):151–7. https://doi.org/10.2353/ajpath.2006.050766 PMID: 16400018

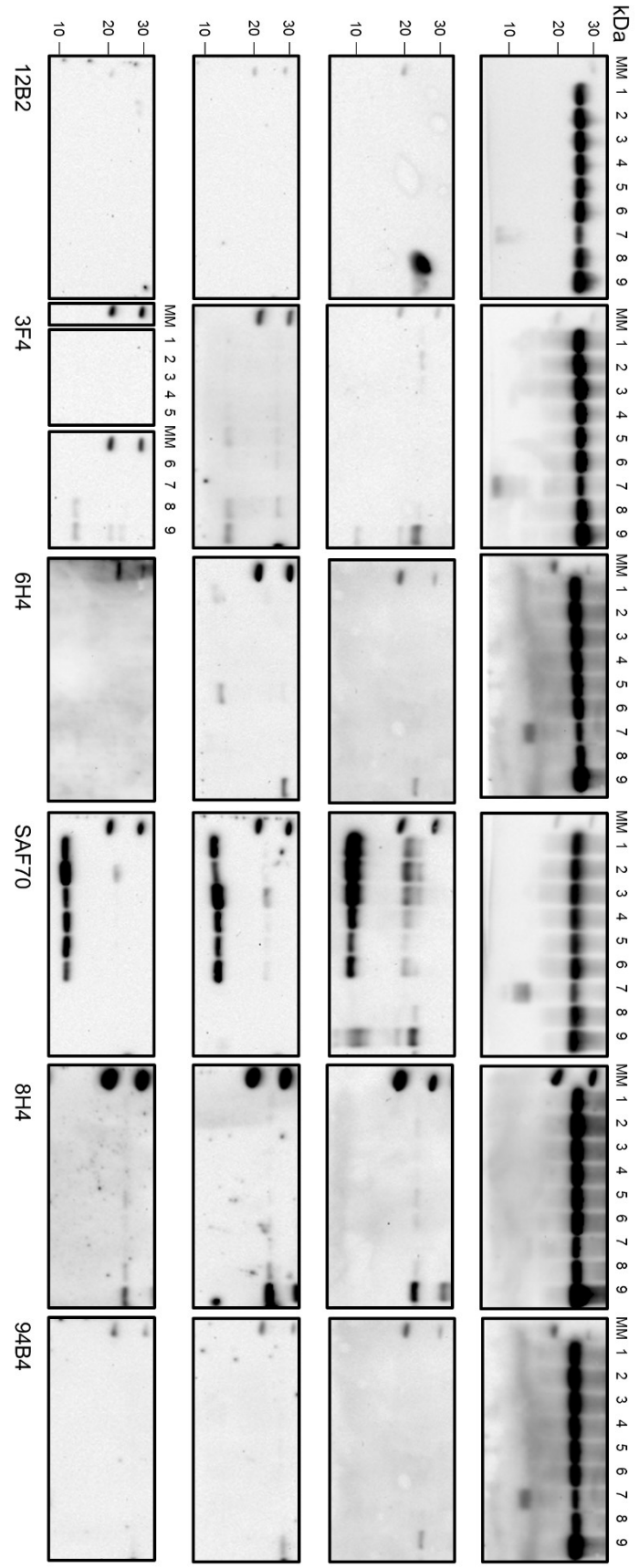

S1 Figure: BH-RT-QuIC reaction products treated with increasing (continued on next page)

(continued) concentrations of PK and analysed by WB with panel of six commercially available mAbs.

Results from each individual mAb are displayed in columns, from left to right, 12B2 1:10000, 3F4 1:10000, 6H4 1:1000, SAF70 1:1000, 8H4 1:2000, 94B4 1:1000. This order mirrors the position on the FLHa-rPrP primary sequence of each mAbs epitope from the N- to the C-terminal. For each blot, Lanes (1–6): products of RT-QuIC reactions seeded with sCJD 10%BH subtypes MM1, MM2c, MV1, MV2, VV1, VV2, respectively. Lane (7): products of reaction seeded with non-CJD 10%BH. Lane 8: unseeded reaction products. Lane (9): RT-QuIC untreated reaction mixture. Row (A) RT-QuIC reaction products before proteolytic treatment, row (B) RT-QuIC reaction products treated with PK 10 µg/mL, row (C) PK 30 µg/mL, row (D) PK 50 µg/mL. Each row displays blots that were transferred on an individual PVDF membrane.

Appendix II

PMCA raw data set

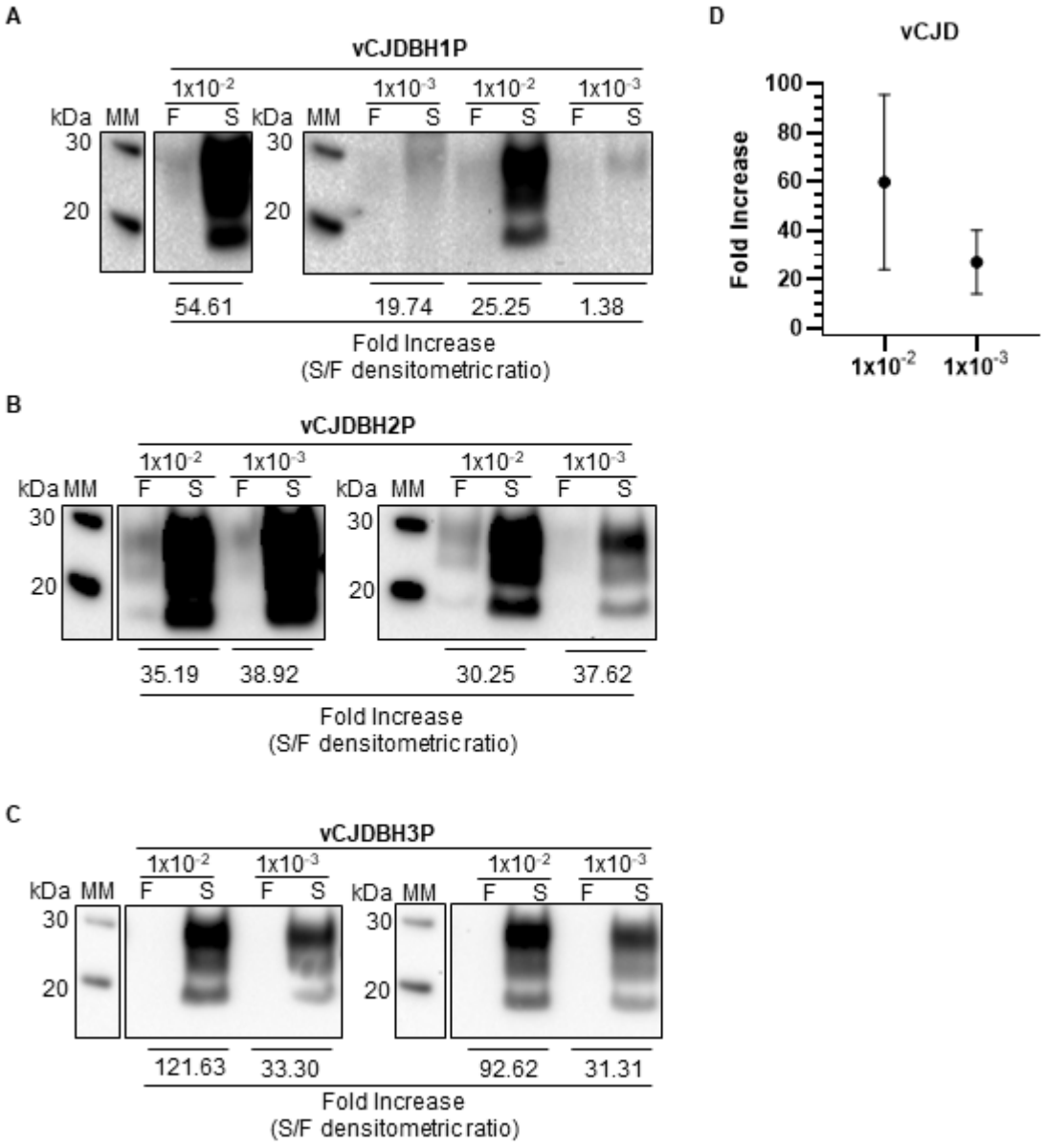

Figure II.1 vCJD seeded PMCA raw data set

Figure A, B and C: WBs for the detection of PMCA reaction products. The identification of the sample is shown on top of each WB picture. The dilution factor (seed-into-substrate) used is indicated below the sample name. For each sample two technical replicates were run in each PMCA experiment. F: Frozen sample; S: Sonicated sample. The S/F values calculated on each pair of S and F samples are indicated at the bottom of each WB picture, in correspondence with the signals analysed. WB immunodetection was with mAb 3F4. MM: molecular weight marker; kDa: kilodalton. Figure D: Graphical representation of the mean average S/F ratios. Each data point represents the mean average of the results of the densitometric analysis performed on the WBs for the detection of PMCA reaction products of each technical replicates tested per seed.

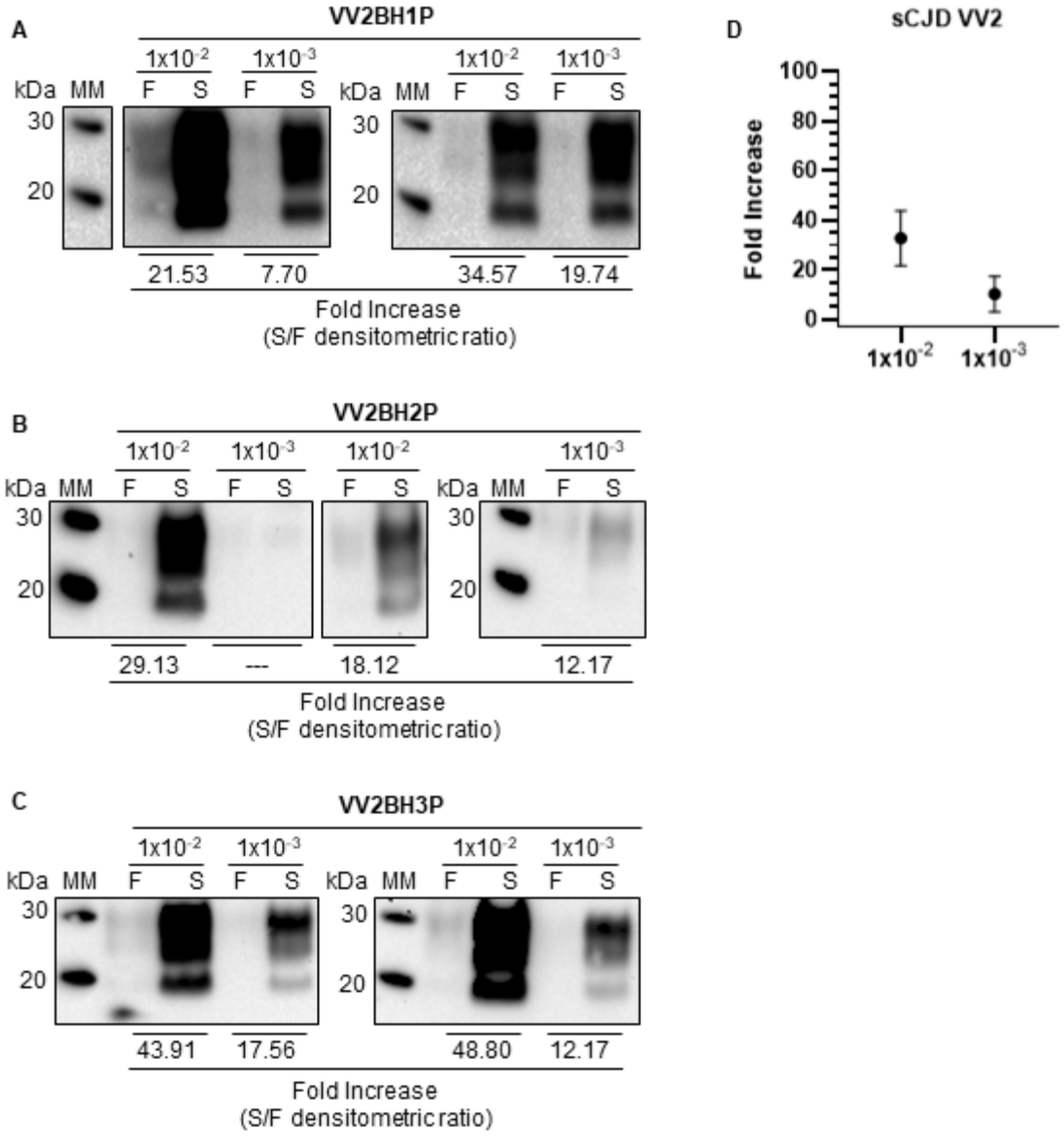

Figure II.2 sCJD subtype VV2 seeded PMCA raw data set

Figure A, B and C: WBs for the detection of PMCA reaction products. The identification of the sample is shown on top of each WB picture. The dilution factor (seed-into-substrate) used is indicated below the sample name. For each sample two technical replicates were run in each PMCA experiment. F: Frozen sample; S: Sonicated sample. The S/F values calculated on each pair of S and F samples are indicated at the bottom of each WB picture, in correspondence with the signals analysed. WB immunodetection was with mAb 3F4. MM: molecular weight marker; kDa: kilodalton. Figure D: Graphical representation of the mean average S/F ratios. Each data point represents the mean average of the results of the densitometric analysis performed on the WBs for the detection of PMCA reaction products of each technical replicates tested per seed.

.

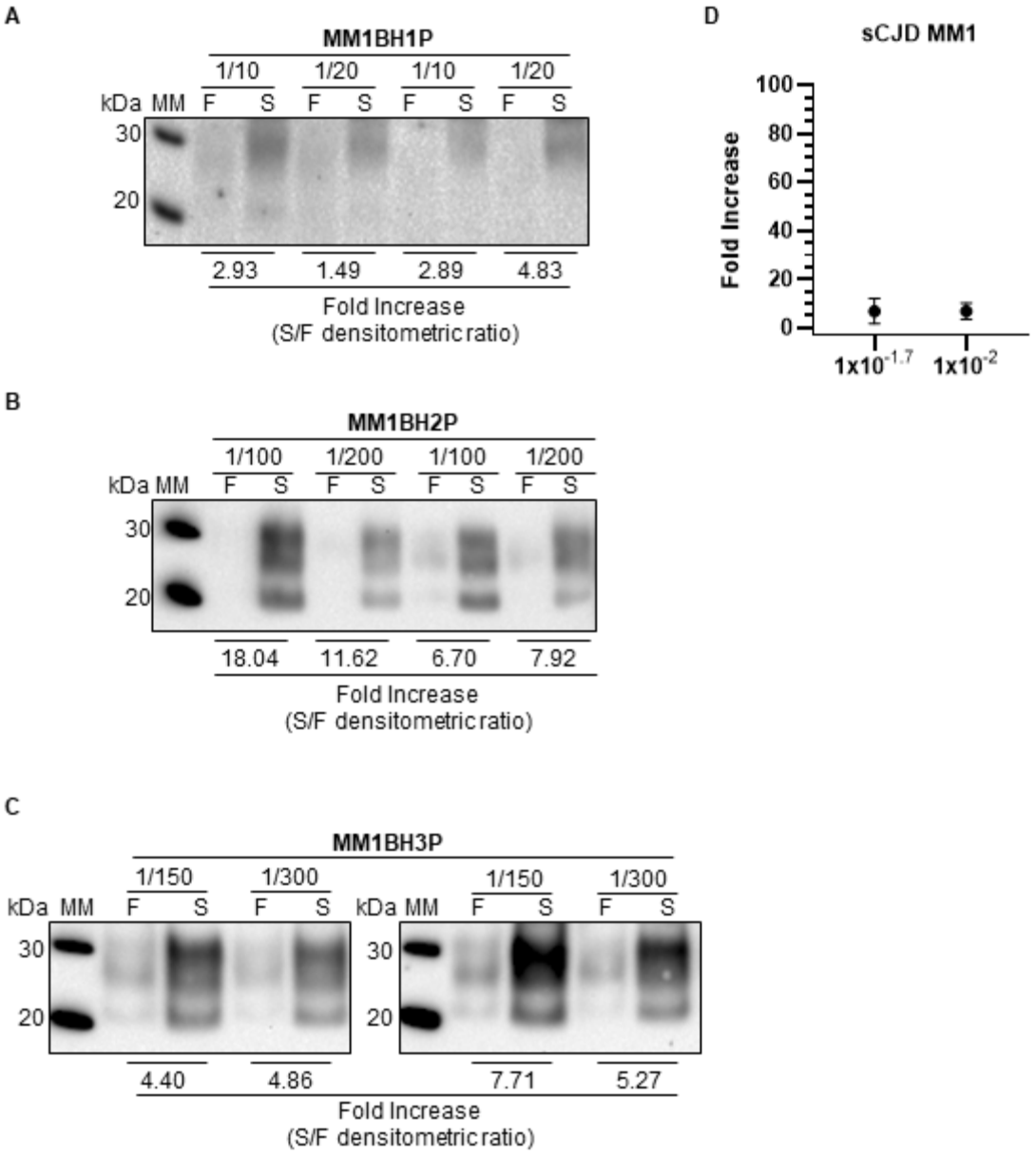

Figure II.3 sCJD subtype MM1 seeded PMCA raw data set

Figure A, B and C: WBs for the detection of PMCA reaction products. The identification of the sample is shown on top of each WB picture. The dilution factor (seed-into-substrate) used is indicated below the sample name. For each sample two technical replicates were run in each PMCA experiment. F: Frozen sample; S: Sonicated sample. The S/F values calculated on each pair of S and F samples are indicated at the bottom of each WB picture, in correspondence with the signals analysed. WB immunodetection was with mAb 3F4. MM: molecular weight marker; kDa: kilodalton. Figure D: Graphical representation of the mean average S/F ratios. Each data point represents the mean average of the results of the densitometric analysis performed on the WBs for the detection of PMCA reaction products of each technical replicates tested per seed.

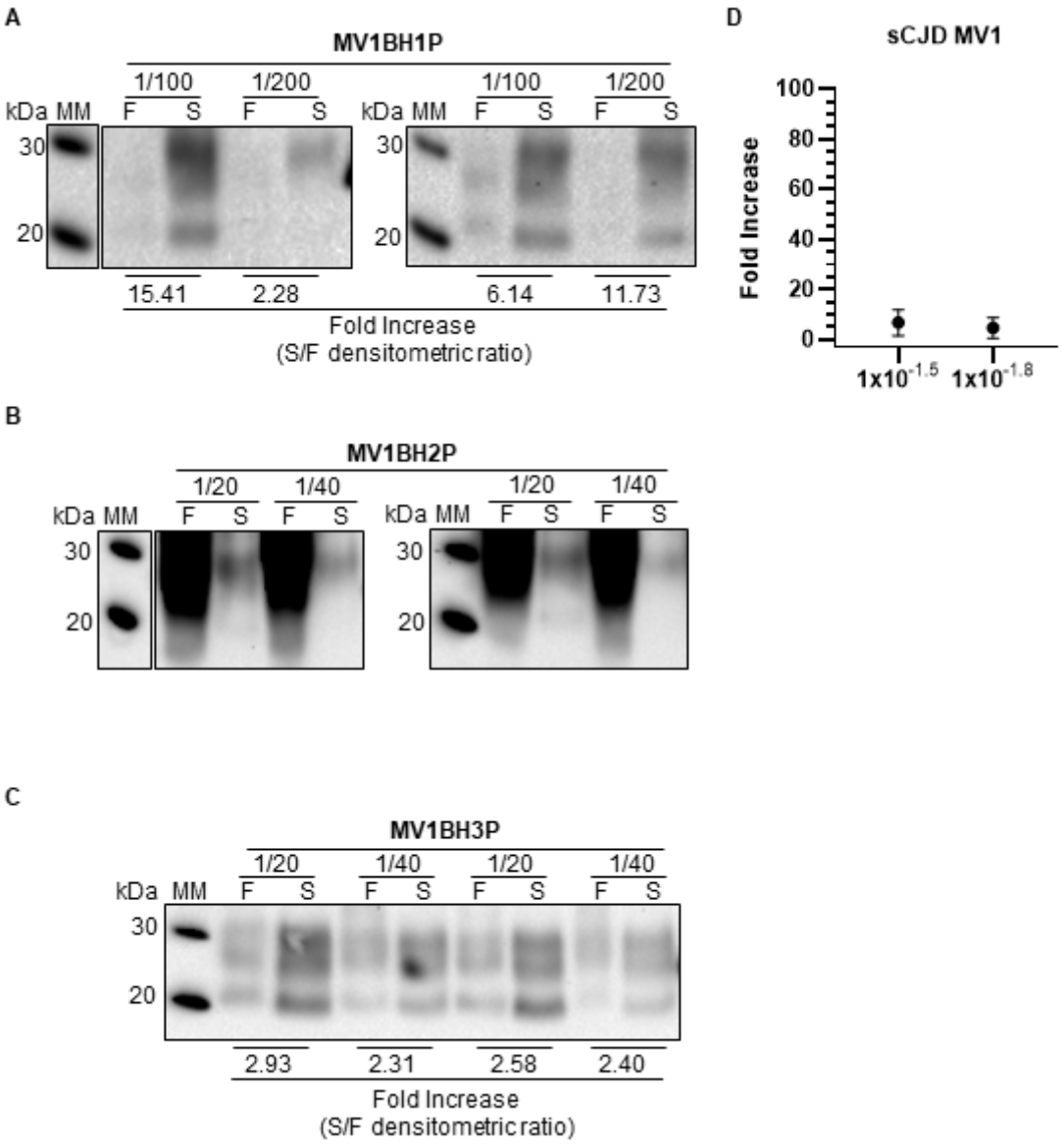

Figure II.4 sCJD subtype MV1 seeded PMCA raw data set

Figure A, B and C: WBs for the detection of PMCA reaction products. The identification of the sample is shown on top of each WB picture. The dilution factor (seed-into-substrate) used is indicated below the sample name. For each sample two technical replicates were run in each PMCA experiment. F: Frozen sample; S: Sonicated sample. The S/F values calculated on each pair of S and F samples are indicated at the bottom of each WB picture, in correspondence with the signals analysed. WB immunodetection was with mAb 3F4. MM: molecular weight marker; kDa: kilodalton. Figure D: Graphical representation of the mean average S/F ratios. Each data point represents the mean average of the results of the densitometric analysis performed on the WBs for the detection of PMCA reaction products of each technical replicates tested per seed.

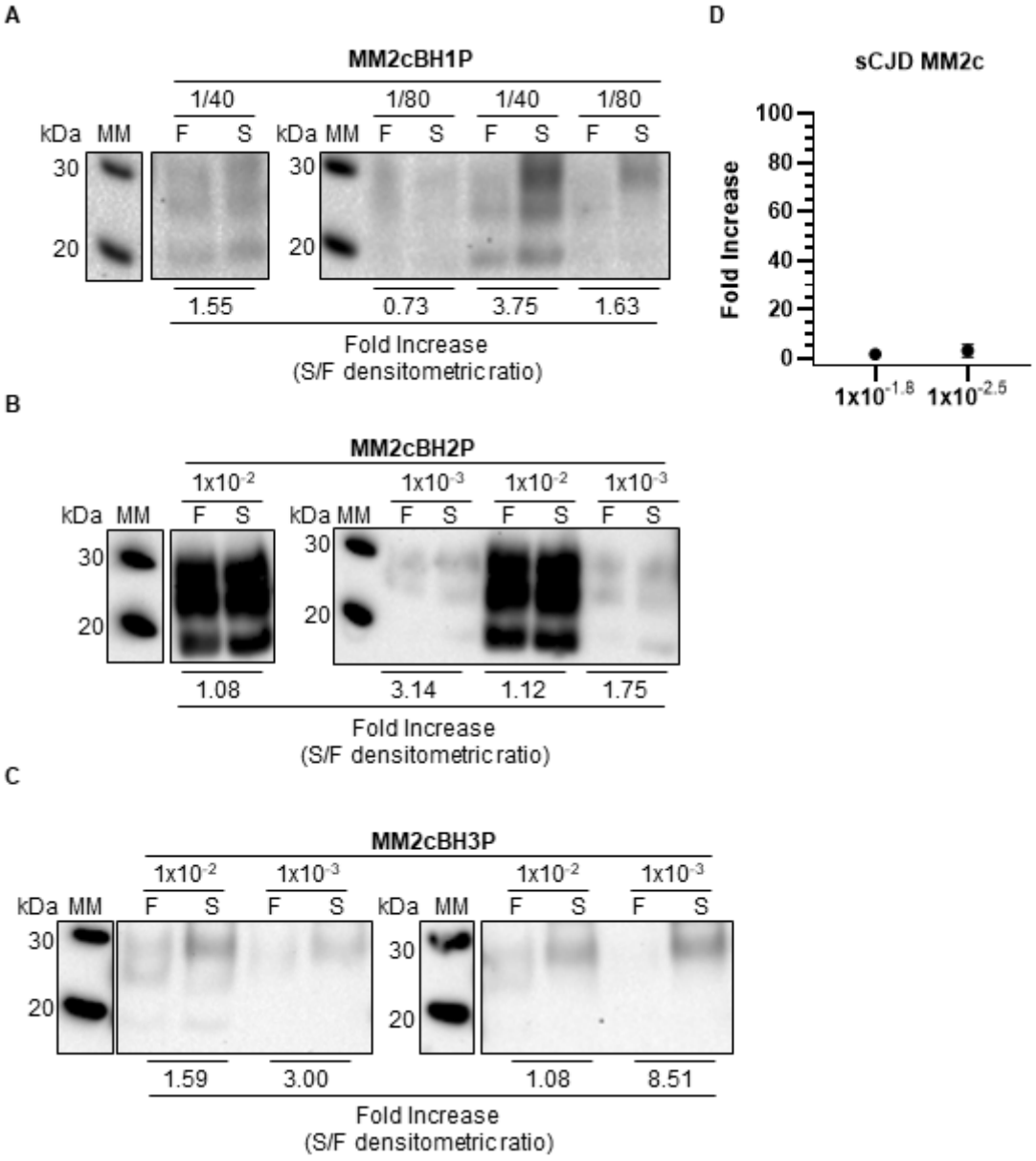

Figure II.5 sCJD subtype MM2c seeded PMCA raw data set

Figure A, B and C: WBs for the detection of PMCA reaction products. The identification of the sample is shown on top of each WB picture. The dilution factor (seed-into-substrate) used is indicated below the sample name. For each sample two technical replicates were run in each PMCA experiment. F: Frozen sample; S: Sonicated sample. The S/F values calculated on each pair of S and F samples are indicated at the bottom of each WB picture, in correspondence with the signals analysed. WB immunodetection was with mAb 3F4. MM: molecular weight marker; kDa: kilodalton. Figure D: Graphical representation of the mean average S/F ratios. Each data point represents the mean average of the results of the densitometric analysis performed on the WBs for the detection of PMCA reaction products of each technical replicates tested per seed.

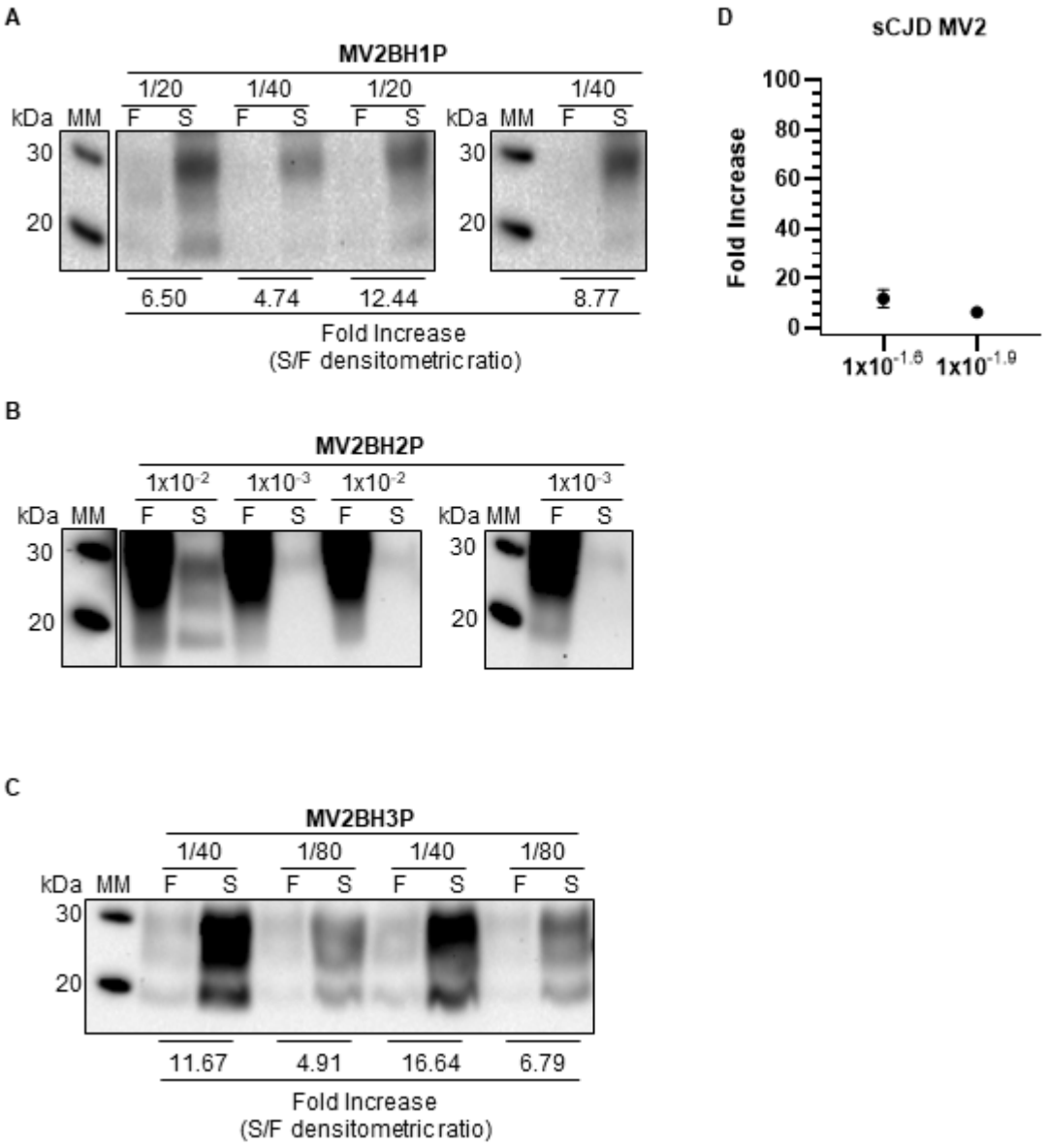

Figure II.6 sCJD subtype MV2 seeded PMCA raw data set

Figure A, B and C: WBs for the detection of PMCA reaction products. The identification of the sample is shown on top of each WB picture. The dilution factor (seed-into-substrate) used is indicated below the sample name. For each sample two technical replicates were run in each PMCA experiment. F: Frozen sample; S: Sonicated sample. The S/F values calculated on each pair of S and F samples are indicated at the bottom of each WB picture, in correspondence with the signals analysed. WB immunodetection was with mAb 3F4. MM: molecular weight marker; kDa: kilodalton. Figure D: Graphical representation of the mean average S/F ratios. Each data point represents the mean average of the results of the densitometric analysis performed on the WBs for the detection of PMCA reaction products of each technical replicates tested per seed.

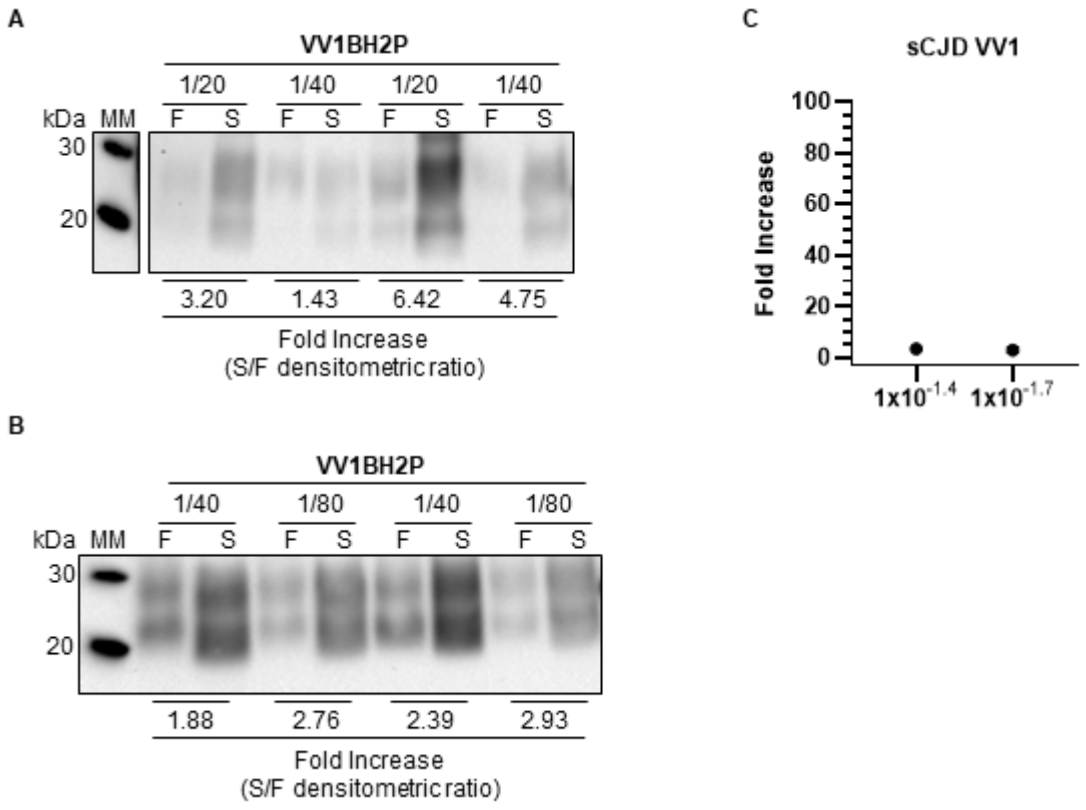

Figure II.7 sCJD subtype MV2 seeded PMCA raw data set

Figure A, B and C: WBs for the detection of PMCA reaction products. The identification of the sample is shown on top of each WB picture. The dilution factor (seed-into-substrate) used is indicated below the sample name. For each sample two technical replicates were run in each PMCA experiment. F: Frozen sample; S: Sonicated sample. The S/F values calculated on each pair of S and F samples are indicated at the bottom of each WB picture, in correspondence with the signals analysed. WB immunodetection was with mAb 3F4. MM: molecular weight marker; kDa: kilodalton. Figure D: Graphical representation of the mean average S/F ratios. Each data point represents the mean average of the results of the densitometric analysis performed on the WBs for the detection of PMCA reaction products of each technical replicates tested per seed.

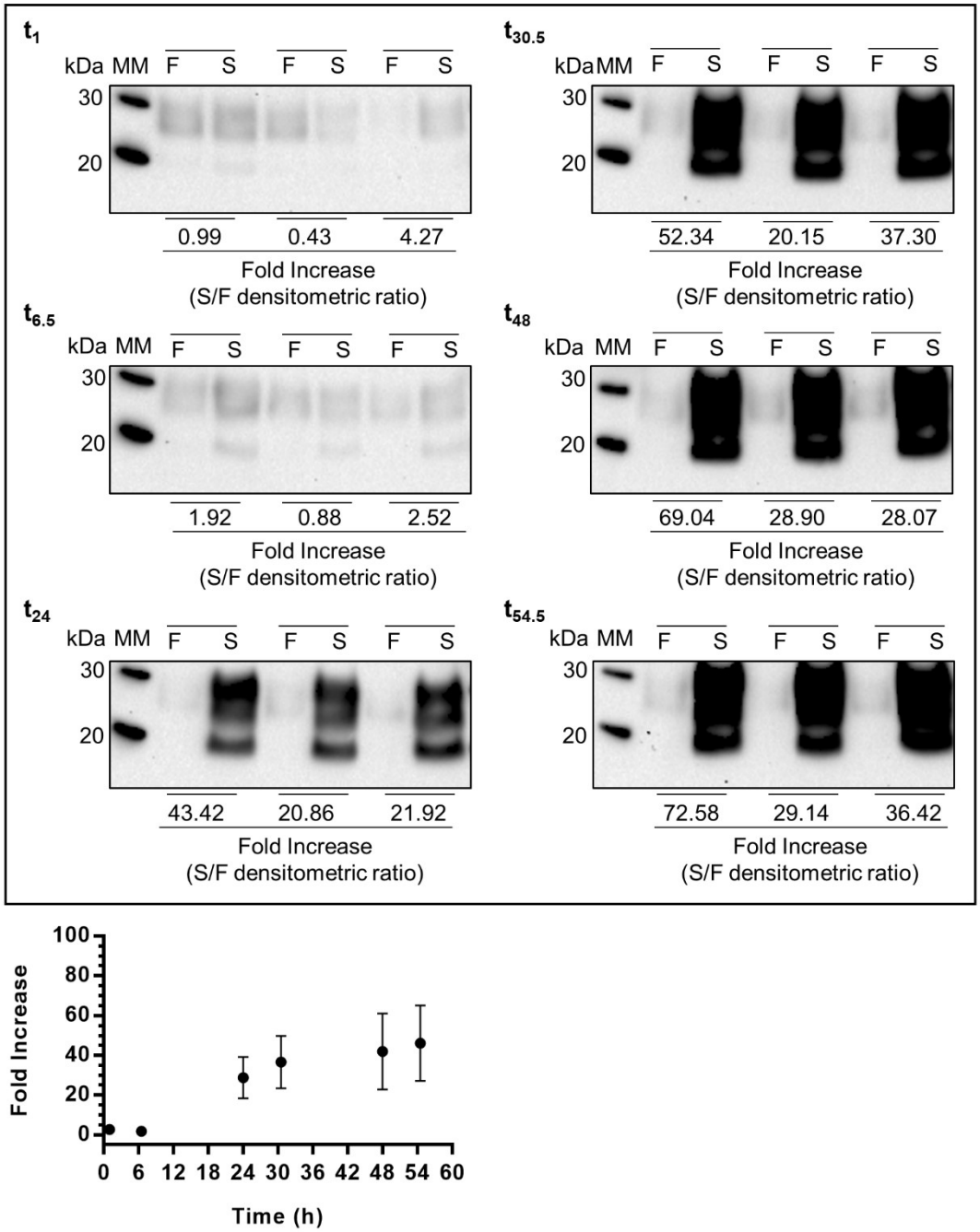

Figure II.8 sCJD subtype BH1VV2P PMCA kinetics study

In the box: WBs for the analysis of PMCA reaction kinetics. PMCA reaction seeded with BH1VV2P at dilution $1x10^{-2}$ was sampled in triplicates at defined time interval (*i.e.* $t_{1, 6.5, 24, 30, 48, 54.5}$). F: Frozen sample; S: Sonicated sample. The S/F values calculated on each pair of S and F samples are indicated at the bottom of each WB picture, in correspondence with the signals analysed. WB immunodetection was with mAb 3F4. MM: molecular weight marker; kDa: kilodalton. Below the box: graph summarizing PMCA reaction kinetics. Each data point indicates the mean average fold increase. Bars indicate standard deviation.

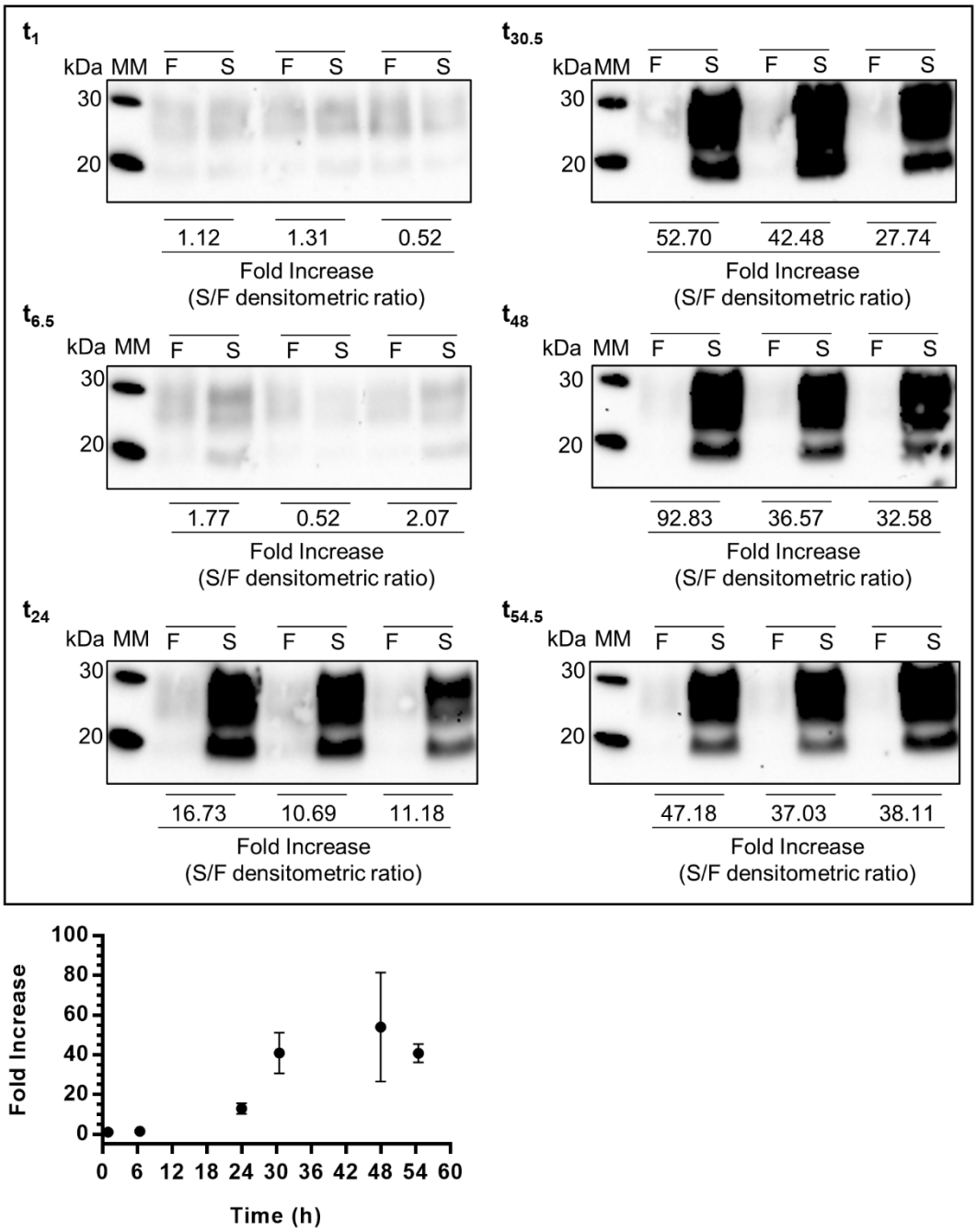

Figure II.9 sCJD subtype BH3VV2P PMCA kinetics study

In the box: WBs for the analysis of PMCA reaction kinetics. PMCA reaction seeded with BH1VV2P at dilution $1x10^{-2}$ was sampled in triplicates at defined time interval (*i.e.* $t_{1, 6.5, 24, 30, 48, 54.5}$). F: Frozen sample; S: Sonicated sample. The S/F values calculated on each pair of S and F samples are indicated at the bottom of each WB picture, in correspondence with the signals analysed. WB immunodetection was with mAb 3F4. MM: molecular weight marker; kDa: kilodalton. Below the box: graph summarizing PMCA reaction kinetics. Each data point indicates the mean average fold increase. Bars indicate standard deviation.

Appendix III

Raw data used for the evaluation of the PrP^{res} levels in the 10%BHs

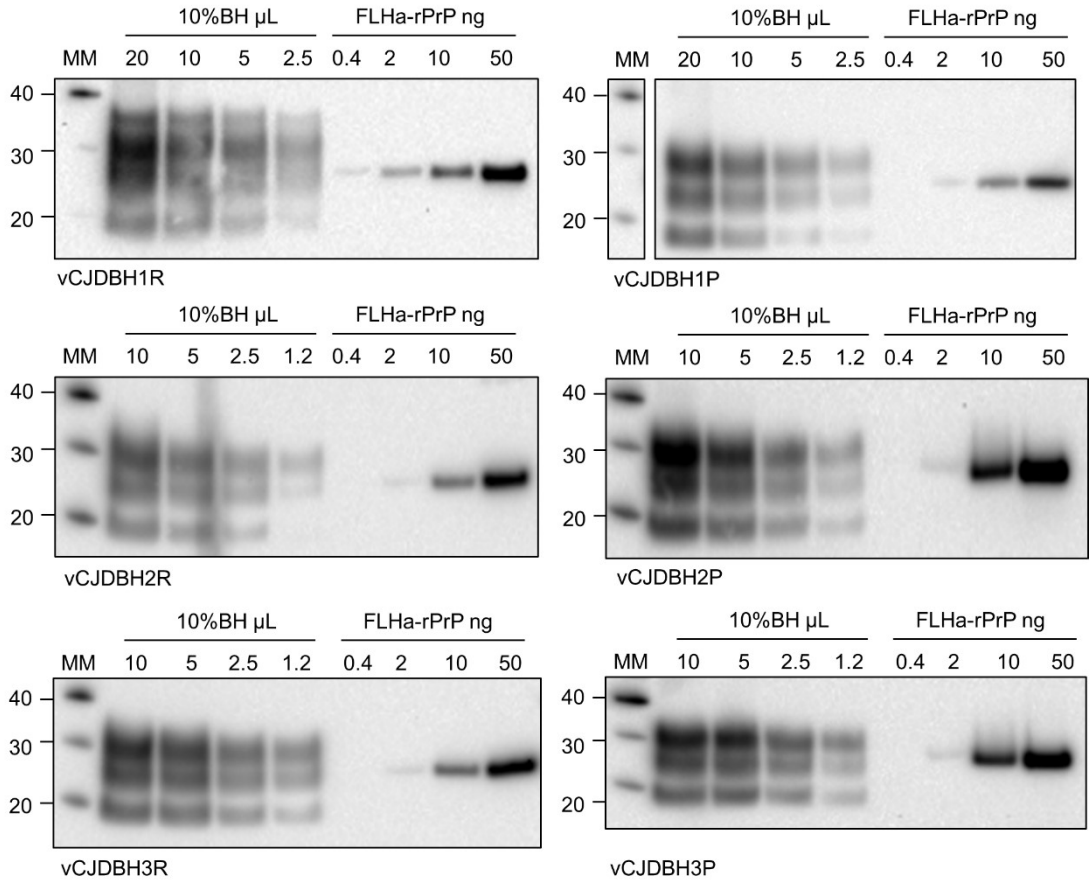

Figure III.1 WB for the evaluation of the PrP^{res} levels in the vCJD 10%BH

WBs for the evaluation of the PrP^{res} levels in the vCJD 10%BH. WB were performed as described in Section 2.4.1. The volume of PK treated 10%BH that was loaded onto the gel is indicated on top of each WB picture, along with the amount of FLHa-rPrP used as standard. The identification of the sample is shown at the bottom of each WB picture. WB immunodetection was with mAb 3F4. MM: molecular weight marker; kDa: kilodalton. FLHa-rPrP: full length hamster recombinant prion protein

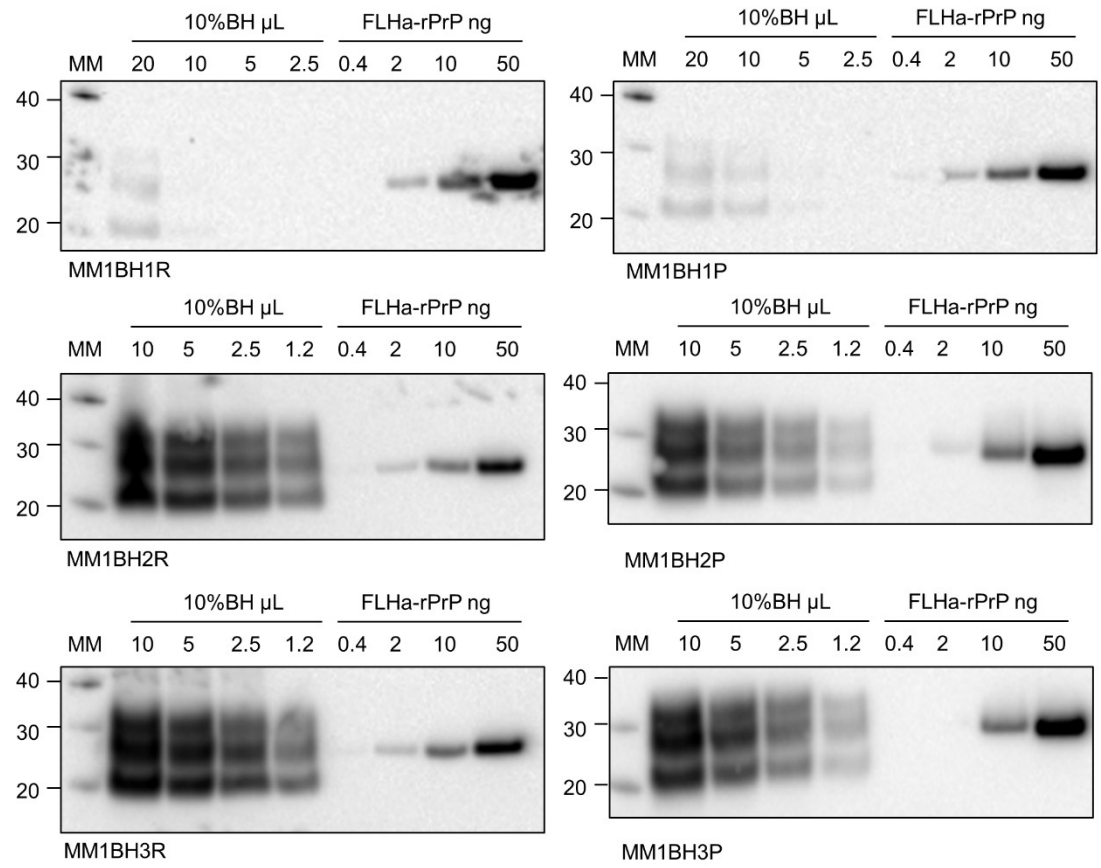

Figure III.2 WB for the evaluation of the PrP^{res} levels in the sCJD MM1 10%BH

WBs for the evaluation of the PrP^{res} levels in the vCJD 10%BH. WB were performed as described in Section 2.4.1. The volume of PK treated 10%BH that was loaded onto the gel is indicated on top of each WB picture, along with the amount of FLHa-rPrP used as standard. The identification of the sample is shown at the bottom of each WB picture. WB immunodetection was with mAb 3F4. MM: molecular weight marker; kDa: kilodalton. FLHa-rPrP: full length hamster recombinant prion protein

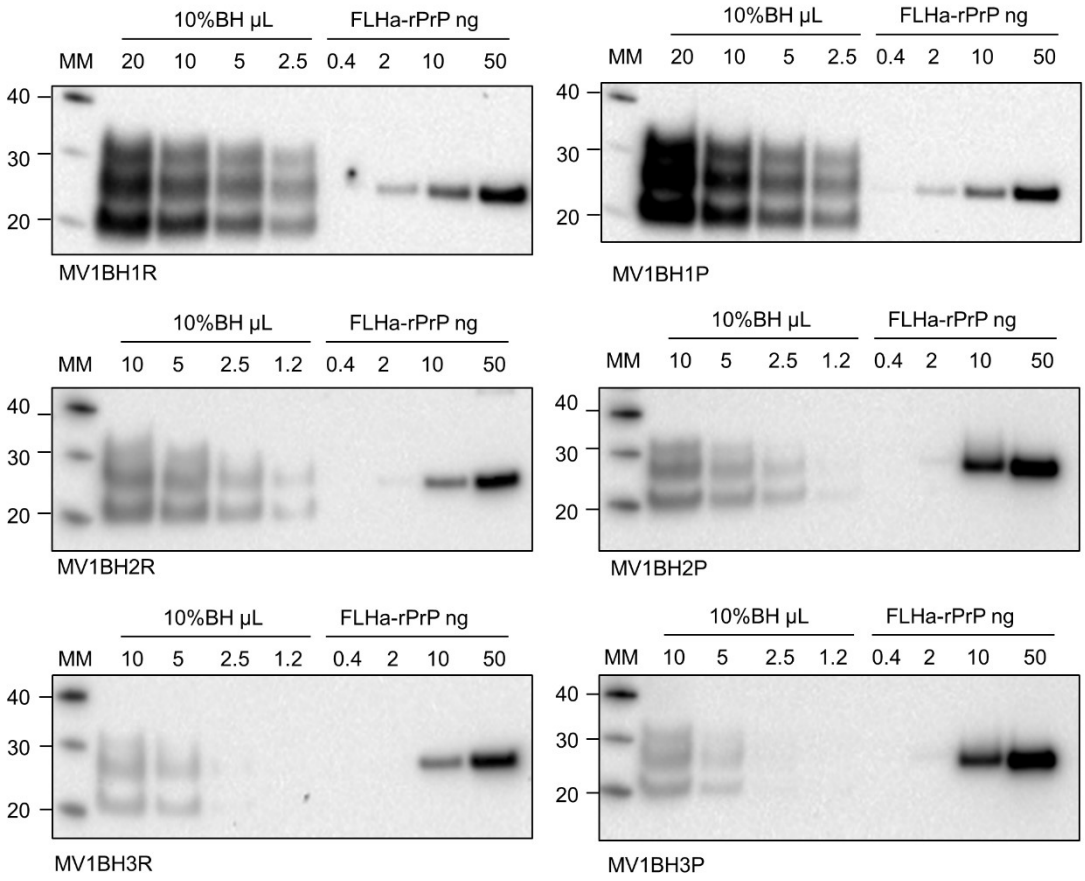

Figure III.3 WB for the evaluation of the PrP^{res} levels in the sCJD MV1 10%BH

WBs for the evaluation of the PrP^{res} levels in the vCJD 10%BH. WB were performed as described in Section 2.4.1. The volume of PK treated 10%BH that was loaded onto the gel is indicated on top of each WB picture, along with the amount of FLHa-rPrP used as standard. The identification of the sample is shown at the bottom of each WB picture. WB immunodetection was with mAb 3F4. MM: molecular weight marker; kDa: kilodalton. FLHa-rPrP: full length hamster recombinant prion protein

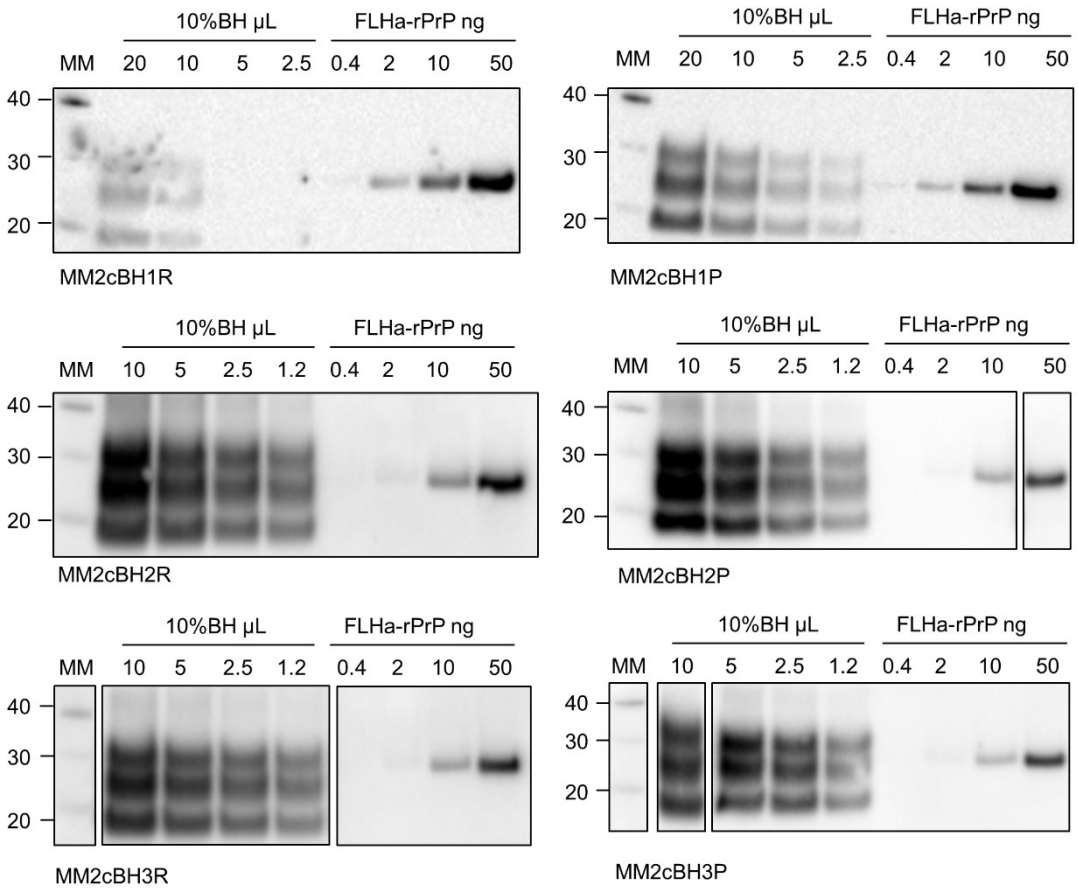

Figure III.4 WB for the evaluation of the PrP^{res} levels in the sCJD MM2c 10%BH

WBs for the evaluation of the PrP^{res} levels in the vCJD 10%BH. WB were performed as described in Section 2.4.1. The volume of PK treated 10%BH that was loaded onto the gel is indicated on top of each WB picture, along with the amount of FLHa-rPrP used as standard. The identification of the sample is shown at the bottom of each WB picture. WB immunodetection was with mAb 3F4. MM: molecular weight marker; kDa: kilodalton. FLHa-rPrP: full length hamster recombinant prion protein

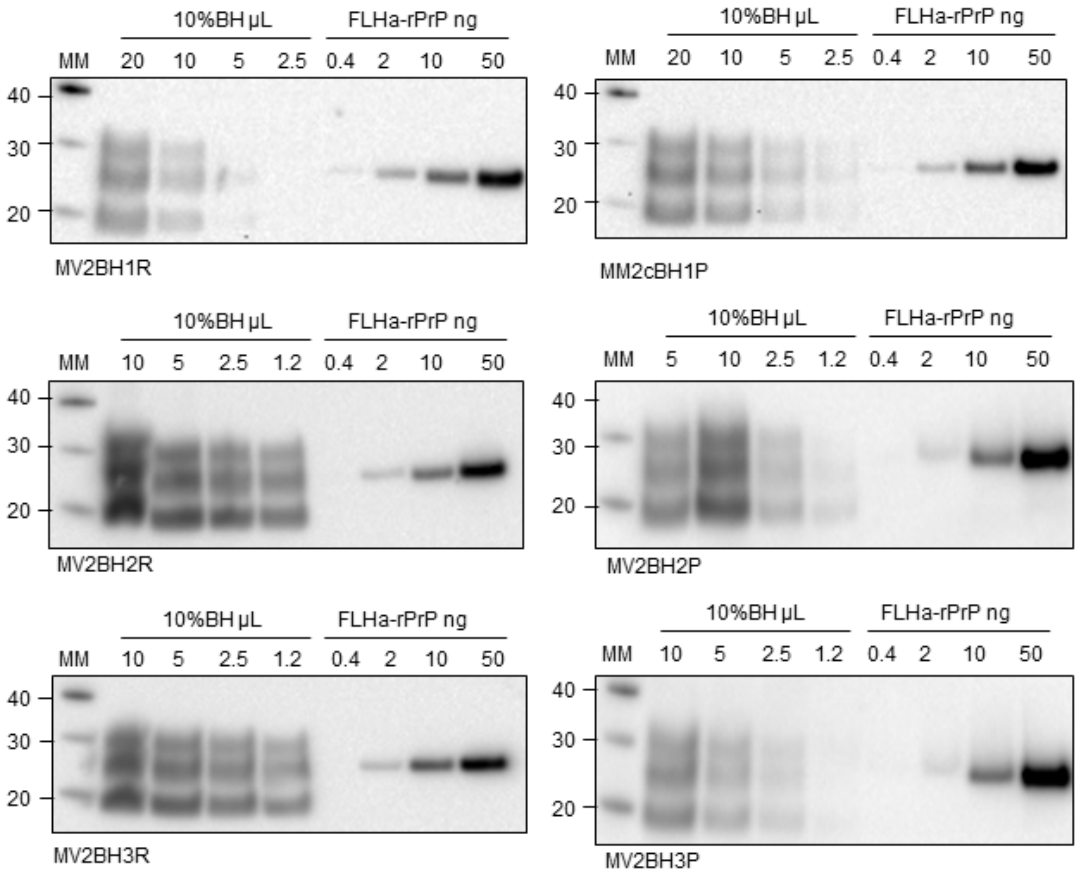

Figure III.5 WB for the evaluation of the PrP^{res} levels in the sCJD MV2 10%BH

WBs for the evaluation of the PrP^{res} levels in the vCJD 10%BH. WB were performed as described in Section 2.4.1. The volume of PK treated 10%BH that was loaded onto the gel is indicated on top of each WB picture, along with the amount of FLHa-rPrP used as standard. The identification of the sample is shown at the bottom of each WB picture. WB immunodetection was with mAb 3F4. MM: molecular weight marker; kDa: kilodalton. FLHa-rPrP: full length hamster recombinant prion protein

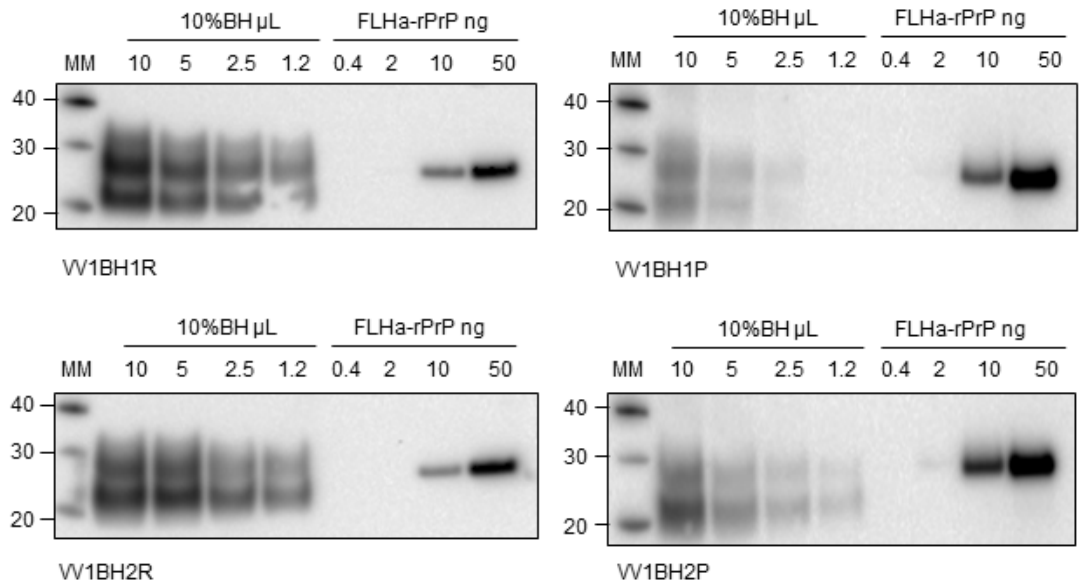

Figure III.6 WB for the evaluation of the PrP^{res} levels in the sCJD VV1 10%BH

WBs for the evaluation of the PrP^{res} levels in the vCJD 10%BH. WB were performed as described in Section 2.4.1. The volume of PK treated 10%BH that was loaded onto the gel is indicated on top of each WB picture, along with the amount of FLHa-rPrP used as standard. The identification of the sample is shown at the bottom of each WB picture. WB immunodetection was with mAb 3F4. MM: molecular weight marker; kDa: kilodalton. FLHa-rPrP: full length hamster recombinant prion protein

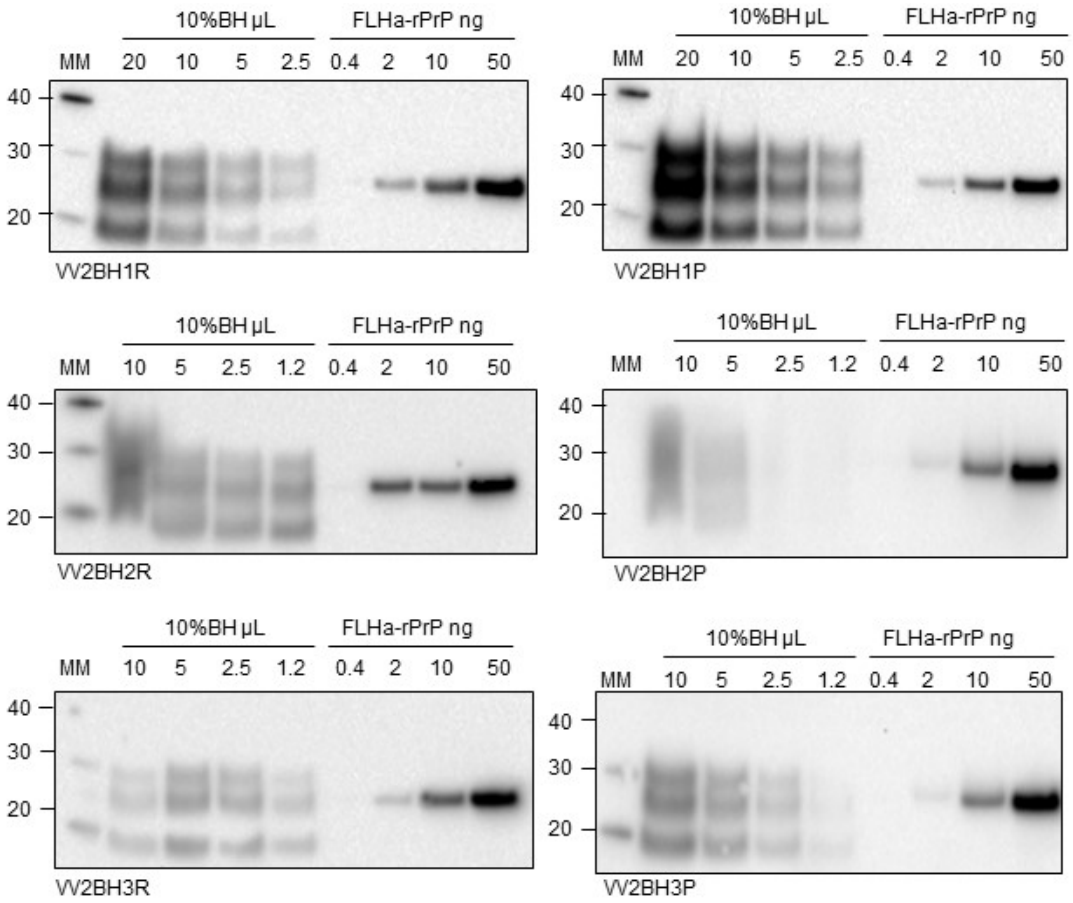

Figure III.7 WB for the evaluation of the PrP^{res} levels in the sCJD VV2 10%BH

WBs for the evaluation of the PrP^{res} levels in the vCJD 10%BH. WB were performed as described in Section 2.4.1. The volume of PK treated 10%BH that was loaded onto the gel is indicated on top of each WB picture, along with the amount of FLHa-rPrP used as standard. The identification of the sample is shown at the bottom of each WB picture. WB immunodetection was with mAb 3F4. MM: molecular weight marker; kDa: kilodalton. FLHa-rPrP: full length hamster recombinant prion protein

Bibliography

Atarashi, R., K. Sano, K. Satoh, and N. Nishida. 2011a. “Real-Time Quaking-Induced Conversion: A Highly Sensitive Assay for Prion Detection.” *Prion*. https://doi.org/10.4161/pri.5.3.16893.

Atarashi, R., K. Satoh, K. Sano, T. Fuse, N. Yamaguchi, D. Ishibashi, T. Matsubara, et al. 2011b. “Ultrasensitive Human Prion Detection in Cerebrospinal Fluid by Real-Time Quaking-Induced Conversion.” *Nature Medicine* 17 (2): 175–78. https://doi.org/10.1038/nm.2294.

Atarashi, Ryuichiro, Jason M. Wilham, Leah Christensen, Andrew G. Hughson, Roger A. Moore, Lisa M. Johnson, Henry A. Onwubiko, S. A Suzette A Priola, and Byron Caughey. 2008. “Simplified Ultrasensitive Prion Detection by Recombinant PrP Conversion with Shaking.” *Nature Methods* 5 (3): 211–12. https://doi.org/10.1038/nmeth0308-211.

Bari, Michele Angelo Di, Francesca Chianini, Gabriele Vaccari, Elena Esposito, Michela Conte, Samantha L. Eaton, Scott Hamilton, et al. 2008. “The Bank Vole (Myodes Glareolus) as a Sensitive Bioassay for Sheep Scrapie.” *Journal of General Virology* 89 (12): 2975–85. https://doi.org/10.1099/vir.0.2008/005520-0.

Barria, M. A. 2014. “Modelling Human Prion Replication in Cell-Free Systems.” University of Edinburgh. https://www.era.lib.ed.ac.uk/handle/1842/10025.

Barria, M. A., A. Balachandran, M. Morita, T. Kitamoto, R. Barron, J.C. Manson, R.S. Knight, J.W. Ironside, and M.W. Head. 2014. “Molecular Barriers to Zoonotic Transmission of Prions.” *Emerging Infectious Diseases* 20 (1): 88–97. https://doi.org/10.3201/eid2001.130858.

Barria, M. A., A. Lee, A.J.E. Green, R.S. Knight, and M.W. Head. 2018. “Rapid Amplification of Prions from Variant Creutzfeldt-Jakob Disease Cerebrospinal Fluid.” *J Path: Clin Res*, no. 4: 86–92. https://doi.org/10.1002/cjp2.90.

Barria, M.A., A. Mukherjee, D. Gonzalez-Romero, R. Morales, and C. Soto. 2009. “De Novo Generation of Infectious Prions in Vitro Produces a New Disease Phenotype.” *PLoS Pathogens* 5 (5). https://doi.org/10.1371/journal.ppat.1000421.

Baskakov, I.V., B. Caughey, J.R. Requena, A.M. Sevillano, W.K. Surewicz, and H. Wille. 2019. “The Prion 2018 Round Tables (I): The Structure of PrP Sc.” In *Prion*. https://doi.org/10.1080/19336896.2019.1569450.

Bessen, R.A., and R.F. Marsh. 1992. “Biochemical and Physical Properties of the Prion Protein from Two Strains of the Transmissible Mink Encephalopathy Agent.” *Journal of Virology* 66 (4): 2096–2101.

Biacabe, Anne Gaëlle, Jean Louis Laplanche, Stephen Ryder, and Thierry Baron. 2004. “Distinct Molecular Phenotypes in Bovine Prion Diseases.” *EMBO Reports* 5 (1): 110–14. https://doi.org/10.1038/sj.embor.7400054.

Bieschke, J., A. Giese, W. Schulz-Schaeffer, I. Zerr, S. Poser, M. Eigen, and H. Kretzschmar. 2000. “Ultrasensitive Detection of Pathological Prion Protein Aggregates by Dual-Color Scanning for Intensely Fluorescent Targets.” *Proceedings of the National Academy of Sciences* 97 (10): 5468–73. https://doi.org/10.1073/pnas.97.10.5468.

Bishop, M.T., P. Hart, L. Aitchison, H.N. Baybutt, C. Plinston, V. Thomson, N.L. Tuzi, et al. 2006. “Predicting Susceptibility and Incubation Time of Human-to-Human Transmission of VCJD.” *Lancet Neurology* 5 (5): 393–98. https://doi.org/10.1016/S1474-4422(06)70413-6.

Bishop, M.T., R.G. Will, and J.C. Manson. 2010. “Defining Sporadic Creutzfeldt-Jakob Disease Strains and Their Transmission Properties.” *Proceedings of the National Academy of Sciences* 107 (26): 12005–10. https://doi.org/10.1073/pnas.1004688107.

Bolton, D.C., M.P. Mckinley, and S.B. Prusiner. 1982. “Identification of a Protein That Purifies with the Scrapie Prion.” *Science* 218 (4579): 1309–11. https://doi.org/10.1126/science.6815801.

Bongianni, M., C.D. Orrù, B.R. Groveman, L. Sacchetto, M. Fiorini, G. Tonoli, G. Triva, et al. 2017. “Diagnosis of Human Prion Disease Using Real-Time Quaking-Induced Conversion Testing of Olfactory Mucosa and Cerebrospinal Fluid Samples.” *JAMA Neurology* 74 (2): 155. https://doi.org/10.1001/jamaneurol.2016.4614.

Bougard, Daisy, Jean Philippe Brandel, Maxime Bélondrade, Vincent Béringue, Christiane Segarra, Hervé Fleury, Jean Louis Laplanche, et al. 2016. “Detection of Prions in the Plasma of Presymptomatic and Symptomatic Patients with Variant Creutzfeldt-Jakob Disease.” *Science Translational Medicine* 8 (370): 1–10. https://doi.org/10.1126/scitranslmed.aag1257.

Brandner, S., A. Raeber, A. Sailer, T. Blattler, M. Fischer, C. Weissmann, and A. Aguzzi. 2002. “Normal Host Prion Protein (PrPC) Is Required for Scrapie Spread within the Central Nervous System.” *Proceedings of the National Academy of Sciences* 93 (23): 13148–51. https://doi.org/10.1073/pnas.93.23.13148.

Brandner, Sebastian, Stefan Isenmann, Alex Raeber, Marek Fischer, Andreas Sailer, Yasushi Kobayashi, Silvia Marino, Charles Weissmann, and Adriano Aguzzi. 1996. “Normal Host Prion Protein Necessary for Scrapie-Induced Neurotoxicity.” *Nature* 379 (6563): 339–43. https://doi.org/10.1038/379339a0.

Brown, P., J. Brandel, T. Sato, Y. Nakamura, J. MacKenzie, R.G. Will, A. Ladogana, M. Pocchiari, E.W. Leschek, and L.B. Schonberger. 2012. “Iatrogenic Creutzfeldt-Jakob Disease, Final Assessment.” *Emerging Infectious Diseases* 18 (6). https://doi.org/10.3201/eid1806.120116.

Brown, P., C. J. Gibbs, P. Rodgers-Johnson, D.M. Asher, M.P. Sulima, A. Bacote, L.G. Goldfarb, and D.C. Gajdusek. 1994. “Human Spongiform Encephalopathy: The National Institutes of Health Series of 300 Cases of Experimentally Transmitted Disease.” *Annals of Neurology* 35 (5): 513–29. https://doi.org/10.1002/ana.410350504.

Bruce, M. E., R. G. Will, J. W. Ironside, I. McConnell, D. Drummond, A. Suttie, L. McCardle, et al. 1997. “Transmissions to Mice Indicate That ‘new Variant’ CJD Is Caused by the BSE Agent.” *Nature* 389 (6650): 498–501. https://doi.org/10.1038/39057.

Büeler, H., A. Aguzzi, A. Sailer, R. A. Greiner, P. Autenried, M. Aguet, and C. Weissmann. 1993. “Mice Devoid of PrP Are Resistant to Scrapie.” *Cell*. https://doi.org/10.1016/0092-8674(93)90360-3.

Cali, I., J. Lavrich, F. Moda, D. Kofskey, S.K. Nemani, B. Appleby, F. Tagliavini, C. Soto, P. Gambetti, and S. Notari. 2019. “PMCA-Replicated PrPD in Urine of VCJD Patients Maintains Infectivity and Strain Characteristics of Brain PrPD: Transmission Study.” *Scientific Reports* 9 (1): 5191. https://doi.org/10.1038/s41598-019-41694-0.

Camacho, M.V., G. Telling, Q. Kong, P. Gambetti, and S. Notari. 2019. “Role of Prion Protein Glycosylation in Replication of Human Prions by Protein Misfolding Cyclic Amplification.” *Laboratory Investigation*, June. https://doi.org/10.1038/s41374-019-0282-1.

Campioni, S., B. Mannini, M. Zampagni, A. Pensalfini, C. Parrini, E. Evangelisti, A. Relini, et al. 2010. “A Causative Link between the Structure of Aberrant Protein Oligomers and Their Toxicity.” *Nature Chemical Biology* 6 (2): 140–47. https://doi.org/10.1038/nchembio.283.

Casalone, C., G. Zanusso, P. Acutis, S. Ferrari, L. Capucci, F. Tagliavini, S. Monaco, and M. Caramelli. 2004. “Identification of a Second Bovine Amyloidotic Spongiform Encephalopathy: Molecular Similarities with Sporadic Creutzfeldt-Jakob Disease.” *Proceedings of the National Academy of Sciences* 101 (9): 3065–70. https://doi.org/10.1073/pnas.0305777101.

Castilla, J., R. Morales, P. Saá, M.A. Barria, P. Gambetti, and C. Soto. 2008. “Cell-Free Propagation of Prion Strains.” *EMBO Journal* 27 (19): 2557–66. https://doi.org/10.1038/emboj.2008.181.

Caughey, B.W., K.S. Bhat, D. Ernst, S.F. Hayes, A. Dong, and W.S. Caughey. 1991. “Secondary Structure Analysis of the Scrapie-Associated Protein PrP 27–30 in Water by Infrared Spectroscopy.” *Biochemistry* 30 (31): 7672–80. https://doi.org/10.1021/bi00245a003.

Chandler, R.L. 1961. “Encephalopathy in Mice Produced by Inoculation with Scrapie Brain Material.” *The Lancet* 277 (7191): 1378–79. https://doi.org/10.1016/S0140-6736(61)92008-6.

Chen, B., R. Morales, M.A. Barria, and C. Soto. 2010. “Estimating Prion Concentration in Fluids and Tissues by Quantitative PMCA.” *Nature Methods* 7 (7): 519–20. https://doi.org/10.1038/nmeth.1465.

Cohen, F.E., K.M. Pan, Z. Huang, M. Baldwin, R.J. Fletterick, and S.B. Prusiner. 1994. “Structural Clues to Prion Replication.” *Science* 264 (5158): 530–31. https://www.ncbi.nlm.nih.gov/pubmed/7909169.

Cohen, S.I.A., M. Vendruscolo, C.M. Dobson, and T.P.J. Knowles. 2013. “The

Kinetics and Mechanisms of Amyloid Formation." In *Amyloid Fibrils and Prefibrillar Aggregates: Molecular and Biological Properties, 1st Edition*, edited by Daniel Erik Otzen.

Colby, D.W., K. Giles, G. Legname, H. Wille, I.V. Baskakov, S.J. DeArmond, and S.B. Prusiner. 2009. "Design and Construction of Diverse Mammalian Prion Strains." *Proceedings of the National Academy of Sciences* 106 (48): 20417–22. https://doi.org/10.1073/pnas.0910350106.

Colby, D.W., Q. Zhang, S. Wang, D. Groth, G. Legname, D. Riesner, and S.B. Prusiner. 2007. "Prion Detection by an Amyloid Seeding Assay." *Proceedings of the National Academy of Sciences of the United States of America* 104 (52): 20914–19. https://doi.org/10.1073/pnas.0710152105.

Collinge, J., and A.R. Clarke. 2007. "A General Model of Prion Strains and Their Pathogenicity." *Science* 318 (5852): 930–36. https://doi.org/10.1126/science.1138718.

Collinge, J., K.C.L. Sidle, J. Meads, J.W. Ironside, and A.F. Hill. 1996. "Molecular Analysis of Prion Strain Variation and the Aetiology of 'new Variant' CJD." *Nature* 383 (6602): 685–90. https://doi.org/10.1038/383685a0.

Collinge, John, Mark S. Palmer, Katie C.L. Sidle, Andrew F. Hill, Ian Gowland, Julie Meads, Emmanuel Asante, Ray Bradley, Lawrence J. Doey, and Peter L. Lantos. 1995. "Unaltered Susceptibility to BSE in Transgenic Mice Expressing Human Prion Protein." *Nature* 378 (6559): 779–83. https://doi.org/10.1038/378779a0.

Collins, S.J., P. Sanchez-Juan, C.L. Masters, G.M. Klug, C. Van Duijn, A. Poleggi, M. Pocchiari, et al. 2006. "Determinants of Diagnostic Investigation Sensitivities across the Clinical Spectrum of Sporadic Creutzfeldt-Jakob Disease." *Brain* 129 (9): 2278–87. https://doi.org/10.1093/brain/awl159.

Concha-Marambio, L., S. Pritzkow, F. Moda, F. Tagliavini, J.W. Ironside, P.E. Schulz, and C. Soto. 2016. "Detection of Prions in Blood from Patients with Variant Creutzfeldt-Jakob Disease TL - 8." *Science Translational Medicine* 8 (370): 370–183. https://doi.org/10.1126/scitranslmed.aaf6188.

Cramm, M., M. Schmitz, A. Karch, E. Mitrova, F. Kuhn, B. Schroeder, A. Raeber, et al. 2015. "Stability and Reproducibility Underscore Utility of RT-QuIC for Diagnosis of Creutzfeldt-Jakob Disease." *Molecular Neurobiology* 53 (3): 1896–1904. https://doi.org/10.1007/s12035-015-9133-2.

Crozet, C., F. Flamant, A. Bencsik, D. Aubert, J. Samarut, and T. Baron. 2001. "Efficient Transmission of Two Different Sheep Scrapie Isolates in Transgenic Mice Expressing the Ovine PrP Gene." *Journal of Virology* 75 (11): 5328–34. https://doi.org/10.1128/jvi.75.11.5328-5334.2001.

Dabaghian, R., I. Zerr, U. Heinemann, and G. Zanusso. 2008. "Detection of Proteinase K Resistant Proteins in the Urine of Patients with Creutzfeldt-Jakob and Other Neurodegenerative Diseases." *Prion* 2 (4): 170–78.

Deleault, N.R., B.T. Harris, J.R. Rees, and S. Supattapone. 2007. "Formation of

Native Prions from Minimal Components in Vitro." *Proceedings of the National Academy of Sciences of the United States of America* 104 (23): 9741–46. https://doi.org/10.1073/pnas.0702662104.

Denkers, N.D., D.M. Henderson, C.K. Mathiason, and E.A. Hoover. 2016. "Enhanced Prion Detection in Biological Samples by Magnetic Particle Extraction and Real-Time Quaking-Induced Conversion." *The Journal of General Virology* 97 (8): 2023–29. https://doi.org/10.1099/jgv.0.000515.

Diack, A.B., D.L. Ritchie, M.T. Bishop, V. Pinion, J.P. Brandel, S. Haik, F. Tagliavini, et al. 2012. "Constant Transmission Properties of Variant Creutzfeldt-Jakob Disease in 5 Countries." *Emerging Infectious Diseases* 18 (10): 1574–79. https://doi.org/10.3201/eid1810.120792.

Dobson, C.M. 2003. "Protein Folding and Misfolding." *Nature* 426 (6968): 884–90. https://doi.org/10.1038/nature02261.

Eigen, M. 1996. "Prionics or the Kinetic Basis of Prion Diseases." *Biophysical Chemistry* 63 (1). https://doi.org/10.1016/S0301-4622(96)02250-8.

Fairfoul, G., L.I. McGuire, S. Pal, J.W. Ironside, J. Neumann, S. Christie, C. Joachim, et al. 2016. "Alpha-Synuclein RT-QuIC in the CSF of Patients with Alpha-Synucleinopathies." *Annals of Clinical and Translational Neurology* 3 (10): 812–18. https://doi.org/10.1002/acn3.338.

Fernández-Borges, N., J. De Castro, and J. Castilla. 2009. "In Vitro Studies of the Transmission Barrier." In *Prion*. Vol. 3. https://doi.org/10.4161/pri.3.4.10500.

Foutz, A., B.S. Appleby, C. Hamlin, X. Liu, S. Yang, Y. Cohen, W. Chen, et al. 2017. "Diagnostic and Prognostic Value of Human Prion Detection in Cerebrospinal Fluid." *Annals of Neurology* 81 (1): 79–92. https://doi.org/10.1002/ana.24833.

Fraser, H., and A.G. Dickinson. 1973. "Scrapie in Mice. Agent-Strain Differences in the Distribution and Intensity of Grey Matter Vacuolation." *Journal of Comparative Pathology* 83 (1): 29–40. https://doi.org/10.1016/0021-9975(73)90024-8.

Gajdusek, D.C., C.J.Jr. Gibbs, and M.P. Alpers. 1967. "Transmission and Passage of Experimental " Kuru " to Chimpanzees." *Science* 155 (3759): 212–14. http://www.jstor.org/stable/1721151.

Gibbs, C.J.Jr., D.C. Gajdusek, D.M. Asher, and M.P. Alpers. 1968. "Creutzfeldt-Jakob Disease (Spongiform Encephalopathy): Transmission to the Chimpanzee." *Science* 161 (10).

Giehm, L., and D.E. Otzen. 2010. "Strategies to Increase the Reproducibility of Protein Fibrillization in Plate Reader Assays." *Analytical Biochemistry* 400 (2): 270–81. https://doi.org/10.1016/j.ab.2010.02.001.

Gregori, L., G. Kovacs, I. Alexeeva, H. Budka, and R.G. Rohwer. 2008. "Excretion of Transmissible Spongiform Encephalopathy Infectivity in Urine." *Emerging Infectious Diseases* 14 (9): 1406–12. https://doi.org/10.3201/eid1409.080259.

Griffith, J.S. 1967. “Self-Replication and Scrapie.” *Nature* 215 (5105): 1043–44.

Groveman, B.R., M.A. Dolan, L.M. Taubner, A. Kraus, R.B. Wickner, and B.W. Caughey. 2014. “Parallel In-Register Intermolecular-Sheet Architectures for Prion-Seeded Prion Protein (PrP) Amyloids.” *Journal of Biological Chemistry* 289 (35): 24129–42. https://doi.org/10.1074/jbc.M114.578344.

Groveman, B.R., C.D. Orrù, A.G. Hughson, M. Bongianni, M. Fiorini, D. Imperiale, A. Ladogana, M. Pocchiari, G. Zanusso, and B.W. Caughey. 2016. “Extended and Direct Evaluation of RT-QuIC Assays for Creutzfeldt-Jakob Disease Diagnosis.” *Annals of Clinical and Translational Neurology* 4 (2): 139–44. https://doi.org/10.1002/acn3.378.

Groveman, B.R., C.D. Orrù, A.G. Hughson, L.D. Raymond, G. Zanusso, B. Ghetti, K.J. Campbell, J. Safar, D. Galasko, and B.W. Caughey. 2018. “Rapid and Ultra-Sensitive Quantitation of Disease-Associated α-Synuclein Seeds in Brain and Cerebrospinal Fluid by ASyn RT-QuIC.” *Journal of Biological Research* 25 (1): 1–10. https://doi.org/10.1186/s40478-018-0508-2.

Groveman, Bradley R., Gregory J. Raymond, Katrina J. Campbell, Brent Race, Lynne D. Raymond, Andrew G. Hughson, Christina D. Orrú, Allison Kraus, Katie Phillips, and Byron Caughey. 2017. “Role of the Central Lysine Cluster and Scrapie Templating in the Transmissibility of Synthetic Prion Protein Aggregates.” *PLoS Pathogens* 13 (9). https://doi.org/10.1371/journal.ppat.1006623.

Hadlow, W.J. 1959. “Scrapie and Kuru.” *The Lancet* 274 (7097): 289–90. https://doi.org/10.1016/S0140-6736(59)92081-1.

Hafner-Bratkovič, I. 2017. “Prions, Prionoid Complexes and Amyloids: The Bad, the Good and Something in Between.” *Swiss Medical Weekly* 147. https://doi.org/10.4414/smw.2017.14424.

Haigh, C.L., and S.C. Drew. 2015. “Cavitation during the Protein Misfolding Cyclic Amplification (PMCA) Method - The Trigger for de Novo Prion Generation?” *Biochemical and Biophysical Research Communications* 461 (3): 494–500. https://doi.org/10.1016/j.bbrc.2015.04.048.

Head, M.W. 2013. “Human Prion Diseases: Molecular, Cellular and Population Biology.” *Neuropathology* 33 (3): 221–36. https://doi.org/10.1111/neup.12016.

Head, M.W., T.J.R. Bunn, M.T. Bishop, V. McLoughlin, S. Lowrie, C.S. McKimmie, M.C. Williams, et al. 2004. “Prion Protein Heterogeneity in Sporadic but Not Variant Creutzfeldt-Jakob Disease: U.K. Cases 1991-2002.” *Annals of Neurology* 55 (6): 851–59. https://doi.org/10.1002/ana.20127.

Head, M.W., and J.W. Ironside. 2012. “Review: Creutzfeldt-Jakob Disease: Prion Protein Type, Disease Phenotype and Agent Strain.” *Neuropathology and Applied Neurobiology* 38 (4): 296–310. https://doi.org/10.1111/j.1365-2990.2012.01265.x.

Head, M.W., J.W. Ironside, B. Ghetti, M. Jeffrey, P. Piccardo, and R.G. Will. 2008. “Prion Diseases.” In *Greenfield’s Neuropathology 8th Edition*, edited by S.

Love, D.N. Louis, D. Ellison, and J.G. Greenfield.

Head, M.W., E. Kouverianou, L. Taylor, A.J Green, and R.S. Knight. 2005. "Evaluation of Urinary PrPScas a Diagnostic Test for Sporadic, Variant, and Familial CJD." *Neurology* 64 (10): 1794–96. https://doi.org/10.1212/01.WNL.0000161842.68793.8A.

Henderson, D.M., K.A. Davenport, N.J. Haley, N.D. Denkers, C.K. Mathiason, and E.A. Hoover. 2015a. "Quantitative Assessment of Prion Infectivity in Tissues and Body Fluids by Real-Time Quaking-Induced Conversion." *Journal of General Virology* 96: 210–19. https://doi.org/10.1099/vir.0.069906-0.

Henderson, D.M., N.D Denkers, C.E. Hoover, N. Garbino, C.K. Mathiason, and E.A. Hoover. 2015b. "Longitudinal Detection of Prion Shedding in Saliva and Urine by Chronic Wasting Disease-Infected Deer by Real-Time Quaking-Induced Conversion." *Journal of Virology* 89 (18): 9338–47. https://doi.org/10.1128/JVI.01118-15.

Hermann, P., M. Laux, M. Glatzel, J. Matschke, T. Knipper, S. Goebel, J. Treig, et al. 2018. "Validation and Utilization of Amended Diagnostic Criteria in Creutzfeldt-Jakob Disease Surveillance." *Neurology* 91 (4): e331–38. https://doi.org/10.1212/wnl.0000000000005860.

Hill, A.F., M. Desbruslais, S. Joiner, K.C.L. Sidle, I. Gowland, J. Collinge, L.J. Doey, and P. Lantos. 1997. "The Same Prion Strain Causes VCJD and BSE." *Nature* 389 (6650): 448–50. https://doi.org/10.1038/38925.

Ironside, J.W., R.S.G. Knight, and M.W. Head. 2011. "Iatrogenic Creutzfeldt-Jakob Disease." In *Neurodegeneration: The Molecular Pathology of Dementia and Movement Disorders 2nd Edn.*, edited by D. W. Dickson and R.O. Weller, 381–386. Oxford: Wiley-Blackwell.

ISS. 2019. "CJD and Related Diseases in Italy." http://old.iss.it/binary/rncj/cont/Tavola31October2019english.pdf.

Jarrett, J.T., and P.T. Lansbury. 1993. "Seeding 'One-Dimensional Crystallization' of Amyloid: A Pathogenic Mechanism in Alzheimer's Disease and Scrapie?" *Cell*. https://doi.org/10.1016/0092-8674(93)90635-4.

John, T.R., H.M. Schatzl, and S. Gilch. 2013. "Early Detection of Chronic Wasting Disease Prions in Urine of Pre-Symptomatic Deer by Real-Time Quaking-Induced Conversion Assay." *Prion* 7 (3): 253–58. https://doi.org/10.4161/pri.24430.

Jones, M., A.H. Peden, D. Wight, C. Prowse, I. MacGregor, J.C. Manson, M.L. Turner, J.W. Ironside, and M.W. Head. 2008. "Effects of Human PrPSc Type and PRNP Genotype in an In-Vitro Conversion Assay." *NeuroReport* 19 (18): 1783–86. https://doi.org/10.1097/WNR.0b013e328318edfa.

Kariv-Inbal, Z., T. Ben-Hur, N.C. Grigoriadis, R. Engelstein, and R. Gabizon. 2006. "Urine from Scrapie-Infected Hamsters Comprises Low Levels of Prion Infectivity." *Neurodegenerative Diseases* 3 (3): 123–28. https://doi.org/10.1159/000094770.

Kaski, D., S. Mead, H. Hyare, S. Cooper, R. Jampana, J. Overell, R.S.G. Knight, J. Collinge, and P. Rudge. 2009. “Variant CJD in an Individual Heterozygous for PRNP Codon 129.” *The Lancet* 374 (9707): 2128. https://doi.org/10.1016/s0140-6736(09)61568-3.

Kayed, R., E. Head, J.L. Thompson, T.M. McIntire, S.C. Milton, C.W. Cotman, and C.G. Glabel. 2003. “Common Structure of Soluble Amyloid Oligomers Implies Common Mechanism of Pathogenesis.” *Science* 300 (5618): 486–89. https://doi.org/10.1126/science.1079469.

Kimberlin, R.H., and C.A. Walker. 1978. “Evidence That the Transmission of One Source of Scrapie Agent to Hamsters Involves Separation of Agent Strains from a Mixture.” *Journal of General Virology* 39 (3): 487–96. https://doi.org/10.1099/0022-1317-39-3-487.

Kobayashi, A., Y. Matsuura, S. Mohri, and T. Kitamoto. 2014. “Distinct Origins of Dura Mater Graft-Associated Creutzfeldt-Jakob Disease: Past and Future Problems.” Vol. 2. https://doi.org/10.1186/2051-5960-2-32.

Kobayashi, A., Y. Matsuura, A. Takeuchi, M. Yamada, I. Miyoshi, S. Mohri, and T. Kitamoto. 2019. “A Domain Responsible for Spontaneous Conversion of Bank Vole Prion Protein.” *Brain Pathology* 29 (2): 155–63. https://doi.org/10.1111/bpa.12638.

Kocisko, D., J. Come, S.A. Priola, B. Chesebro, G.J. Raymond, P.T. Lansbury, and B.W. Caughey. 1994. “Cell-Free Formation of Protease-Resistant Prion Protein.” *Nature* 370 (066/21): 471–74.

Kocisko, D.A., S.A. Priola, G.J. Raymond, B. Chesebro, P.T. Lansbury, and B.W. Caughey. 2006. “Species Specificity in the Cell-Free Conversion of Prion Protein to Protease-Resistant Forms: A Model for the Scrapie Species Barrier.” *Proceedings of the National Academy of Sciences* 92 (9): 3923–27. https://doi.org/10.1073/pnas.92.9.3923.

Ladogana, A., M. Puopolo, E.A. Croes, H. Budka, C. Jarius, S. Collins, G.M. Klug, et al. 2005. “Mortality from Creutzfeldt-Jakob Disease and Related Disorders in Europe, Australia, and Canada.” *Neurology* 64 (9): 1586–91. https://doi.org/10.1212/01.WNL.0000160117.56690.B2.

Ladogana, A., P. Sanchez-Juan, E. Mitrová, A.J.E. Green, N. Cuadrado-Corrales, R. Sánchez-Valle, S. Koscova, et al. 2009. “Cerebrospinal Fluid Biomarkers in Human Genetic Transmissible Spongiform Encephalopathies.” *Journal of Neurology* 256 (10): 1620–28. https://doi.org/10.1007/s00415-009-5163-x.

Legname, G., I.V. Baskakov, H.B. Nguyen, D. Reisner, F.E. Cohen, S.J. Dearmond, and S.B. Prusiner. 2004. “Synthetic Mammalian Prions.” *Science* 305 (July): 673–76.

Levavasseur, E., A.G. Biacabe, E. Comoy, A. Culeux, K. Grznarova, N. Privat, S. Simoneau, et al. 2017. “Detection and Partial Discrimination of Atypical and Classical Bovine Spongiform Encephalopathies in Cattle and Primates Using Real-Time Quaking-Induced Conversion Assay.” *PLoS ONE* 12 (2). https://doi.org/10.1371/journal.pone.0172428.

Levavasseur, E., N. Privat, J.C.E. Martin, S. Simoneau, T. Baron, B. Flan, J.M. Torres, and S. Haïk. 2014. “Molecular Modeling of Prion Transmission to Humans.” *Viruses* 6 (10): 3766–77. https://doi.org/10.3390/v6103766.

Li, R., T. Liu, B.S. Wong, T. Pan, M. Morillas, W. Swietnicki, K. O’Rourke, P. Gambetti, W.K. Surewicz, and M.S. Sy. 2000. “Identification of an Epitope in the C Terminus of Normal Prion Protein Whose Expression Is Modulated by Binding Events in the N Terminus.” *Journal of Molecular Biology* 301 (3): 567–73. https://doi.org/10.1006/jmbi.2000.3986.

Masel, J., V.A.A. Jansen, and M.A. Nowak. 1999. “Quantifying the Kinetic Parameters of Prion Replication.” *Biophysical Chemistry* 77 (2–3): 139–52. https://doi.org/10.1016/S0301-4622(99)00016-2.

Masters, C.L., J.O. Harris, D.C. Gajdusek, C.J. Gibbs, C. Bernoulli, and D.M. Asher. 1979. “Creutzfeldt-Jakob Disease: Patterns of Worldwide Occurrence and the Significance of Familial and Sporadic Clustering.” *Annals of Neurology* 5 (2): 177–88. https://doi.org/10.1002/ana.410050212.

Masujin, K., C.D. Orrù, K. Miyazawa, B.R. Groveman, L.D. Raymond, A.G. Hughson, and B.W. Caughey. 2016. “Detection of Atypical H-Type Bovine Spongiform Encephalopathy and Discrimination of Bovine Prion Strains by Real-Time Quaking-Induced Conversion.” *Journal of Clinical Microbiology* 54 (3): 676–86. https://doi.org/10.1128/JCM.02731-15.

McGuire, L.I., A.H. Peden, C.D. Orrù, J.M. Wilham, N.E. Appleford, G. Mallinson, M. Andrews, et al. 2012. “Real Time Quaking-Induced Conversion Analysis of Cerebrospinal Fluid in Sporadic Creutzfeldt-Jakob Disease.” *Annals of Neurology* 72 (2): 278–85. https://doi.org/10.1002/ana.23589.

McGuire, L.I., A. Poleggi, I. Poggiolini, S. Suardi, K. Grznarova, S. Shi, B. de Vil, et al. 2016. “Cerebrospinal Fluid Real-Time Quaking-Induced Conversion Is a Robust and Reliable Test for Sporadic Creutzfeldt-Jakob Disease: An International Study.” *Annals of Neurology* 80 (1): 160–65. https://doi.org/10.1002/ana.24679.

Moda, F., P. Gambetti, S. Notari, L. Concha-Marambio, M. Catania, K.-W. Park, Emanuela Maderna, et al. 2014. “Prions in the Urine of Patients with Variant Creutzfeldt–Jakob Disease.” *New England Journal of Medicine* 371 (6): 530–39. https://doi.org/10.1056/NEJMoa1404401.

Moda, F., S. Pritzkow, and C. Soto. 2013. “Protein Misfolding Cyclic Amplification.” In *Prions and Diseases: Volume 1, Physiology and Pathophysiology*, edited by W.-Q. Zou and P. Gambetti, 83–92. New York, NY: Springer. https://doi.org/10.1007/978-1-4614-5305-5_6.

Moda, F., S. Suardi, G. Di Fede, A. Indaco, L. Limido, C. Vimercati, M. Ruggerone, et al. 2012. “MM2-Thalamic Creutzfeldt-Jakob Disease: Neuropathological, Biochemical and Transmission Studies Identify a Distinctive Prion Strain.” *Brain Pathology* 22 (5): 662–69. https://doi.org/10.1111/j.1750-3639.2012.00572.x.

Mok, T., Z. Jaunmuktane, S. Joiner, T. Campbell, C. Morgan, B. Wakerley, F. Golestani, et al. 2017. “Variant Creutzfeldt–Jakob Disease in a Patient with

Heterozygosity at PRNP Codon 129." *New England Journal of Medicine* 376 (3): 292–94. https://doi.org/10.1056/nejmc1610003.

Morales, R., C. Duran-Aniotz, R. Diaz-Espinoza, M.V. Camacho, and C. Soto. 2012. "Protein Misfolding Cyclic Amplification of Infectious Prions." *Nature Protocols* 7 (June): 1397. https://doi.org/10.1038/nprot.2012.067.

Moudjou, M., J. Chapuis, M. Mekrouti, F. Reine, L. Herzog, P. Sibille, H. Laude, et al. 2016. "Glycoform-Independent Prion Conversion by Highly Efficient, Cell-Based, Protein Misfolding Cyclic Amplification." *Scientific Reports* 6 (July): 1–12. https://doi.org/10.1038/srep29116.

Noble, Geoffrey P., and Surachai Supattapone. 2015. "Dissociation of Recombinant Prion Autocatalysis from Infectivity." *Prion* 9 (6): 405–11. https://doi.org/10.1080/19336896.2015.1123843.

Nonno, Romolo, Michele A Di Bari, Franco Cardone, Gabriele Vaccari, Paola Fazzi, Giacomo Dell'Omo, Claudia Cartoni, et al. 2006. "Efficient Transmission and Characterization of Creutzfeldt–Jakob Disease Strains in Bank Voles." *PLoS Pathogens* 2 (2): e12. https://doi.org/10.1371/journal.ppat.0020012.

Notari, S., L. Qing, M. Pocchiari, A. Dagdanova, K. Hatcher, A. Dogterom, J.F. Groisman, et al. 2012. "Assessing Prion Infectivity of Human Urine in Sporadic Creutzfeldt-Jakob Disease." *Emerging Infectious Diseases* 18 (1): 21–28. https://doi.org/10.3201/eid1801.110589.

Nowak, M.A., D.C. Krakauer, A. Klug, and R.M. May. 1998. "Prion Infection Dynamics." *Integrative Biology: Issues, News, and Reviews* 1 (1): 3–15. https://doi.org/10.1002/(SICI)1520-6602(1998)1:1<3::AID-INBI2>3.0.CO;2-9.

Orrù, C.D., M. Bongianni, G. Tonoli, S. Ferrari, A.G. Hughson, B.R. Groveman, M. Fiorini, et al. 2014. "A Test for Creutzfeldt–Jakob Disease Using Nasal Brushings." *New England Journal of Medicine* 371 (6): 519–29. https://doi.org/10.1056/NEJMoa1315200.

Orrù, C.D., B.R. Groveman, A.G. Hughson, G. Zanusso, M.B. Coulthart, and B.W. Caughey. 2015a. "Rapid and Sensitive RT-QuIC Detection of Human Creutzfeldt-Jakob Disease Using Cerebrospinal Fluid." *MBio* 6 (1): e02451-14. https://doi.org/10.1128/mBio.02451-14.

Orrù, C.D., B.R. Groveman, L.D. Raymond, A.G. Hughson, R. Nonno, W. Zou, B. Ghetti, P. Gambetti, and B.W. Caughey. 2015b. "Bank Vole Prion Protein As an Apparently Universal Substrate for RT-QuIC-Based Detection and Discrimination of Prion Strains." *PLoS Pathogens* 11 (6). https://doi.org/10.1371/journal.ppat.1004983.

Orrù, C.D., J.M. Wilham, S. Vascellari, A.G. Hughson, and B.W. Caughey. 2012. "New Generation QuIC Assays for Prion Seeding Activity." *Prion* 6 (2): 147–52. https://doi.org/10.4161/pri.19430.

Orrù, C.D., J. Yuan, B.S. Appleby, B. Li, Y. Li, D. Winner, Z. Wang, et al. 2017. "Prion Seeding Activity and Infectivity in Skin Samples from Patients with Sporadic Creutzfeldt-Jakob Disease." *Science Translational Medicine* 9 (417).

https://doi.org/10.1126/scitranslmed.aam7785.

Orrú, Christina D., Matilde Bongianni, Giovanni Tonoli, Sergio Ferrari, Andrew G. Hughson, Bradley R. Groveman, Michele Fiorini, et al. 2014. “A Test for Creutzfeldt–Jakob Disease Using Nasal Brushings.” *New England Journal of Medicine* 371 (6): 519–29. https://doi.org/10.1056/NEJMoa1315200.

Pan, K. M., M. Baldwin, J. Nguyen, M. Gasset, A. Serban, D. Groth, I. Mehlhorn, Z. Huang, R. J. Fletterick, and F. E. Cohen. 1993. “Conversion of Alpha-Helices into Beta-Sheets Features in the Formation of the Scrapie Prion Proteins.” *Proceedings of the National Academy of Sciences of the United States of America* 90 (23): 10962–66. https://doi.org/10.1073/pnas.90.23.10962.

Parchi, P., R. Castellani, S. Capellari, B. Ghetti, K. Young, S.G. Chen, M. Farlow, et al. 1996. “Molecular Basis of Phenotypic Variability in Sporadic Creutzfeldt-Jakob Disease.” *Annals of Neurology* 39 (6): 767–78. https://doi.org/10.1002/ana.410390613.

Parchi, P., A. Giese, S. Capellari, P. Brown, W. Schulz-Schaeffer, O. Windl, I. Zerr, et al. 1999. “Classification of Sporadic Creutzfeldt-Jakob Disease Based on Molecular and Phenotypic Analysis of 300 Subjects.” *Annals of Neurology* 46 (2): 224–33. http://www.ncbi.nlm.nih.gov/pubmed/10443888.

Parchi, P., and D. Saverioni. 2012. “Molecular Pathology, Classification, and Diagnosis of Sporadic Human Prion Disease Variants.” *Folia Neuropathologica* 50 (1): 20–45.

Pattison, I. H., and G. C. Millson. 1961. “Scrapie Produced Experimentally in Goats with Special Reference to the Clinical Syndrome.” *Journal of Comparative Pathology* 71 (April): 101–9. http://www.ncbi.nlm.nih.gov/pubmed/13733383.

Peden, A. H., L. I. McGuire, N. E. J. Appleford, G. Mallinson, J. M. Wilham, C. D. Orru, B. Caughey, et al. 2012. “Sensitive and Specific Detection of Sporadic Creutzfeldt-Jakob Disease Brain Prion Protein Using Real-Time Quaking-Induced Conversion.” *Journal of General Virology* 93 (2): 438–49. https://doi.org/10.1099/vir.0.033365-0.

Peden, A.H., M.W. Head, D.L. Ritchie, J.E. Bell, and J.W. Ironside. 2004. “Preclinical VCJD after Blood Transfusion in a PRNP Codon 129 Heterozygous Patient.” *Lancet* 364 (9433): 527–29. https://doi.org/10.1016/S0140-6736(04)16811-6.

Peden, A.H., D.P. Sarode, C.R. Mulholland, M.A. Barria, D.L. Ritchie, J.W. Ironside, and M.W. Head. 2014. “The Prion Protein Protease Sensitivity, Stability and Seeding Activity in Variably Protease Sensitive Prionopathy Brain Tissue Suggests Molecular Overlaps with Sporadic Creutzfeldt-Jakob Disease.” *Acta Neuropathologica Communications* 2 (1): 1–17. https://doi.org/10.1186/s40478-014-0152-4.

Piconi, G., A.H. Peden, M.A. Barria, and A.J.E. Green. 2019. “Epitope Mapping of the Protease Resistant Products of RT-QuIC Does Not Allow the Discrimination of SCJD Subtypes.” *PLOS ONE* 14 (6): e0218509. https://doi.org/10.1371/journal.pone.0218509.

Piening, N., P. Weber, A. Giese, and H. Kretzschmar. 2005. “Breakage of PrP Aggregates Is Essential for Efficient Autocatalytic Propagation of Misfolded Prion Protein.” *Biochemical and Biophysical Research Communications* 326 (2): 339–43. https://doi.org/10.1016/j.bbrc.2004.11.039.

Pirisinu, L., S. Marcon, M.A. Di Bari, C. D’Agostino, U. Agrimi, and R. Nonno. 2013. “Biochemical Characterization of Prion Strains in Bank Voles.” *Pathogens* 2 (3): 446–56. https://doi.org/10.3390/pathogens2030446.

Prusiner, S. B. 2004. *Prion Biology and Diseases*. Edited by Stanley B. Prusiner. 2nd ed. Cold Spring Harbor Laboratory Press.

Prusiner, S.B. 1982. “Novel Proteinaceous Infectious Particles Cause Scrapie.” *Science* 216 (4542): 136–44. https://doi.org/10.1126/science.6801762.

———. 1998. “Prions.” *Proc Natl Acad Sci USA Nobel Lecture* 95 (11): 13363–83.

Prusiner, S.B., D.F. Groth, S.P. Cochran, F.R. Masiarz, M.P. McKinley, and H.M. Martinez. 1980. “Molecular Properties, Partial Purification, And Assay By Incubation Period Measurements Of The Hamster Scrapie Agent.” *Biochemistry* 19 (21): 4883–91. https://doi.org/10.1021/bi00562a028.

Prusiner, S.B., M.P. Mckinley, D.F. Groth, K.A. Bowman, N.I. Mock, S.P. Cochran, and F.R. Masiarz. 1981. “Scrapie Agent Contains a Hydrophobic Protein” 78 (11): 6675–79.

Prusiner, S.B., M. Scott, D. Foster, K.M. Pan, D. Groth, C. Mirenda, M. Torchia, et al. 1990. “Transgenetic Studies Implicate Interactions between Homologous PrP Isoforms in Scrapie Prion Replication.” *Cell* 63 (4): 673–86. https://doi.org/10.1016/0092-8674(90)90134-Z.

Ritchie, D.L., M.A. Barria, A.H. Peden, H.M. Yull, J. Kirkpatrick, P. Adlard, J.W. Ironside, and M.W. Head. 2017. “UK Iatrogenic Creutzfeldt–Jakob Disease: Investigating Human Prion Transmission across Genotypic Barriers Using Human Tissue-Based and Molecular Approaches.” *Acta Neuropathologica* 133 (4): 579–95. https://doi.org/10.1007/s00401-016-1638-x.

Rossetti, G., and P. Carloni. 2017. “Structural Modeling of Human Prion Protein’s Point Mutations.” In *Progress in Molecular Biology and Translational Science*, 150:105–22. Academic Press. https://doi.org/10.1016/bs.pmbts.2017.07.001.

Saborio, G.P., B. Permanne, and C. Soto. 2001. “Sensitive Detection of Pathological Prion Protein by Cyclic Amplication of Protein Misfolding.” *Nature* 411 (June): 1–4. https://doi.org/10.1038/35081095.

Saborio, G.P., C. Soto, R.J. Kascsak, E. Levy, R. Kascsak, D.A. Harris, and B. Frangione. 1999. “Cell-Lysate Conversion of Prion Protein into Its Protease-Resistant Isoform Suggests the Participation of a Cellular Chaperone.” *Biochemical and Biophysical Research Communications* 258 (2): 470–75. https://doi.org/10.1006/bbrc.1999.0660.

Safar, J.G., H. Wille, V. Itri, D.F. Groth, H. Serban, M. Torchia, F.E. Cohen, and S.B. Prusiner. 1998. “Eight Prion Strains Have PrPSc Molecules with Different

Conformations." *Nature Medicine* 4 (10): 1157–65. https://doi.org/10.1038/2654.

Saijo, Eri, Bernardino Ghetti, Gianluigi Zanusso, Adrian Oblak, Jennifer L. Furman, Marc I. Diamond, Allison Kraus, and Byron Caughey. 2017. "Ultrasensitive and Selective Detection of 3-Repeat Tau Seeding Activity in Pick Disease Brain and Cerebrospinal Fluid." *Acta Neuropathologica* 133 (5): 751–65. https://doi.org/10.1007/s00401-017-1692-z.

Sailer, A., H. Büeler, M. Fischer, A. Aguzzi, and C. Weissmann. 1994. "No Propagation of Prions in Mice Devoid of PrP." *Cell*. https://doi.org/10.1016/0092-8674(94)90436-7.

Sang, J.C., J.-E. Lee, A.J. Dear, S. De, G. Meisl, A.M. Thackray, R. Bujdoso, T.P.J. Knowles, and D. Klenerman. 2019. "Direct Observation of Prion Protein Oligomer Formation Reveals an Aggregation Mechanism with Multiple Conformationally Distinct Species." *Chemical Science* 10 (17): 4588–97. https://doi.org/10.1039/C8SC05627G.

Sano, K., R. Atarashi, D. Ishibashi, T. Nakagaki, K. Satoh, and N. Nishida. 2014. "Conformational Properties of Prion Strains Can Be Transmitted to Recombinant Prion Protein Fibrils in Real-Time Quaking-Induced Conversion." *Journal of Virology* 88 (20): 11791–801. https://doi.org/10.1128/JVI.00585-14.

Sano, K., R. Atarashi, and N. Nishida. 2015. "Structural Conservation of Prion Strain Specificities in Recombinant Prion Protein Fibrils in Real-Time Quaking-Induced Conversion." *Prion* 9 (4): 237–43. https://doi.org/10.1080/19336896.2015.1062201.

Scheckel, C., and A. Aguzzi. 2018. "Prions, Prionoids and Protein Misfolding Disorders." *Nature Reviews Genetics* 19 (7): 405–18. https://doi.org/10.1038/s41576-018-0011-4.

Scott, M., D. Foster, C. Mirenda, D. Serban, F. Coufal, M. Wälchli, M. Torchia, et al. 1989. "Transgenic Mice Expressing Hamster Prion Protein Produce Species-Specific Scrapie Infectivity and Amyloid Plaques." *Cell* 59 (5): 847–57. https://doi.org/10.1016/0092-8674(89)90608-9.

Scott, M.R., D. Groth, J. Tatzelt, M. Torchia, P. Tremblay, S.J. DeArmond, and S.B. Prusiner. 1997. "Propagation of Prion Strains through Specific Conformers of the Prion Protein." *Journal of Virology* 71 (12): 9032–44. https://www.ncbi.nlm.nih.gov/pmc/articles/PMC230204/pdf/719032.pdf.

Seeger, H. 2005. "Coincident Scrapie Infection and Nephritis Lead to Urinary Prion Excretion." *Science* 310 (5746): 324–26. https://doi.org/10.1126/science.1118829.

Shaked, G.M., Y. Shaked, Z. Kariv-Inbal, M. Halimi, I. Avraham, and R. Gabizon. 2001. "A Protease-Resistant Prion Protein Isoform Is Present in Urine of Animals and Humans Affected with Prion Diseases." *Journal of Biological Chemistry* 276 (34): 31479–82. https://doi.org/10.1074/jbc.C100278200.

Shi, S., J. Wagner, G. Mitteregger-Kretzschmar, S. Ryazanov, A. Leonov, C.

Griesinger, and A. Giese. 2015. “Quantitative Real-Time Quaking-Induced Conversion Allows Monitoring of Disease-Modifying Therapy in the Urine of Prion-Infected Mice.” *Journal of Neuropathology and Experimental Neurology* 74 (9): 924–33. https://doi.org/10.1097/NEN.0000000000000233.

Sigurdson, C.J., K.P.R. Nilsson, S. Hornemann, G. Manco, N. Fernández-Borges, P. Schwarz, J. Castilla, K. Wüthrich, and A. Aguzzi. 2010. “A Molecular Switch Controls Interspecies Prion Disease Transmission in Mice.” *Journal of Clinical Investigation* 120 (7): 2590–99. https://doi.org/10.1172/JCI42051.

Silva, C.J., E. Vázquez-Fernández, B. Onisko, and J.R. Requena. 2015. “Proteinase K and the Structure of PrPSc: The Good, the Bad and the Ugly.” *Virus Research*. https://doi.org/10.1016/j.virusres.2015.03.008.

Silveira, J.R., G.J. Raymond, A.G. Hughson, R.E. Race, V.L. Sim, S.F. Hayes, and B.W. Caughey. 2005. “The Most Infectious Prion Protein Particles.” *Nature* 437 (7056): 257–61. https://doi.org/10.1038/nature03989.

Stahl, N., M.A. Baldwin, S.B. Prusiner, and A.L. Burlingame. 1990. “Identification of Glycoinositol Phospholipid Linked and Truncated Forms of the Scrapie Prion Protein.” *Biochemistry*. https://doi.org/10.1021/bi00490a001.

Stoeck, K., P. Sanchez-Juan, J. Gawinecka, A.J.E. Green, A. Ladogana, M. Pocchiari, R. Sanchez-Valle, et al. 2012. “Cerebrospinal Fluid Biomarker Supported Diagnosis of Creutzfeldt-Jakob Disease and Rapid Dementias: A Longitudinal Multicentre Study over 10 Years.” *Brain* 135 (10): 3051–61. https://doi.org/10.1093/brain/aws238.

Telling, G. C., P. Parchi, S. J. DeArmond, P. Cortelli, P. Montagna, R. Gabizon, J. Mastrianni, E. Lugaresi, P. Gambetti, and S. B. Prusiner. 1996. “Evidence for the Conformation of the Pathologic Isoform of the Prion Protein Enciphering and Propagating Prion Diversity.” *Science* 274 (5295): 2079–82. https://doi.org/10.1126/science.274.5295.2079.

Tessier, P.M., and S. Lindquist. 2007. “Prion Recognition Elements Govern Nucleation, Strain Specificity and Species Barriers.” *Nature* 447 (7144): 556–61. https://doi.org/10.1038/nature05848.

The National CJD Research & Surveillance Unit. 2017. “CJD Surveillance in the UK, 26th Annual Report.” Edinburgh. www.cjd.ed.ac.uk.

Thomzig, A., F. Cardone, D. Krüger, M. Pocchiari, P. Brown, and M. Beekes. 2006. “Pathological Prion Protein in Muscles of Hamsters and Mice Infected with Rodent-Adapted BSE of VCJD.” *Journal of General Virology* 87 (1): 251–54. https://doi.org/10.1099/vir.0.81277-0.

Towbin, H., T. Staehelin, and J. Gordon. 1979. “Electrophoretic Transfer of Proteins from Polyacrylamide Gels to Nitrocellulose Sheets: Procedure and Some Applications.” *Proceedings of the National Academy of Sciences of the United States of America* 76 (9): 4350–54. https://doi.org/10.1073/pnas.76.9.4350.

Vilotte, J.-L., S. Soulier, R. Essalmani, M.-G. Stinnakre, D. Vaiman, L. Lepourry, J. C. Da Silva, et al. 2001. “Markedly Increased Susceptibility to Natural Sheep

Scrapie of Transgenic Mice Expressing Ovine PrP." *Journal of Virology* 75 (13): 5977–84. https://doi.org/10.1128/jvi.75.13.5977-5984.2001.

Walker, L.C., and H. LeVine. 2003. "The Cerebral Proteopathies." *Molecular Neurobiology* 21 (1–2): 083–096. https://doi.org/10.1385/mn:21:1-2:083.

Wang, F., X. Wang, C.G. Yuan, and J. Ma. 2010. "Generating a Prion with Bacterially Expressed Recombinant Prion Protein." *Science* 327 (5969): 1132–35. https://doi.org/10.1126/science.1183748.

Ward, H.J.T., D. Everington, S.N. Cousens, B. Smith-Bathgate, M. Leitch, S. Cooper, C. Heath, R.S.G. Knight, P.G. Smith, and R.G. Will. 2006. "Risk Factors for Variant Creutzfeldt-Jakob Disease: A Case-Control Study." *Annals of Neurology* 59 (1): 111–20. https://doi.org/10.1002/ana.20708.

Watts, J.C., K. Giles, S. Patel, A. Oehler, S.J. DeArmond, and S.B. Prusiner. 2014. "Evidence That Bank Vole PrP Is a Universal Acceptor for Prions." *PLoS Pathogens* 10 (4): 1003990. https://doi.org/10.1371/journal.ppat.1003990.

Wilham, Jason M., Christina D. Orrú, Richard A. Bessen, Ryuichiro Atarashi, Kazunori Sano, Brent Race, Kimberly D. Meade-White, Lara M. Taubner, Andrew Timmes, and Byron Caughey. 2010. "Rapid End-Point Quantitation of Prion Seeding Activity with Sensitivity Comparable to Bioassays." *PLoS Pathogens* 6 (12). https://doi.org/10.1371/journal.ppat.1001217.

Will, R.G., J.W. Ironside, M. Zeidler, K. Estibeiro, S.N. Cousens, P.G. Smith, A. Alperovitch, S. Poser, M. Pocchiari, and A. Hofman. 1996. "A New Variant of Creutzfeldt-Jakob Disease in the UK." *The Lancet* 347 (9006): 921–25. https://doi.org/10.1016/S0140-6736(96)91412-9.

Wille, H., and J. Requena. 2018. "The Structure of PrPSc Prions." *Pathogens* 7 (1): 20. https://doi.org/10.3390/pathogens7010020.

World Health Organisation. 2003. *WHO Manual for Surveillance of Human Transmissible Spongiform Encephalopathies Including Variant Creutzfeldt-Jakob Disease*. *WHO*.

Wüthrich, K., and R. Riek. 2001. "Three-Dimensional Structures of Prion Proteins." *Advances in Protein Chemistry* 57 (January): 55–82. https://doi.org/10.1016/S0065-3233(01)57018-7.

Yuan, J., M. Kinter, J. McGeehan, G. Perry, G. Kneale, P. Gambetti, and W.-Q. Zou. 2005. "Concealment of Epitope by Reduction and Alkylation in Prion Protein." *Biochemical and Biophysical Research Communications* 326 (3): 652–59. https://doi.org/10.1016/j.bbrc.2004.11.088.

Yull, H.M., D.L. Ritchie, J.P.M. Langeveld, F.G. van Zijderveld, M.E. Bruce, J.W. Ironside, and M.W. Head. 2006. "Detection of Type 1 Prion Protein in Variant Creutzfeldt-Jakob Disease." *The American Journal of Pathology* 168 (1): 151–57. https://doi.org/10.2353/AJPATH.2006.050766.

Zahn, R., A. Liu, T. Luhrs, R. Riek, C. von Schroetter, F. Lopez Garcia, M. Billeter, L. Calzolai, G. Wider, and K. Wuthrich. 2000. "NMR Solution Structure of the

Human Prion Protein." *Proceedings of the National Academy of Sciences* 97 (1): 145–50. https://doi.org/10.1073/pnas.97.1.145.

Zanusso, G., D. Liu, S. Ferrari, I. Hegyi, X. Yin, A. Aguzzi, S. Hornemann, et al. 1998. "Prion Protein Expression in Different Species: Analysis with a Panel of New MAbs." *Proceedings of the National Academy of Sciences* 95 (15): 8812–16. https://doi.org/10.1073/pnas.95.15.8812.

Zerr, I., and P. Parchi. 2018. "Sporadic Creutzfeldt–Jakob Disease." In *Handbook of Clinical Neurology*, edited by M. Pocchiari and J. C. Manson, 153:155–74. Elsevier B.V. https://doi.org/10.1016/B978-0-444-63945-5.00009-X.

Zobeley, E., E. Flechsig, A. Cozzio, M. Enari, and C. Weissmann. 1999. "Infectivity of Scrapie Prions Bound to a Stainless Steel Surface." *Molecular Medicine (Cambridge, Mass.)* 5: 240–43.